Reliable and Sustainable Electric Power and Energy Systems Management

Roy Billinton
Rajesh Karki
Ajit Kumar Verma *Editors*

Reliability and Risk Evaluation of Wind Integrated Power Systems

Springer

Reliable and Sustainable Electric Power and Energy Systems Management

Series Editors

Roy Billinton
Ajit Kumar Verma
Rajesh Karki

For further volumes:
http://www.springer.com/series/10855

Roy Billinton · Rajesh Karki · Ajit Kumar Verma
Editors

Reliability and Risk Evaluation of Wind Integrated Power Systems

Springer

Editors
Roy Billinton
Rajesh Karki
Department of Electrical and Computer Engineering
University of Saskatchewan
Saskatoon, SK
Canada

Ajit Kumar Verma
Stord/Haugesund University College
Haugesund
Norway

ISBN 978-81-322-0986-7 ISBN 978-81-322-0987-4 (eBook)
DOI 10.1007/978-81-322-0987-4
Springer New Delhi Heidelberg New York Dordrecht London

Library of Congress Control Number: 2013931513

Printed on acid-free paper

Springer is part of Springer Science+Business Media (www.springer.com)

Preface

The importance of power and energy in modern society is well established and it is impossible to create a modern society and country without the existence of reliable power and energy systems. The continued development of reliable systems has been the main focus of power and energy system engineers for over a century. Reliability issues are integral elements in the planning and economics associated with any engineering system, and are embedded in basic project planning and appraisal techniques. As the complexities of modern power and energy systems grow, new approaches, techniques, and methods will be proposed for the evaluation and analysis of these systems. While rapid developments in the field of computational technologies have solved many issues related to the analysis of complex systems, the incorporation of new constraints arising from the use of particular technologies will dictate the solution techniques to be more creative and require considerable time to remodel, system test, and validate.

This Book Series entitled, "Reliable and Sustainable Electric Power and Energy Systems Management", is intended to provide a platform for researchers, planners and policy makers to share their research outputs, ideas and opinions on the critical issue of sustainable and reliable power and energy systems. It also aims to provide impetus for critical research in this highly important area for modern society in the context of a meshed and complex environment that is affected by events taking place throughout the world. This book series is intended to be produced in separate volumes. The present book is the first volume of the Book Series. This volume is focused on new innovative research from academia and industry on understanding, quantifying and managing the risks associated with the uncertainty in wind variability. These are important issues in planning and operating electric power systems with acceptable levels of reliability and high proportions of wind power generation.

Five of the eight chapters in this book are extended versions of papers presented at the PMAPS-2012 Conference, June 10–14, 2012 in Istanbul, Turkey. The biennial Probability Methods Applied to Power Systems conferences are highly focused gatherings of international experts. Reliability analysis of renewable energy sources in electric power systems has been a major presentation and discussion topic in recent years and this activity is expected to continue in the future. All of the chapter authors

in this book are actively involved in PMAPS and many of them actively participated in the recent conference in Istanbul.

Wind power behaves quite differently from conventional electric power generating units due to its intermittent and diffuse nature. An important requirement in planning a wind integrated power system is to ascertain the capacity credit that can be assigned to both existing and planned wind power facilities. Chapter 1 illustrates the procedures used by a large Regional Transmission Organization and Independent System Operator to determine the capacity value of the wind resources in their jurisdiction. This chapter demonstrates the method developed to calculate the system-wide capacity value of wind resources and illustrates how the capacity credit is designated to the individual wind sites.

The increasing trend towards renewable forms of generation, and in particular wind, is creating new operating challenges. The uncertainty associated with the wind is an issue which must be considered in order for wind power to be successfully integrated into an existing electric power system. This uncertainty may be managed through the use of suitable wind forecasting methodologies. The error inherent in forecasting will impact system reliability and cost as will inaccuracies in assumptions about the forecast error. Chapter 2 presents a methodology adopted for use in a Scenario Tree Tool constructed to allow for closer examination of the effect of forecast error assumptions and properties in unit commitment scheduling models.

Chapter 3 presents a new approach to the critical problem of detecting or forecasting ramping events in the context of wind power prediction. The novelty of the model relies on departing from the probability density function estimated for the wind power and building a probabilistic representation of encountering, at each time step, a ramp event according to some definition. The model allows the assignment of a probability value to each possible magnitude of a predicted ramp and its worth is assessed by several metrics including receiver operating characteristic curves which show the relationship between true positive and false positive ramp rates.

The increasing wind power penetration in electric power systems creates growing operational difficulties in maintaining system reliability due to the uncertain nature of wind power. An appreciation of the available wind power in the next few hours can assist the system operator to optimize the required regulating margin. Chapter 4 illustrates a process in which time series Auto Regressive Moving Average (ARMA) models have been used to quantify the uncertainty associated with wind power commitment in a short future time such as 1–4 h using a conditional probability approach. Knowledge of available wind power a day ahead or even longer is also required by system operators to schedule the conventional generating units in the system. This chapter extends the future time of interest up to 24 h to examine the impact of initial wind speed/wind power conditions and to evaluate the wind power commitment based on a probabilistic wind power commitment risk.

Chapter 5 proposes a novel framework for designing an N-1 secure generation day-ahead dispatch for power systems with a high penetration of fluctuating power sources, e.g., wind or PV power. This is achieved by integrating the security constraints in a DC optimal power flow optimization and formulating a stochastic program with chance constraints, which encode the probability of satisfying

the transmission capacity constraints of the lines. The resulting problem is solved numerically by transforming the initial problem into a tractable one using the so-called scenario approach, which is based on sampling the uncertain parameter (in this case the wind power) while keeping the desired probabilistic guarantees. A Markov chain-based model is employed to generate the wind power scenarios. The effectiveness of the proposed technique is illustrated by application to the IEEE 30-bus network, and comparing it with the solution of a deterministic variant of the problem, where the operator determines a secure generation dispatch based only on the available wind power forecast. A Monte Carlo simulation study is applied to collect statistical results regarding the performance of the method.

Substantial integration of intermittent renewable energy resources such as wind generation in an electric power system can have significant impacts on the system reliability. Chapter 6 illustrates the application of system well-being analysis to address both generation system adequacy and security concerns. Sequential Monte Carlo simulation is utilized in the system well-being analysis to capture the characteristics associated with adequacy and security. A deterministic criterion of the loss of the largest generating unit is utilized as the security measure. The expected values and probability distributions of the system well-being indices associated with different generation scenarios are investigated and compared. The study results are demonstrated using the two test systems designated as the RBTS and IEEE-RTS.

Chapter 7 presents an approach which can be used to represent the correlation between any number of time series in a reliability evaluation based on non-sequential Monte Carlo simulation. The technique is illustrated in this chapter by application to generating capacity adequacy assessment with correlation between wind time series related to wind generation located at different sites and/or the system time-varying load. The developed model can be applied in a reliability study (generating system, composite system, etc.) where several time series are present. The calculated generating system adequacy indices are compared to those obtained by sequential Monte Carlo simulation and show that the model captures the dependence between correlated random variables.

Methodologies based on probability concepts are extremely useful in assessing the reliability performance of electric power systems and have been successfully applied to many areas including generating capacity planning, operating reserve assessment, distribution systems, etc. Many studies in these areas have been conducted in the last few years in order to evaluate the behavior of electric power systems due to the volatility of renewable sources. New methods and models to assess the reliability of power networks with a high penetration of these sources have been proposed in the literature. Most of these methods, however, utilize simplified models, considering only generation reliability or the representation of energy constraints through clustered data models. Chapter 8 presents an application of a flexible non-sequential Monte Carlo simulation approach to evaluate the main reliability indices of composite generation and transmission systems, considering renewable energy, comprising mainly hydro, mini-hydro, wind, co-generation (e.g. biomass), and solar power sources. The renewable capacity is calculated based on

monthly (hydro and mini-hydro) or hourly (wind, co-generation, and solar) series of primary energy. Case studies using variations of the IEEE RTS-96 are presented and discussed. The feasibility of the proposed method is demonstrated by application to an existing large electric power system.

Roy Billinton
Rajesh Karki
Ajit Kumar Verma

Contents

Bio Sketch of Editors

Dr Roy Billinton received the B.Sc. and M.Sc. degrees from the University of Manitoba, Winnipeg, MB, Canada, and the Ph.D. and D.Sc. degrees in electrical engineering from the University of Saskatchewan, Saskatoon, SK, Canada. He was with the System Planning and Production Divisions, Manitoba Hydro. In 1964, he joined the University of Saskatchewan, where he served as the Head of the Electrical Engineering Department, Associate Dean for Graduate Studies, Research and Extension, and the Acting Dean of Engineering, and is currently a Professor Emeritus in the Department of Electrical Engineering. He has authored or coauthored eight books and more than 940 papers on power system reliability evaluation, economic system operation, and power system analysis. Dr. Billinton is a Fellow of the Engineering Institute of Canada, the Canadian Academy of Engineering, the Royal Society of Canada, a Foreign Associate of the United States National Academy of Engineering, and a Professional Engineer in the Province of Saskatchewan, Canada. The IEEE-PES honored Dr Billinton by initiating the Roy Billinton Power System Reliability Award in 2010.

Dr Rajesh Karki obtained his B.E. degree in electrical engineering from the Regional Engineering College (renamed National Institute of Technology), West Bengal, India in 1991, and MSc and PhD degress in electrical power engineering in 1997 and 2000 respectively from the University of Saskatchewan, Canada. He worked for academic institutions and different industries in Nepal between 1991 and 1995. He worked for GE Industrial Systems, Peterborough, ON, Canada during 2000–2002. He joined the University of Saskatchewan, Canada as an Assistant Professor in 2002, where he currently works as an Associate Professor. He chaired the Power Systems Research Group at the University of Saskatchewan during 2005–2012. His research interests include power system reliability and planning, and reliability modeling and analysis of renewable energy systems. He has served in various capacities in international conferences held in Canada and abroad. He has published over 70 papers in reputable international journals and peer reviewed conferences. He has completed several consulting projects on system planning and reliability for Canadian electric utilities. Dr Karki is a Senior Member of the IEEE, and a Professional Engineer in the Province of Saskatchewan, Canada.

Dr Ajit Kumar Verma obtained B.Tech (Electrical Engineering) and PhD (Reliability Engineering) from Indian Institute of Technology Kharagpur, India in 1984 and 1988 respectively. He joined Indian Institute of Technology Bombay in 1988 where he holds the position of Professor of Electrical Engineering. He is currently working as Professor of Technical Safety at University College Stord/ Haugesund, Norway. He has supervised/co-supervised 28 PhDs and 88 Masters thesis in the area of Software Reliability, Reliable Computing, Power Systems Reliability (PSR), Reliability Centred Maintenance (RCM) and Probabilistic Safety/Risk Assessment (PSA). He has over 195 publications in various journals and conferences. He is a senior member of IEEE and a life fellow of IETE. He is the Editor-in-Chief of OPSEARCH published by Springer as well as the Editor-in-Chief of International Journal of Systems Assurance Engineering and Management (IJSAEM) published by Springer. He has served as a Guest Editor of many international journal including IEEE Transactions on Reliability March, 2010. He has been Conference Chairman of various International Conferences and symposia.

Contributors

Göran Andersson Power Systems Laboratory, Department of Electrical Engineering, ETH Zürich, Zurich, Switzerland, e-mail: andersson@eeh.ee.ethz.ch

Roy Billinton Power System Research Group, Department of Electrical and Computer Engineering, University of Saskatchewan, Saskatoon, Canada, e-mail: roy.billinton@usask.ca

Carmen L. T. Borges Electrical Engineering Department, Federal University of Rio de Janeiro, Rio de Janeiro, Brazil, e-mail: carmen@nacad.ufrj.br

A. Botterud Argonne National Laboratory, Decision and Information Sciences Division, Lemont, UK, e-mail: abotterud@anl.gov

Mauro A. da Rosa INESC Tech, Power System Unit, 4200-465 Porto, Portugal, e-mail: marosa@inescporto.pt

Armando M. Leite da Silva Institute of Electrical Systems and Energy, Federal University of Itajubá – UNIFEI, Itajubá, MG 37.500-903, Brazil, e-mail: am.leitedasilva@gmail.com

Julio A. S. Dias PSR, Rio de Janeiro, Brazil, e-mail: alberto@psr-inc.com

C. Ferreira LIAAD/INESC TEC and ISEP/IPP, Polytechnic Institute of Porto, Porto, Portugal, e-mail: cgf@isep.ipp.pt

Silvan A. Flávio Institute of Electrical Systems and Energy, Federal University of Itajubá – UNIFEI, Itajubá, MG 37.500-903, Brazil, e-mail: silvanflavio@yahoo.com.br

J. Gama LIAAD/INESC TEC and FEP, University of Porto, Porto, Portugal, e-mail: jgama@liaad.up.pt

Brandon Heath Regulatory and Economic Studies Department, MISO, Saint Paul, MN, USA, e-mail: bheath@misoenergy.org

Rajesh Karki Power System Research Group, Department of Electrical and Computer Engineering, University of Saskatchewan, Saskatoon, Canada, e-mail: rajesh.karki@usask.ca

John Lawhorn Regulatory and Economic Studies Department, MISO, Saint Paul, MN, USA, e-mail: jlawhorn@misoenergy.org

Wenyuan Li BC Hydro and Power Authority, Vancouver, BC, Canada, e-mail: wen.yuan.li@bchydro.com

Colm Lowery Electricity Research Centre, University College Dublin, Dublin, Ireland, e-mail: Colm.Lowery@ucdconnect.ie

John Lygeros Automatic Control Laboratory, Department of Electrical Engineering, ETH Zürich, Zurich, Switzerland, e-mail: lygeros@control.ee.ethz.ch

Mark O'Malley Electricity Research Centre, University College Dublin, Dublin, Ireland, e-mail: mark.omalley@ucd.ie

Luiz Antônio F. Manso Electrical Engineering Department, Federal University of São João del-Rei – UFSJ, São João del-Rei, MG 36.307-440, Brazil, e-mail: lmanso@ufsj.edu.br

Kostas Margellos Automatic Control Laboratory, Department of Electrical Engineering, ETH Zürich, Zürich, Switzerland, e-mail: margellos@control.ee.ethz.ch

Vladimiro Miranda INESC TEC (formerly INESC Porto), University of Porto, Porto, Portugal, e-mail: vmiranda@inescporto.pt

Leonidas C. Resende Electrical Engineering Department, Federal University of São João del-Rei – UFSJ, São João del-Rei, MG 36.307-440, Brazil, e-mail: leonidas@ufsj.edu.br

Suman Thapa Power System Research Group, Department of Electrical and Computer Engineering, University of Saskatchewan, Saskatoon, Canada, e-mail: suman.thapa@usask.ca

Charles Tyson Regulatory and Economic Studies Department, MISO, Saint Paul, MN, USA, e-mail: ctyson@misoenergy.org

Maria Vrakopoulou Power Systems Laboratory, Department of Electrical Engineering, ETH Zürich, Zurich, Switzerland, e-mail: vrakopoulou@eeh.ee.ethz.ch

Wijarn Wangdee Electricity Research Centre, University College Dublin, Dublin, Ireland, e-mail: wijarn.wangdee@bchydro.com

Determining Capacity Credit for Wind Used in MISO Resource Adequacy

Brandon Heath, Charles Tyson and John Lawhorn

1 Introduction and Background

The primary objective of resource adequacy is making sure that there is enough generation capacity available when needed. The MISO is a Regional Transmission Organization and Independent System Operator in the United States that covers approximately 1.05 million square kilometers (406 thousand square miles), serves over 40 million people and comprises 135,000 MW of generation of which currently 11,000 MW is wind, Fig. 1. The wind is located at over 140 sites across the MISO footprint and is comprised of nearly 10,000 separate wind turbines. The MISO also operates a $27.5 billion annual energy market that incorporates 1,975 Commercial Pricing Nodes (CPnodes). MISO is currently adding 1,000 MW of wind on its system every year, and it is expected to have 25,000 MW by 2025. As more new wind resources are being integrated into the MISO footprint and used in meeting the resource adequacy requirements, the capacity value to assign this intermittent resource has taken on ever-increasing importance. This chapter discusses the techniques and processes used to accurately evaluate and assign the correct value of capacity for the wind resources.

Since 2009, MISO has embarked on a process to determine the capacity value for the increasing fleet of wind generation in the system. The MISO process as developed and vetted through the MISO stakeholder community consists

B. Heath (✉) · C. Tyson · J. Lawhorn
Regulatory and Economic Studies Department, MISO, Saint Paul, MN, USA
e-mail: bheath@misoenergy.org

C. Tyson
e-mail: ctyson@misoenergy.org

J. Lawhorn
e-mail: jlawhorn@misoenergy.org

R. Billinton et al. (eds.), *Reliability and Risk Evaluation of Wind Integrated Power Systems*, Reliable and Sustainable Electric Power and Energy Systems Management,
DOI: 10.1007/978-81-322-0987-4_1, © Springer India 2013

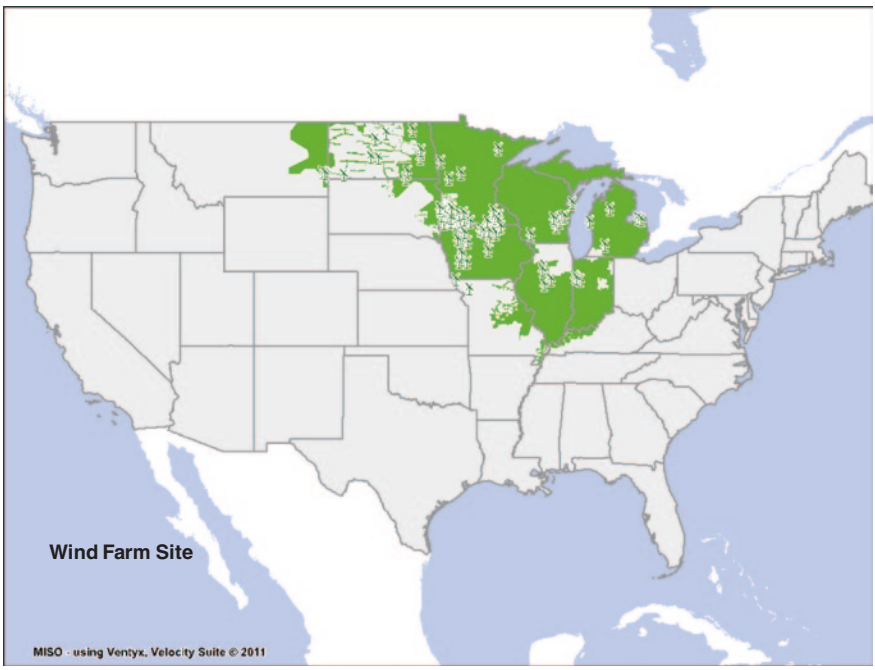

Fig. 1 MISO market footprint

of a two-step method. The first step utilizes a probabilistic approach to calculate the MISO system-wide effective load-carrying capability (ELCC) value for all wind resources in the MISO footprint. The second step employs a deterministic approach using specific information about the location of each wind resource "period metric" to allocate the single system-wide ELCC value across all wind CPnodes in the MISO system, to determine a wind capacity credit for each wind node.

As the geographic distance between wind generation increases, the correlation with the wind output decreases, as shown in Fig. 2. This leads to a higher average output from wind for a more geographically diverse set of wind plants, relative to a closely clustered group of wind plants. Due to the increasing diversity and the interannual variability in wind generation over time, the process needs to be repeated annually to incorporate the most recent historical performance of wind resources into the analysis. So, for each upcoming planning year, the wind capacity credit values in MISO are updated to account for both the stochastic nature of wind generation and the ever-increasing integration of new resources into the system. The sections of this write-up and current results illustrated here are broken down to describe the details of the two-step method adopted by MISO for determining wind capacity credit for the 2012 planning year.

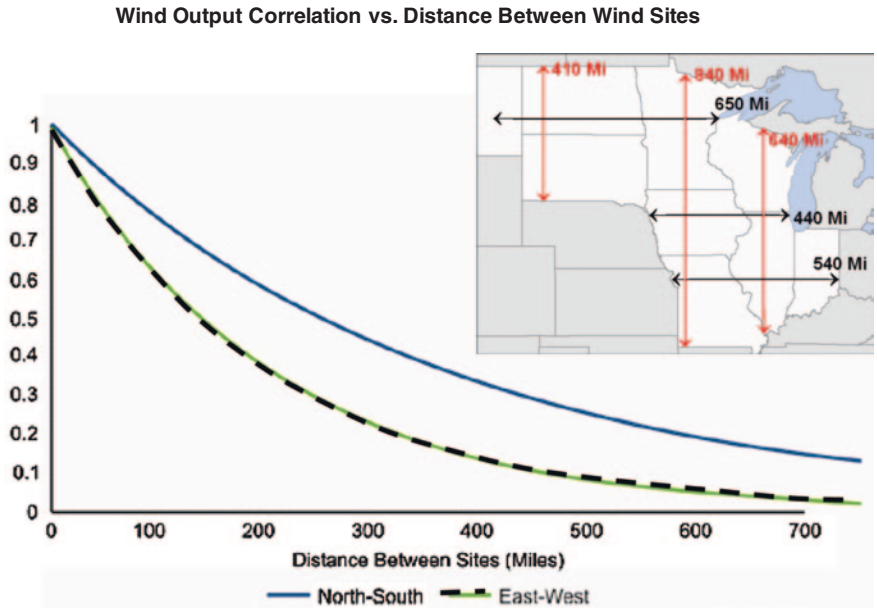

Fig. 2 Wind output correlation to distance between wind sites

2 Step-1: MISO System-Wide Wind ELCC Study

2.1 Probabilistic Analytical Approach

The probabilistic measure of load not being served is known as loss-of-load probability, and when this probability is summed over a time frame, for example 1 year, it is known as loss-of-load expectation (LOLE). The industry-accepted standard for what has been considered a reliable system has been the "less than 1 day in 10 years" criteria for LOLE. This measure is often expressed as 0.1 day/year, as that is often the time period (1 year) over which the LOLE index is calculated.

ELCC is defined as the amount of incremental load a resource, such as wind, can dependably and reliably serve while considering the probabilistic nature of generation shortfalls and random forced outages as driving factors to load not being served. Using ELCC in the determination of capacity value for generation resources has been around for nearly half a century. In 1966, Garver demonstrated the use of loss-of-load probability mathematics in the calculation of ELCC [1].

To measure ELCC of a particular resource, the reliability effects need to be isolated for the resource in question, from those of all the other sources. This is accomplished by calculating the LOLE of two different cases: one "with" and one "without" the resource. Inherently, the case "with" the resource should be more reliable and consequently have fewer days per year of expected loss of load (smaller LOLE).

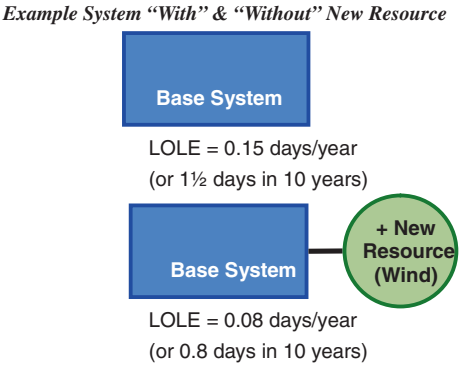

Fig. 3 Example system "with" and "without" new resource

The new resource in the example shown in Fig. 3 made the system 0.07 day/year more reliable, but there is another way to express the reliability contribution of the new resource besides the change in LOLE. This way requires establishing a common baseline reliability level and then adjusting the load in each case "with" and "without" the new resource to this common LOLE level. A common baseline that is chosen is the industry-accepted reliability standard of 1 day in 10 years (0.1 day/year) LOLE criteria.

With each case being at the same reliability level, as shown in Fig. 4, the only difference between the two cases is that the load was adjusted. This difference is the amount of ELCC expressed in load or megawatts, which is 300 MW (100 to −200) for the new resource in this example. Sometimes this number is divided by the nameplate rating of the new resource and then expressed in percentage (%) form. The new resource in the ELCC example Fig. 4 has an ELCC of 30 % of the resource nameplate.

The same methodology illustrated in the simple example of Fig. 4 was utilized as the analytical approach for the determination of the system-wide ELCC of the wind resource in the much more complex MISO system. For each historic year studied, there were two types of cases analyzed, one with and one without the

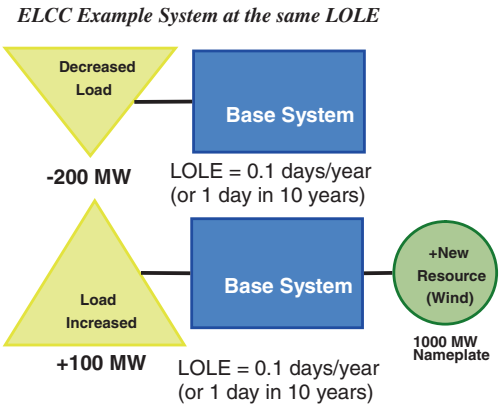

Fig. 4 ELCC example system at the same LOLE

wind resources. Each case was adjusted to the same common baseline LOLE and the ELCC was measured off those load adjustments. Using ELCC is the preferred method of calculation for determining the capacity value of wind [2].

2.2 LOLE Model Inputs and Assumptions

To apply the ELCC calculation methodology, MISO uses the Multi-Area Reliability Simulation (MARS) program by GE Energy to calculate LOLE values with and without the wind resource modeled. This model consisted of three major inputs:

1. Generator forced outage rates (FORs)
2. Actual historic hourly load values
3. Actual historic hourly wind output values

FORs are used for the conventional type of units in the LOLE model. These FORs are calculated from the Generator Availability Data System (GADS) that MISO uses to collect historic operation performance data for all conventional-type units in the MISO system as well as the capacity throughout the country.

To incorporate historical information, the actual 2005–2011 historical hourly concurrent load and wind output at the wind CPnodes are used to calculate the historic ELCC values for the wind generation in the MISO on a system-wide basis. The last two columns in Table 1 illustrate the ELCC results for the 7 years of MISO historic data.

2.3 MISO System-Wide ELCC Results

MISO calculated ELCC percentage results for historic years 2005–2011 and at multiple scenarios of penetration levels, corresponding to 10, 20, and 30 GW of installed wind capacity. This creates an ELCC penetration characteristic for each year, as illustrated by the different curves in Fig. 5. The initial leftmost data point for each curve is at the lowest penetration point on each characteristic curve and represents

Table 1 MISO historical wind ELCC values

Years	MISO peak load (MW)	Registered wind max capacity (MW)	Historical wind penetration (%)	System-wide ELCC (MW)	System-wide ELCC (%)
2005	109,473	908	0.8	152	16.7
2006	113,095	1,251	1.1	495	39.6
2007	101,800	2,065	2.0	57	2.8
2008	96,321	3,086	3.2	395	12.8
2009	94,185	5,636	6.0	173	3.1
2010	107,171	8,179	7.6	1,548	18.9
2011	102,804	9,996	9.7	3,007	30.1

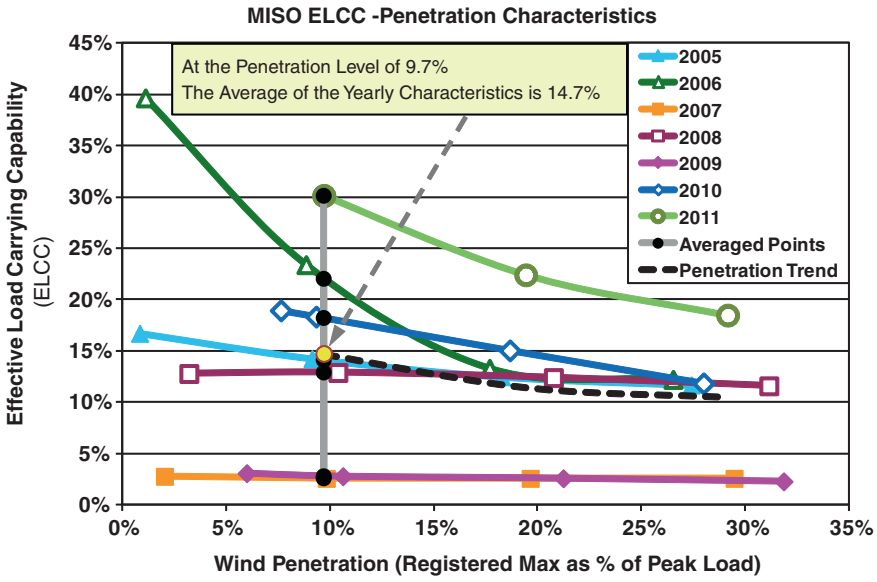

Fig. 5 Seven years of historical ELCC penetration characteristics

the actual annual ELCC for that year, and the values are shown in the right column in Table 1. The values along each year's characteristic curve at the higher penetration levels reflect what that year's wind resource would have as an ELCC if more capacity had been installed in that year, over the same MISO footprint. The high-end 30 GW level of penetration is an estimate of the amount of wind generation that could result in MISO, as the load-serving entities collectively meet renewable resource mandates of the various MISO States. Figure 5 illustrates the ELCC versus penetration characteristic of seven historical years, and how those characteristics, from multiple years, were merged to set an ongoing wind capacity credit percent.

The end of a second quarter is the convention used to set the capacity going into the next planning year. The penetration level at the end of the second quarter 2011 was 9.7 %. Specifically as a percentage, the 2011 penetration level is the second quarter 9,996 MW in column-4 of Table 1 divided by the 102,804 MW peak load in column-1. The vertical line in Fig. 5 illustrates where the most recent historical 9.7 % penetration level intersects each year's ELCC characteristic curve. The average of these seven intersect values is the 14.7 % system-wide ELCC assigned for the upcoming planning year 2012.

The ELCC characteristic of each year can be represented by a trend-line equation that has an R^2 coefficient of no less than 0.9996. This is the basis for achieving accuracy with sparse or few years of data. Alternative attempts to directly find a composite suitable single-trend-line curve to represent the aggregate 28 ELCC characteristic points of all 7 years met with poor R^2 coefficients in the range of 0.04 to 0.11. Figure 6 shows the resulting trend line along with the associated

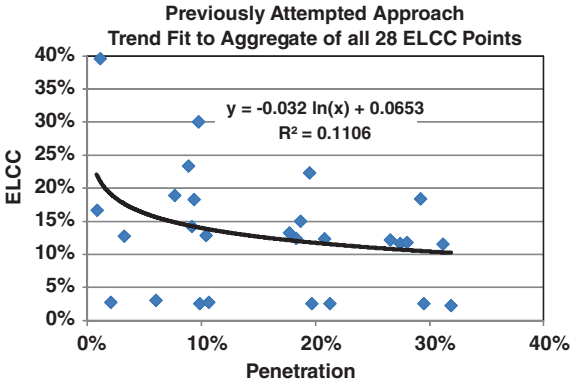

Fig. 6 Penetration trend by fitting to all 28 ELCC calculated points

equation and R^2 coefficient. While the trend line appears to represent a reasonable fit when compared to the dashed black line for the penetration trend in Fig. 5, the R^2 value of 0.1106 indicates that the process would be mathematically inferior.

3 Step-2: Wind Capacity Credit by CPnode Calculation

3.1 Deterministic Analytical Technique

Since there are many wind CPnodes throughout the MISO system (143 in 2011), a deterministic approach involving an historic period metric is used to allocate the single system-wide ELCC value of wind to all the registered wind CPnodes. While evaluation of all CPnodes captures the benefit of the geographic diversity, it is important to assign the capacity credit of wind at the individual CPnode locations, because in the MISO market, the location relates to deliverability due to possible congestion on the transmission system. Also, in a market, it is important to convey the correct incentive signal regarding where wind resources are relatively more effective. The location and relative performance is a valuable input in determining the trade-offs between constructing wind facilities in high–capacity factor locations, which in the case of the MISO are located in more remote locations far from load centers, and requiring more transmission investment versus locating wind-generating facilities at less effective wind resource locations that may require less transmission build-out. Figure 7 illustrates that the most economical solution in the MISO is a combination of both remote and local wind resources.

The system-wide wind ELCC value of 14.7 % times the 2011 installed registered wind capacity of 9,996 MW results in 1,469 MW of system-wide capacity. The 1,469 MW is then allocated to the 143 different CPnodes in the MISO system. The historic output has been tracked for each wind CPnode over the top 8 daily peak hours for each year 2005–2011. The average capacity factor for each

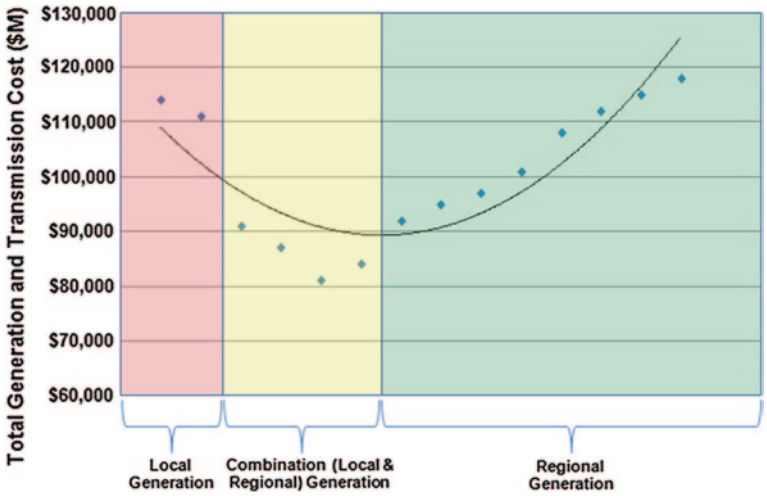

Fig. 7 Conceptual wind generation siting cost *curve*

CPnode during all 56 (8 hours × 7 years) historical daily peak hours is called the "$\text{PKmetric}_{\text{CPNode}}$" for that CPnode. The capacity factor over those 56 h and the installed capacity at each CPnode are the basis for allocating the 1,469 MW of capacity to the 143 CPnodes. MISO has developed business practice rules for the handling of new wind CPnodes that do not have historic output data and for CPnodes with less than 7 years of data.

Tracking the top 8 daily peak hours in a year is sufficient to capture the peak load times that contribute to the annual LOLE of 0.1 day/year. For example, in the LOLE run for year 2011, all of the 0.1 day/year LOLE occurred in the month of July, but only 4 of the top 8 daily peaks occurred in the month of July. Therefore, no more than 4 of the top daily peaks contributed to the LOLE. Other years have LOLE contributions due to more than 4 days; however, 8 days was found sufficient to capture the correlation between wind output and peak load times in all cases. If many more years of historical data were available, one could simply utilize the single peak hour from each year as the basis for determining the $\text{PKmetric}_{\text{CPNode}}$ over multiple years.

3.2 Wind CPnode Equations

Registered maximum (RMax) is the MISO market term for the installed capacity of a resource. The relationship of the wind capacity rating to a CPnode's installed capacity value and capacity credit percent is expressed as follows:

$$(\text{Wind Capacity Rating})_{\text{CPnode } n} = \text{RMax}_{\text{CPnode } n} \times (\text{Capacity Credit \%})_{\text{CPnode } n} \tag{1}$$

where $\text{RMax}_{\text{CPNode } n}$ = registered maximum installed capacity of the wind facility at the CPnode n. The rightmost term in (1), the (capacity credit %)$_{\text{CPNode } n}$ can be replaced by the expression (2):

$$\text{K} \times (\text{PKmetric}_{\text{CPnode } n}\%) \tag{2}$$

where "K" for the year 2011 was found by obtaining the PKmetric at each CPnode over the 7-year period and solving expression (3):

$$\text{K} = \frac{\text{ELCC}}{\sum_{1}^{143} \text{RMax}_{\text{CPnode } n} \times \text{PKmetric}_{\text{CPnode } n}} \tag{3}$$

This results in the sum of the MW ratings calculated for the CPnodes equal to the system-wide ELCC 1,479 MW. The values in (3) are

$$\text{ELCC} = 1,469\,\text{MW}$$

$$\sum \text{RMax}_{\text{CPnode } n} \times \text{PKmetric}_{\text{CPnode } n} = 1{,}803\,\text{MW}$$

$$\text{Therefore, K} = 0.8148 = 1,469/1,803.$$

3.3 Wind CPnode Capacity Credit Results and Examples

The individual PKmetric's$_{\text{CPNode}}$ of the CPnodes ranged from zero to 39.9 %. The individual capacity credit percent for CPnodes therefore ranged from zero to 32.5 %, by applying expression (2).

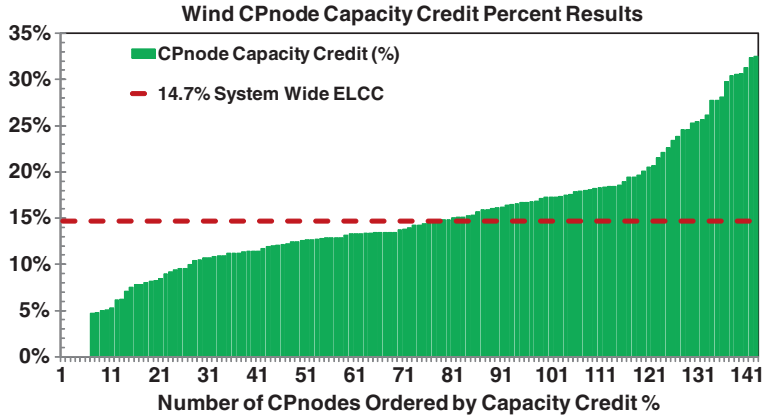

Fig. 8 Allocation of 14.7 % capacity credit over 143 CPnodes

Example (1): For the best-performing CPnode through 2011 data, the 39.89 % PKmetric drives the capacity credit equal to 32.5 % = 39.9 % × 0.8148 and therefore 32.5 % times that CPnode's RMax would equal the unforced capacity (UCAP) rating for the best-performing CPnode.

Example (2): For the CPnode nearest the nominal 14.7 % capacity credit through 2011 data, the 18.2 % PKmetric drives the capacity credit equal to 14.8 % = 18.2 % × 0.8148 and therefore 14.8 % times that CPnode's RMax would equal the UCAP rating for that CPnode.

Figure 8 shows how the system-wide 14.7 % ELCC value compares with the individual capacity credit percentages for the 143 CPnodes sorted in ascending order. The UCAP rating for each CPnode would equal the installed RMax capacity of the CPNode times the CPnode's capacity credit percent.

4 Conclusions

The MISO capacity credit method uses actual historical power output as a basis for setting the capacity rating of wind resources. While MISO is currently limited to applying 7 years of historical power outputs from the wind resources, by applying the developed ELCC and merging techniques, the results are converging and are reflective as if one had more years of historical data available for the process. Figure 9 illustrates the method over a range of limited data results. The leftmost point on the x-axis is the system-wide result while utilizing only 1 year of data; the second point represents having 2 years of historical data available for the process. Progressively, the seventh point illustrates where MISO is currently at with seven years of data, and a projection sensitive to penetration is shown. As data from each new successive year become available, the subsequent capacity credit for successive years is expected to stabilize and be more exclusively driven by penetration.

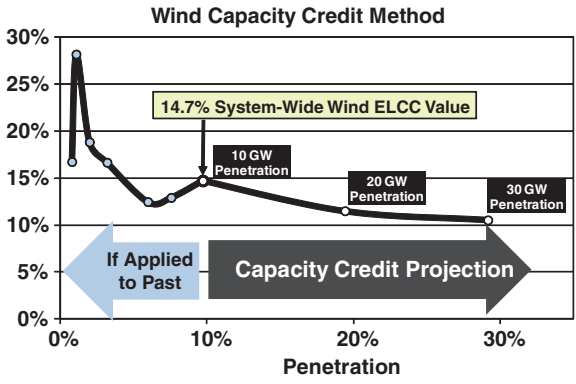

Fig. 9 Applying capacity credit method starting with 2005 data

While the process discussed here represents a consistent and repeatable way to calculate the MISO market needs, MISO will continue to track and consider adjustments that may be required to deal with further aspects of common-mode failure of wind generation. The MISO believes that the capacity credit for wind will be near 10 % as the system approaches 25,000–30,000 MW of installed wind generation.

References

1. Garver LL (1966) Effective load carrying capability of generating units. IEEE Trans Power Apparatus Syst PAS-85(8):910–919
2. Keane A, Milligan M, Dent CJ, Hasche B, D'Annunzio C, Dragoon K, Holttinen H, Samaan N, Soder L, O'Malley M (2011) Capacity value of wind power. IEEE Trans Power Syst 26(2):564–572

Wind Power Scenario Tree Tool: Development and Methodology

Colm Lowery and Mark O'Malley

1 Introduction

The nature of power system operation is changing worldwide. Plans are in place to increase the proportion of demand met through wind power throughout the European continent [1], Ireland [2], the Great Britain [3] and the United States [4]. In Europe, for example, this change is driven by EU policy which aims to reduce CO_2 emissions and dependency on imported fuel. Primarily, this policy encourages the growth of renewable generation including wind power [5]. It is expected that this increase in renewable generation will displace conventional generation—causing a decrease in system operation costs as less conventional fuel is consumed in meeting system demand.

However, displacing conventional generation with non-synchronous renewable generation is creating new system operation challenges. Wind is by its nature variable. It is of limited predictability, and control of the resource is limited to curtailment. As wind cannot be forecast with perfect accuracy, additional reserve must be carried and conventional units must be operated in a more flexible, adaptable manner—leading to reduced efficiency through partial loading and an increase in the number of start-ups required for conventional power plants [6]. While the effects of this uncertainty can be disregarded for low wind penetrations, with high wind penetrations, the uncertainty associated with wind forecasting error will impact upon the reliability, efficiency and economic performance of unit commitment [7, 8].

Ideally, the system will be scheduled in such a way that the expected value of the operating costs is minimized given the uncertainty of wind generation and the

C. Lowery (✉) · M. O'Malley
Electricity Research Centre, University College Dublin, Dublin 4, Ireland
e-mail: Colm.Lowery@ucdconnect.ie

M. O'Malley
e-mail: mark.omalley@ucd.ie

R. Billinton et al. (eds.), *Reliability and Risk Evaluation of Wind Integrated Power Systems*, Reliable and Sustainable Electric Power and Energy Systems Management,
DOI: 10.1007/978-81-322-0987-4_2, © Springer India 2013

constraints on the system. This can be approximated by treating unit commitment as a stochastic problem where the distribution of possible wind generation is represented by a number of probability-weighed time series scenarios. In many forms of stochastic unit commitment, the operational cost of a unit commitment is evaluated for each of these scenario tree branches, similar to deterministic treatments of wind generation [9]. However, it is the expected cost of the entire scenario tree which is the objective to be minimized for the unit commitment.

While stochastic treatments of wind uncertainty have previously been investigated, the contributions to solution quality of specific statistical properties of forecast error have not been considered. These properties are available from analysis of the error between historical forecasts and realized data. In ideal circumstances, a system operator will have the necessary information prioritized in the form best suited for decision making. In practice, and in many prior studies, quantification of forecast error has often been limited to simple statistical properties such as variance and mean error and an assumed Gaussian distribution [10]. While traditional measures of forecast performance such as mean average error or root-mean-square error do not distinguish between distributions with the same mean and variance, more sophisticated methods of analysis of information content such as Renyi entropies indicate that significant information is missed by these simplifications [11, 12].

The WILMAR project developed a stochastic unit commitment scheduling model to analyse the integration of wind power in a large liberalized electricity system [13]. The WILMAR scheduling model uses a rolling sequence of scenario tree forecasts to model the impact of error information (see Fig. 1) This model has previously been used to study the benefits of stochastic treatment of wind uncertainty over deterministic treatments as well as the impact of accounting for more of the wind uncertainty by increasing the frequency of rolling planning [8].

This chapter presents the methodology adopted for use in a Scenario Tree Tool (STT) constructed to allow for closer examination of the effect of forecast error assumptions and properties when combined with a suitable unit commitment model such as WILMAR [14]. Due to the requirement for direct control of the statistical properties in several areas of interest, ARMA series/scenario reduction methodologies were not considered suitable for this tool. A new STT was designed using a methodology based on a moment-matching technique where each time period, within a tree, has a defined variance, skewness and kurtosis. These statistics together with the autocorrelations of the scenario determine the values of the scenarios at that time period. While alternative heuristic methodologies have been proposed for deriving a scenario tree that matches specific moments [15], the methodology used in this tool is based on a nonlinear optimization moment-matching method [16, 17].

Section 2 briefly describes the sections of the STT and details the structure of the programme.

Section 3 describes the methodologies related to the STT. It details the methodologies (moment matching and scenario grouping) used to generate wind and load scenarios within the current STT as well as the method used to account for diurnal/seasonal variations. In addition to describing the new methodology, it also briefly describes the preceding scenario reduction/ARMA series method which was used by older versions of the STT.

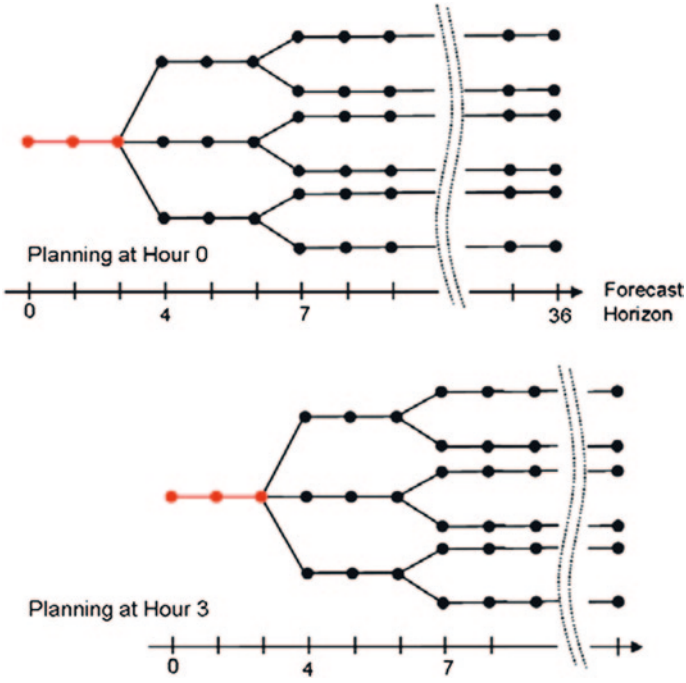

Fig. 1 Illustration of rolling planning scenario trees

Section 4 covers the methodologies used for calculating the replacement reserve, the amount of reserve required to be available after a short delay, from these trees as well as detailing, for completeness, the assumptions about spinning reserve, the amount of reserve required to be available from online generators at a given time and the semi-Markov chain methodology used to simulate forced outages as required by the replacement reserve methodology.

Section 5 displays example graphical outputs from the preceding sections.

A conclusion is presented in Sect. 6.

2 Structure of the Scenario Tree Tool

The overall structure of the STT can be seen in Fig. 2. Each functional box represents a separate module or submodule in the STT, which will be covered in the subsequent sections. Entries on the same level represent parallel operations which can be run simultaneously. The detail of these modules is as follows:

- Initial Inputs: this module loads and prepares data from input libraries.
- Scenario Generation: this module utilizes forecast error information to generate wind and load power scenarios and branching structures. This module contains multiple submodules detailed in Sect. 3 and Fig. 3.

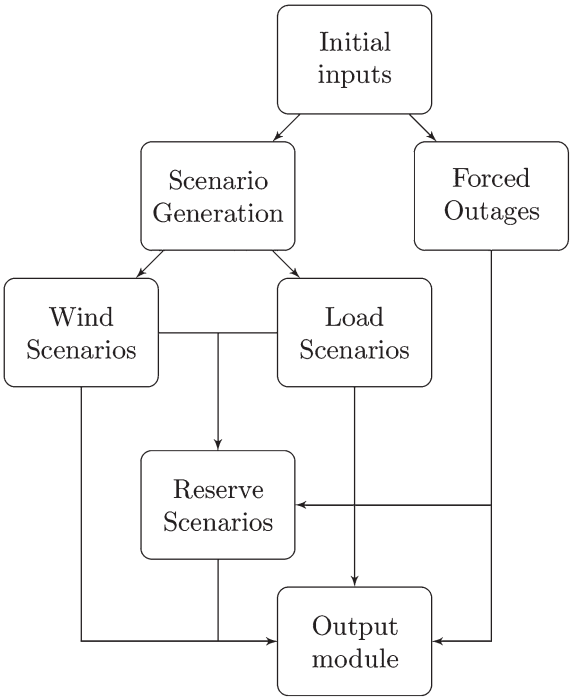

Fig. 2 Structure of the scenario tree tool

- Forced Outages: this module utilizes semi-Markov Chains to calculate a random sequence of plant availability (Sect. 4.2).
- Reserve Scenarios: this module uses the outputs of the scenario generation and forced outage modules, along with plant capacity information to calculate replacement and spinning reserves (Sect. 4.1).
- Output Module: this module collates and converts the information from the other module into input files for the WILMAR model.

3 Development and Methodology of the Scenario Tree Tool

In power plant scheduling, decisions must be made on both information known with certainty and uncertainty which must be forecasted. In stochastic unit commitments, wind forecasts, demand forecasts and their forecast error can be accounted for by representative branching trees consisting of probability-weighed scenarios for available wind generation (Fig. 1). The number of scenarios has been restricted to minimize dimensionality in the unit commitment solution while retaining accuracy in the specified statistical information. For computational reasons, the first stage of these trees is assumed to be known with perfect certainty.

Each scenario in the tree consists of an assigned probability and two time series values—one for load and one for wind. Each of these time series can be

represented as a forecast time series, common to all scenarios within the tree, and an error time series which, together with the error time series of the other scenarios, represents the error distribution of the forecast.

In the All-Island Grid Study (AIGS), these scenario trees were generated by an STT using a methodology based on scenario reduction in ARMA series [18]. Specifically, the wind forecast error was based on the assumption of a Gaussian distribution of wind speed error with standard deviation dependent upon the forecast horizon [19, 20].

In brief, scenario reduction aims to take an initially large number of scenarios and then remove scenarios until only the desired number remains while maintaining as close a representation of the original distribution as possible according to the methodology given here:

1. Generate 1,000 wind speed scenarios, with a length of 36 periods, using ARMA (1,1) series of equal probability [21].
2. Add these scenarios to the wind speed forecast.
3. Convert these wind speed scenarios to wind power forecasts using a normalized aggregated multi-turbine curve.
4. Scale these scenarios to the required level taking account of the spacial correlation of the wind power forecast [22].
5. Calculate the Kantorovich distance between each pair of scenarios [23, 24].
6. Merge the probability of the scenarios with the lowest Kantorovich distance and delete the scenario of smaller probability.
7. Repeat steps 2 and 3 until the desired number of scenarios is achieved.
8. To create the branching scenario tree, this process is repeated omitting the hours in the third stage to reduce the scenarios further.

Due to the requirement for direct control of the statistical properties in several areas of interest, ARMA series/scenario reduction methodologies were not considered suitable for this tool. A new STT was designed using a methodology based on a moment-matching technique where each time period, within a tree, has a defined variance, skewness and kurtosis.

These statistics together with the autocorrelations of the scenario determine the values of the scenarios at that time period. While alternative heuristic methodologies have been proposed for deriving a scenario tree that matches specific moments [15], the methodology used in this tool is based on a nonlinear optimization moment-matching method [16, 17].

The overall structure of scenario generation can be seen in Fig. 3 where W is wind scenarios, L is load scenarios and P is the probability of each scenario. The steps in brief are as follows:

1. Set initial parameters and begin from the final stage of the tree.
2. Generate the scenarios for the current stage of the tree using moment matching (II.A).
3. Calculate the degree of similarity between each subset (size determined by the ratio of branching) in terms of Kantorovich distance and autocorrelations (II.B).

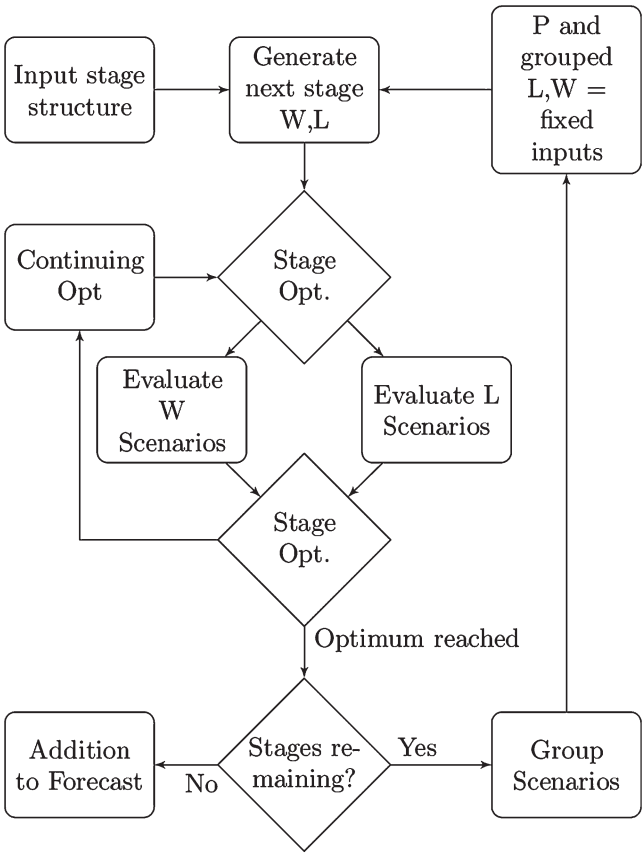

Fig. 3 Structure of the scenario generation

4. Generate an optimal branching structure between the current stage and its predecessor using the subsets which minimize the disparity between merging scenario branches.
5. Repeat the preceding steps for the earlier stages using the branching structure and scenario values as further inputs into the objective function (1).

3.1 Moment Matching

For each stage in the tree, a nonlinear optimization was used to produce a matrix of scenarios consisting of wind, demand and probability values matching the specified statistics as closely as possible. In addition, stages which have already been

determined are used to provide additional autocorrelation information for subsequent stages.

In each stage, the optimization acts to minimize the following objective function (1) while meeting the constraints (4, 5, 6) given the stages and branch connections that have already been defined:

$$\sum_{n=1}^{S} W_n \left(f_n\left(x_t, P_t\right) - S_n\right)^2 \tag{1}$$

where S is the set of statistical properties under consideration. W_n is the optimization weight assigned to the statistical property. S_n are the components of the set S (mean, variance, kurtosis, skewness, the first four autocorrelations). $x_{t,j}$ is the set of values for scenario j during the given time step t. P_t are the probabilities assigned to the scenarios in time step t.

The individual components $(f_n(x))$ of the objective function (1) are calculated using the following formulas for the moment (2) and autocorrelation (3):

$$M_l = \sum_{j=1}^{s} P_j \left(x_{j,t} - \mu_t\right)^l \tag{2}$$

$$AC_{\tau,j} = \sum_{j=1}^{N-\tau} \frac{(Y_i - \mu_j)(Y_{i+\tau} - \mu_j)}{\sum_{j=1}^{N} (Y_i - \mu_j)^2} \tag{3}$$

where M_l is the lth moment at time t. $AC_{\tau,j}$ is the autocorrelation at time lag τ for scenario j. μ_t is the mean of the scenario set at time t. μ_k is the mean of the scenario k, and τ the time lag of the autocorrelation. k is the index of a given scenario. jk are the indices of the scenarios which branch from scenario k.

In order to ensure probability remains consistent across scenarios and time periods, the constraints upon the objective function are as follows:

$$\sum P_{jk,t} = P_{k,t-1} \tag{4}$$

$$\sum P_t = 1 \tag{5}$$

$$P_{jk,t} > 0 \tag{6}$$

3.2 Scenario Grouping

The scenario stages produced by moment matching are divided into groupings according to the branching of the scenario tree and the similarity of their autocorrelations. This is done to ensure that when joined to the relevant scenario in the preceding stage, the autocorrelation of each branch of the tree is consistent across the stage boundaries. This prevents the creation of suboptimal scenario branching as a result of joining two disparate scenarios. Scenario ordering is determined by finding the ordering which minimizes the difference in autocorrelation and the Euclidean distance between the short term (stage II) values of each scenario.

$$D(j1, j2) = E_D(j1, j2) + AC_D(j1, j2) \tag{7}$$

$$E_D(j1, j2) = \sum_{t=1}^{T} \frac{\left(x_{j_1,t} - x_{l,t}\right)^2}{\left(x_{j_2,t}\right)^2} \tag{8}$$

$$AC_D(j1, j2) = \sum_{z=1}^{\tau} \frac{\left(AC_{\tau,j_1} - AC_{\tau,j_2}\right)^2}{\left(AC_{\tau,j_1}\right)^2} \tag{9}$$

where $D\,(j1, j2)$ is the measure of similarity, $E_D\,(j1, j2)$ is the Euclidean distance and $AC_D\,(j1, j2)$ is the difference in autocorrelation.

These groupings and scenarios are then used in the optimization of any subsequent moment-matching steps to provide consistent autocorrelations for each scenario throughout the tree stages.

While the WILMAR model uses tree structures which branch evenly from each node at a time point and never merge, the scenario tree methodology allows for uneven branching and hence can generate topologies which have different scenario resolutions at different time horizons and in different regions of the tree.

3.3 Diurnal and Seasonal Variation

The word "data" is plural, not singular. Wind and load forecasts exhibit different behaviour at different times of the year and day. In order to account for seasonal and diurnal variation, the error trees can be altered before being added to the individual forecasts by the addition of a mean error adjustment time series, $\mu(j)$ to each scenario and the use of a scaling constant ε.

The values of $\mu(j)$ and ε are chosen through fitting the general forecast error to the forecast error of each seasonal period and time period within the day. This is achieved by subdividing the known forecast information by seasonal period, calculating the same metrics as the main data and deriving the necessary adjustments from the proportional difference in standard deviation and mean between the general case and the specific case. This process is repeated for the starting hour of the forecast to derive the adjustment for time of day.

4 Replacement Reserve and Forced Outages

4.1 Replacement Reserve

Replacement reserve is estimated for each individual scenario branch of wind and demand within the tree and is calculated using a similar methodology to that presented in the AIGS [18]. However, the AIGS used methods assuming prior scenario reduction, which calculate reserve from the 90th percentile of the unreduced set of scenarios used to generate the scenario tree. This method can therefore not be used with the new STT as the new methodology uses moment matching and does not generate the large initial number of scenarios required by the AIGS methodology. Instead, the reserve is calculated from the 90th percentile of a distribution based on the variation in wind and demand error represented by those scenarios (10) according to the following method:

The n scenario combinations are mapped onto the wind scenario s from which they came, and the reserve is taken to be the 90th percentile of the difference between the reference power balance P_{Ref} (11) and the forecasted power balance, P, for the scenario combinations n at each wind scenario s (12):

$$\Delta P\,(t_0, f, s) = P_{Ref}(t) - P\,(t_0, f, s) \tag{10}$$

The power balance P_{Ref} at time t is calculated for the realized values of wind W_R, load L_R and available conventional capacity C:

$$P_{Ref}(t) = \sum_{g \varepsilon G} C(g) + W_R(t) - L_R(t) \tag{11}$$

The power balance P of each combination of wind and load scenarios n is calculated for the scenario wind W_E and load L_E as well as for the forced outages. Time t is calculated for the realized values of wind W_R, load and available conventional capacity C:

$$P\,(r, t_0, f, n) = \sum_{g \varepsilon G} C(g) Y(g, t) \; + \; W_E\,(t_0, f, n) - L_E\,(t_0, f, n) \tag{12}$$

In addition to this, required spinning reserve is estimated from the largest infeed to the system and forecasted wind using the methodology presented in the AIGS [10].

4.2 Forced Outages

While no new changes have been made to this methodology, it is included here for completeness as it is necessary for the reserve calculations as well as being a required input for the unit commitments it is currently in use with. Within the model, distinction is drawn between two types of outage (forced outages and

scheduled outages). As scheduled outages are defined by the user and by the test system, the STT simulates forced outages from the information provided about the test system including the information provided on scheduled outages.

The time series of forced outages for each conventional unit are simulated using semi-Markov chains [25], where the failure and repair rates are expressed by the mean time to failure and the mean time to repair. The methodology used in the STT is derived from that presented in the AIGS [18] and is detailed in brief below:

$$P_{\text{Available}} = \frac{\text{MTTF}}{\text{MTTR} + \text{MTTF}} \tag{13}$$

$P_{\text{Available}}$ is the probability that a plant will be available derived from the mean time to failure (MTTF) and mean time to repair (MTTR) for each plant.

$$P_{\text{Unavailable}} = \frac{\text{MTTR}}{\text{MTTR} + \text{MTTF}} = \text{FOR} \tag{14}$$

$P_{\text{Unavailable}}$ is the probability that a plant will be unavailable and is equivalent to the forced outage rate (FOR.)

$$\text{FOR} = \frac{t_{fo}}{t} \tag{15}$$

t_{fo} is the total number of hours the plant is unavailable, and is the total time period.

Figure 4 shows the structure of the forced outage algorithm. The initial state of the unit is determined by drawing a random number from a uniform distribution and comparing it with the full outage percentage (FOP) calculated according to Eq. (16).

$$\text{FOP} = \frac{\text{FOR}}{\text{MTTR}} \tag{16}$$

The result of this determines whether or not the model will draw a time to repair (TTR) or a time to failure ((TTF)) from the Weibull distribution.

$$f(t, \mu, k) = \frac{k}{\mu}\left(\frac{t}{\mu}\right)^{k-1} \cdot e^{-\left(\frac{t}{\mu}\right)^{k}} \tag{17}$$

where the shape factor $k = 1$ is used for the TTF (as time to failure is captured by an exponential distribution), $k = 5$ is used for the TTR (time to failure represented by a bell-shaped distribution) and μ is calculated from MTTF and MTTR, respectively.

In the event that a forced outage extends into the period of a scheduled outage, the scheduled outage is run for its full time period as the scheduled repairs cannot be assumed to be equivalent in nature to those forced by the unscheduled outage.

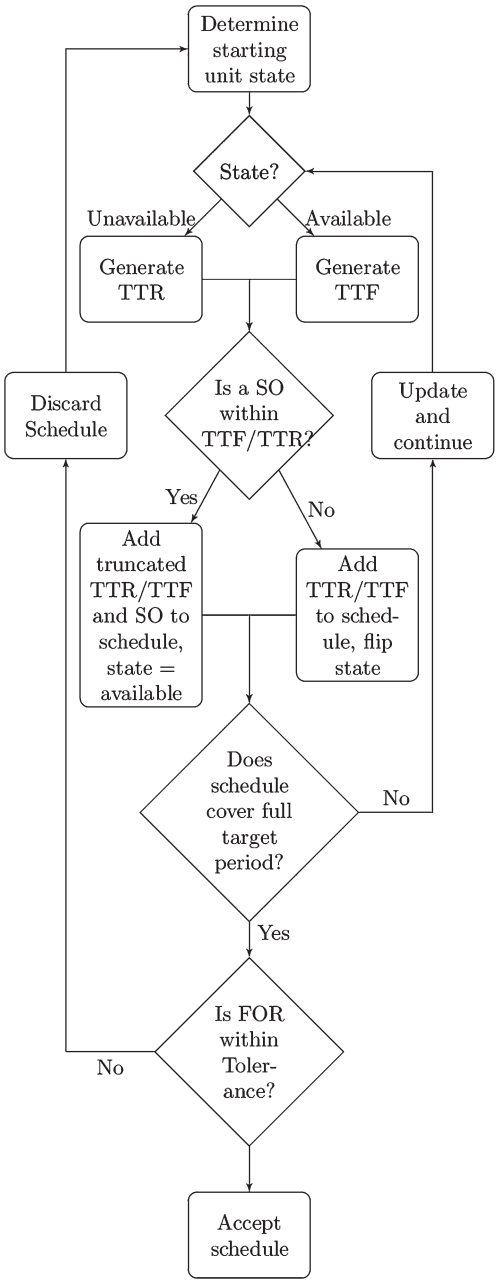

Fig. 4 Algorithm for forced outage calculation

5 Results

This section presents example scenario tree outputs from the STT which demonstrate the impact of changes in forecast error statistics such as kurtosis, skewness and autocorrelation between time periods.

Figure 5 gives an example of the points contained in a statistically accurate scenario tree overlayed upon the realized and forecasted values (thick dashed line and line, respectively). In addition, a single scenario is shown (thin line with squared points) to demonstrate the impact of including autocorrelation in the optimization.

Figure 6 presents the same tree with inverted skewness. While it is similar in shape to Fig. 5, its shape appears transposed around the forecast as its skewness

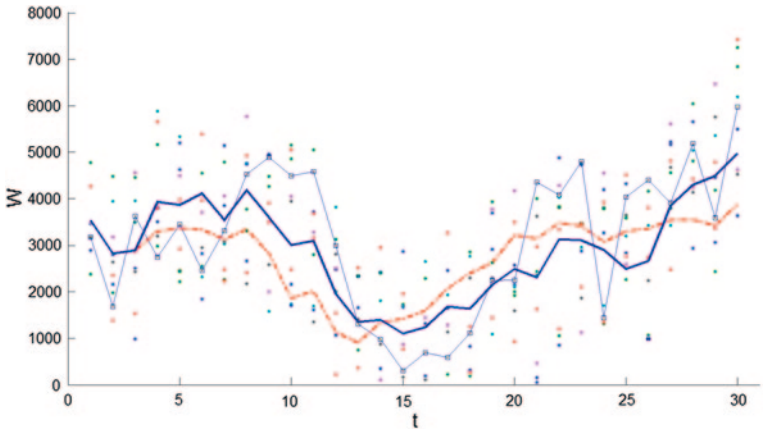

Fig. 5 Example autocorrelated scenario, *thin line*, imposed onto scenario tree points. Deterministic forecast is shown by the *thick line*, and realized value is shown by the *thick dashed line*

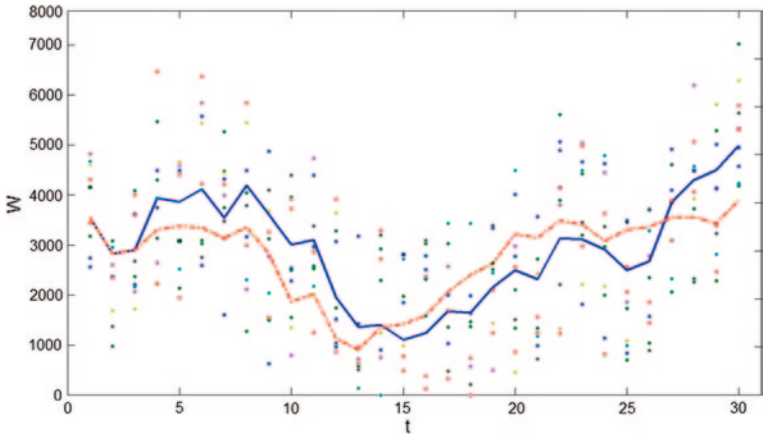

Fig. 6 Example of a figure caption. Scenario tree with inverted skewness. Note the tree is skewed to the opposite side of the deterministic forecast

is of the opposite sign. The scenario tree constructed in this fashion assumes the opposite trend in terms of overestimating or underestimating the forecast.

Figure 7 presents a tree constructed from identical information without autocorrelation considered. Due to this, the included scenario in this version contains considerably more sharp changes than the reality entails. As a result, despite the statistics of each individual time period being correct, the grouped scenarios do not present useful information due to prediction of frequent unrealistic ramp events.

Figure 8 demonstrates the effect of increasing kurtosis—this tree clusters close to the forecast and contains an increased number of extreme values.

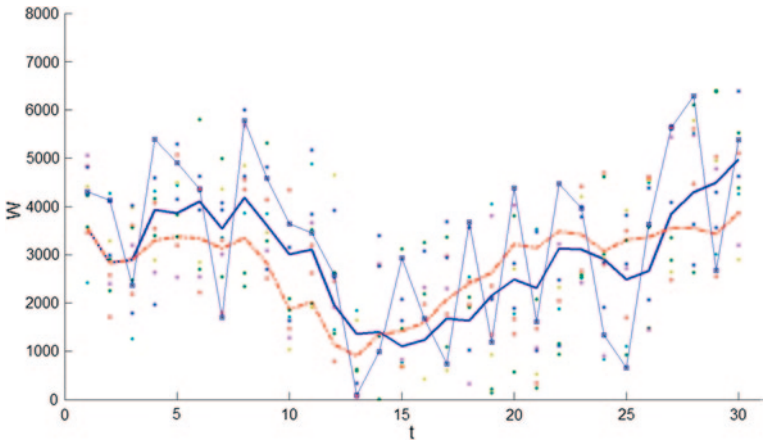

Fig. 7 Example unautocorrelated scenario, *thin line*, imposed onto scenario tree points. Deterministic forecast is shown by the *thick line*, and realized value is shown by the *thick dashed line*

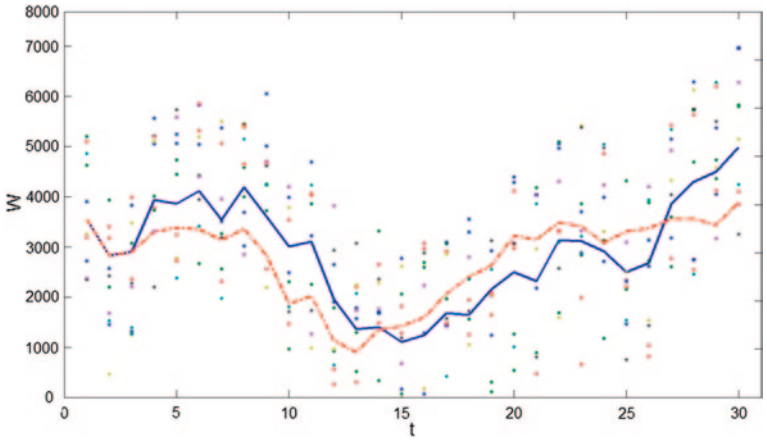

Fig. 8 Scenario tree with *increased kurtosis*. Note the increase in points clustered at the mean and at the extremes

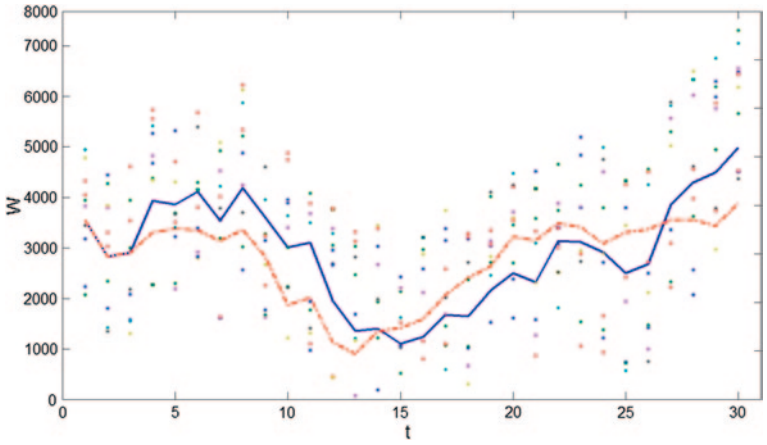

Fig. 9 Scenario tree with *decreased kurtosis*. Note the reduction in clustering and the more even spread of points

In contrast, Fig. 9 demonstrates the effect of reducing kurtosis—a tree which is comparatively evenly spread throughout the distribution without many extreme values or much clustering around the forecast.

6 Conclusion

This chapter presented the methodology of the WILMAR STT based on moment matching. Example outputs demonstrating some of the converted to a graphical format were also included. This tool is under development to examine the impact of wind forecast error statistics on unit commitment for high wind penetration test systems.

Acknowledgments This work was conducted in the Electricity Research Centre, University College Dublin, Ireland, which is supported by the Commission for Energy Regulation, Bord Gáis Energy, Bord na Móna Energy, Cylon Controls, EirGrid, Electric Ireland, EPRI, ESB International, ESB Networks, Gaelectric, Intel, SSE Renewables, UTRC and Viridian Power and Energy.

This publication has emanated from research conducted with the financial support of Science Foundation Ireland under grant number 06/CP/E005.

References

1. Pure power: wind energy targets for 2020 and 2030, EWEA, (2010) Available: http://www.ewea.org/
2. Delivering a sustainable energy future for Ireland, Government White Paper (2007) Available: http://www.dcmnr.gov.ie

3. Meeting the energy challenge, U.K. Government White Paper (2007) Available: http://www.dti.gov.co.uk
4. Second Quarter 2011 Market Report, AWEA. Available: http://www.awea.org/
5. Directive 2009/72/EC of the European Parliament. Available: http://eur-lex.europa.eu
6. Troy N, Denny E, O'Malley M (2010) Base-load cycling on a system with significant wind penetration. IEEE Trans Power Syst 25(2):1088–1097
7. Marti I et al. (2006) Evaluation of advanced wind power forecasting model results of the anemos project. Available: http://anemos.cma.fr. pp 1088–1097 (2010)
8. Tuohy A, Meibom P, Denny E, O'Malley M (2009) Unit commitment for systems with significant wind penetration. IEEE Trans Power Syst 24(2):592–601
9. Takriti S, Birge J, Long E (1996) A stochastic model for the unit commitment problem. IEEE Trans Power Syst 11(3):1497–1508
10. Doherty R, O'Malley M (2005) A new approach to quantify reserve demand in systems with significant installed wind capacity. IEEE Trans Power Syst 20:587–595
11. Hodge B, Orwig K, Milligan M (2012) Examining information entropy approaches as wind power forecasting performance metrics. In: Proceedings of PMAPS Istanbul
12. Hodge B, Milligan M Wind Power Forecasting Error Distributions over Multiple Timescales (2011) NREL Report No. CP-5500-50614. Available: http://www.nrel.gov/
13. Wind Power Integration in Liberalised Electricity Markets (WILMAR) Project. Available: http://www.wilmar.risoe.dk
14. Lowery C, O'Malley M (2012) Impact of wind forecast error statistics upon unit commitment. IEEE Trans Sust Energy 3(4):760–768
15. Hoyland K, Kaut M, Wallace SW (2003) A heuristic for moment-matching scenario generation. Comput Appl Optim 24:169–185
16. Hoyland K, Wallace SW (2001) Generating scenario trees for multistage decision problems. Manag Sci 47(2):295–307
17. Hasche B (2008) Scenario tree generation for an electricity market model. Available: http://www.netmod.org/
18. Meibom P, Barth R, Brand H, Swider D, Ravn H, Weber C (2007) All Island Renewable Grid Study Work stream 2b—Wind Variability Management Studies. Available: http://www.dcmnr.gov.ie
19. Lange M, Focken U (2006) Physical approach to short-term wind power prediction. Springer, Berlin
20. Lange M (2005) On the uncertainty of wind power predictions: analysis of the forecast accuracy and statistical distribution of errors. J Sol Energy Eng 127:177–184
21. Barth R, Soder L, Weber C, Brand H, Swider D (2006) Methodology of the Scenario Tree Tool. Available: http://www.wilmar.risoe.dk
22. Söder L (2004) Simulation of wind speed forecast errors for operation planning of multi-area power systems. In: Proceedings of 8th international conference on probabilistic methods applied to power systems, Ames
23. Dupacova J, Growe-Kuska N, Romisch W (2003) Scenario reduction in stochastic programming: an approach using probability metrics. Math Program Ser. A 95, vol 3, pp 493–511
24. Heitsch H, Roemisch W (2003) Scenario reduction algorithms in stochastic programming. Comput Appl Optim 24(2–3):187–206
25. Valenzuela J, Mazumdar M (2001) Monte-Carlo computation of power generation production costs under operating constraints. IEEE Trans Power Syst 16:671–677

Probabilistic Ramp Detection and Forecasting for Wind Power Prediction

C. Ferreira, J. Gama, V. Miranda and A. Botterud

1 Introduction

This chapter proposes a new way to detect and represent the probability of ramping events in short-term wind power forecasting. Ramping is one notable characteristic in a time series associated with a drastic change in value in a set of consecutive time steps. Two properties of a ramp event forecast, that is, slope and phase error, are important from the point of view of the system operator (SO): they have important implications in the decisions associated with unit commitment or generation scheduling, especially if there is thermal generation dominance in the power system. Unit commitment decisions, generally taken some 12–48 h in advance, must prepare the generation schedule in order to smoothly accommodate forecasted drastic changes in wind power availability. A comprehensive analysis of ramp modeling and prediction may be found in Ref. [1]. Some important works in this area are mentioned in the following paragraphs.

C. Ferreira (✉)
LIAAD/INESC TEC and ISEP/IPP, Polytechnic Institute of Porto, Porto, Portugal
e-mail: cgf@isep.ipp.pt

J. Gama
LIAAD/INESC TEC and FEP, University of Porto, Porto, Portugal
e-mail: jgama@liaad.up.pt

V. Miranda
INESC TEC (Formerly INESC Porto), and FEUP, University of Porto, Porto, Portugal
e-mail: vmiranda@inescporto.pt

A. Botterud
Argonne National Laboratory, Decision and Information Sciences Division,
Argonne, IL, USA
e-mail: abotterud@anl.gov

R. Billinton et al. (eds.), *Reliability and Risk Evaluation of Wind Integrated Power Systems*, Reliable and Sustainable Electric Power and Energy Systems Management,
DOI: 10.1007/978-81-322-0987-4_3, © Springer India 2013

The authors of Refs. [2, 3] define *direction, duration* and *magnitude* for ramps in two basic types: upward (or *ramp-ups*) and downward (or *ramp-downs*), related with meteorological phenomena [4]. To consider a ramp event, the minimum duration is assumed in Ref. [3] to be of 1 h; however, in Ref. [5], one finds events in intervals of 5–60 min. The magnitude of a ramp is given as a percentage of the wind farm nominal power.

In Ref. [2], the authors define a ramp event to be a power output change higher than 50 % of the wind farm nominal power, occurring over a period of 4 h or less. They define two metrics: forecast accuracy and ramp capture—these metrics correspond to precision and recall defined in Sect. 5 below.

In Ref. [6], the authors combine feature selection and five data-mining algorithms to predict power ramp rates 10–60 min ahead. They use the *mean standard deviation*, *maximum* and *minimum* wind speed over all turbines and also the measured wind farm *power* and *power ramp rate*. Considering that the huge number of predictors can degrade the performance, *a boosting tree* algorithm was adopted to select the most interesting features, which are used to train five data-mining algorithms: multilayer perceptron, support vector machines, random forest, classification and regression trees and pace regression.

In Ref. [7], the authors present the development, by WEPROG, of a special purpose tool that provides real-time uncertainty weather forecasts for wind ramp prediction. The tool uses data from their multi-scheme ensemble prediction system (MSEPS), taking 75 forecasts to represent uncertainty for several weather parameters. An extreme ramp event would be a change in power of more than 80 MW over an hour.

In Ref. [8], the authors present the development, by AWS Truepower, of a model that predicts wind ramps between 0 and 6 h ahead. The system capabilities include the following: a probabilistic ramp forecast module that can predict ramp rate probabilities for different time resolutions; a hybrid deterministic probabilistic ramp event forecast that outputs deterministic values; and a confidence interval for the events satisfying the ramp event definition and also the average power production for 15 min intervals. The ramp detection methodology associates algorithms with ramp types. The system learns models for significantly different weather conditions. To access the performance of probabilistic ramp rate forecasts and to compare two forecast methodologies, the critical success index (CSI) [9] and the ranked probability skill score (RPSS) [9] were computed.

In Ref. [10], the authors identify ramps by mapping the initial wind power series into a signal that results from computing the average of time power differences. The authors propose two probabilistic forecasting methods aiming to predict wind power output using ramp information, as well as to predict ramp timing. One method uses information extracted from the translated space, ramp intensity and ramp forecast time information. A method predicting ramping translates the signal of an ensemble of wind power curves and then uses the ensemble votes to define a confidence interval for the ramp timing. The quality of results depends on the number of ensemble members predicting the interval time of ramp occurrence and the size of the time intervals.

In Ref. [11], hard constraints are added to decision-making applications: for instance, in stochastic optimization or risk assessment. In Ref. [3], a probabilistic ramp event forecasting system is presented. It was shown that by using probabilistic forecasting systems, higher economic benefits can be obtained.

The approach proposed in this chapter requires and departs from a probabilistic wind power forecasting model. This model must allow a form of representation (implicit or explicit) of a joint probability density function (pdf) for the wind power, taking as variables the wind power prediction at different time stamps within the forecasting horizon. Such a representation already includes or takes into account the possible cross-time-step dependencies. This is a designation more general than just cross-correlations, which are called autocorrelation in the context of time series, and it involves cross-relations in moments of order higher than the second order. In theory, given such a pdf, a Monte Carlo sampling process may allow the generation of scenarios, each consisting of a sequence of predictions for a number of successive time steps, in a time series fashion.

Our new model departs from a scenario generation procedure and builds a new ramp detection process and a new probabilistic assessment phase. The scenario generation model acts as a sampling mechanism in the Monte Carlo sense. Then, a counting procedure to be detailed below and within the generated sample allows the definition of probabilities for each ramp event in each hour of the forecasting horizon.

A refinement of this procedure allows one to build a histogram, for each hour, of the probability of having a ramping event above a certain magnitude: ramping becomes represented as a random variable associated with a probability distribution. This leads to the use of the results for decision making because the risk (or probability) of having a ramp exceeding a given threshold is quantified.

The robustness of the method, its capacity to avoid false alarms or missed alarms and its tuning are addressed in this chapter. We present a comparative evaluation of performance in the ROC space (i.e., receiver operating characteristic, plotting true-positive vs. false-positive rates)—from a case study using data from a wind farm in the USA [12].

2 Generating Wind Power Scenarios

The key piece of the method developed is the availability of an estimate for the probability density function (pdf) of the wind power prediction. This chapter will not discuss the methods to obtain such pdf estimate nor their validity. This pdf is taken as a multivariate function in a high-dimensional space (the number of dimensions equal to the number of time steps represented in the forecasting horizon). The probability of a ramping event of a given nature then becomes assimilated to the calculation of a special marginal distribution associated with some matching filter describing, in the multivariate space, the ramping event defined. In order to do this, a discrete representation of the pdf by wind power scenarios is necessary.

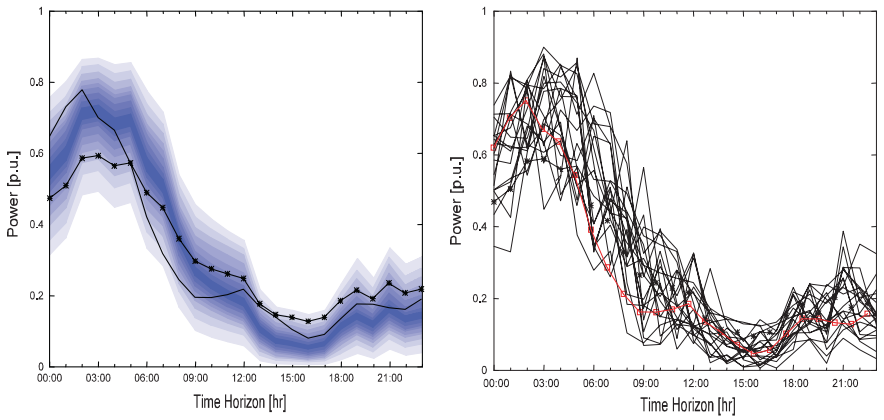

Fig. 1 Representation of wind power forecast as intervals (quantiles gathered by pairs and centered in the median), on the *left*, and scenarios of wind power generation, on the *right*

By a scenario, one understands a sequence of predicted wind power values spanning the entire prediction horizon, and by a discrete representation of the pdf one means a set of scenarios with an empirical density similar to the original pdf.

This is equivalent to some method of generating scenarios from a known pdf by using a sampling technique and turns the ramp event model into a Monte Carlo generating process.

Figure 1 shows a usual representation of the uncertainty associated with wind power in short-term 24-h-ahead prediction, based on quantiles [11], and a discrete representation. In the work reported in this chapter, a state of the art method to generate scenarios according to a Monte Carlo sampling was followed [11]. We should note that we use both historical data and weather forecasts as input to our scenario generator. Moreover, our ramp detection model is independent of the scenario generation method used.

3 Detecting Ramp Events

3.1 Defining Ramps

A *ramp* is a change in power output (from a wind farm) with large enough amplitude and over a relatively short period of time. Figure 2 illustrates this concept. Ramps may be up or down; in both cases, when not predicted, they may cause serious problems in system operation and dispatch, with high costs and additional risks incurred.

There is no consensually accepted formal definition of a ramp. The ramp concept is related with the power signal $P(t)$, a defining threshold ΔP_{ramp} and a time interval Δt. Some definitions adopted by different authors are as follows.

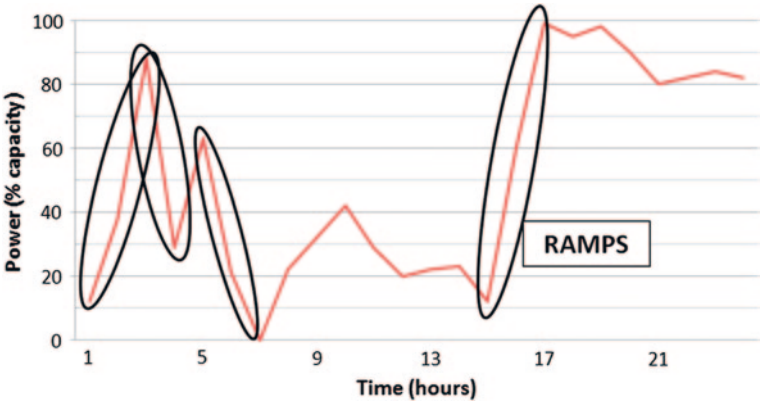

Fig. 2 Illustration of ramp events, defined as a change of at least 50 % in power in an interval of 4 h

Definition 1 Reference [5]: A ramp event is considered to occur at the beginning of an interval, if the magnitude of the increase or decrease in the power signal, at time Δt ahead of the interval, is greater than the ramping threshold value, ΔP_{ramp}:

$$|P\,(t+\Delta t) - P\,(t)| \;>\; \Delta P_{\text{ramp}} \tag{1}$$

Definition 2 Reference [5]: A ramp is considered to occur in a time interval Δt if the difference between the maximum and the minimum power output measured in that interval is greater than the threshold value, ΔP_{ramp}:

$$\max\left(P\,[t,\, t+\Delta t]\right) - \min\left(P\,[t,\, t+\Delta t]\right) \;>\; \Delta P_{\text{ramp}} \tag{2}$$

Definition 3 Reference [6]: A ramp occurs if the difference between the power measured at the initial and final points of a time interval Δt is greater than a predefined reference value to the power ramp rate, ΔP_{ramp}:

$$|P\,(t+\Delta t) - P\,(t)|\,/\Delta t \;>\; \Delta P_{\text{ramp}} \tag{3}$$

The definitions above work directly with the wind power signal. Other approaches transform the signal into a more appropriate representation, for example, considering k-order differences in the power amplitude (see Ref. [10]). Let, P_t be the wind power time series and P_t^f the associated transformed signal that was obtained according to

$$P_t^f = \text{mean}\{P_{t+h} - P_{t+h-n_{\text{am}}}; h = 1, \ldots, n_{\text{am}}\} \tag{4}$$

where n_{am} stands for the number of averaged power differences to consider. Then,

Definition 4 Reference [9]: A ramp event is said to occur in an interval, if the absolute value of the filtered signal P_t^f exceeds a given threshold value, ΔP_{ramp}:

$$\left| P_t^f \right| > \Delta P_{\text{ramp}} \tag{5}$$

Definition 5 This is a new definition developed under the project. It uses a high-pass filter, that is, a filter that passes high-frequency signals and attenuates (reduces the amplitude of) signals with frequencies lower than the cutoff frequency. The simpler high-pass filter can be formulated as follows:

$$y[i] = \alpha(y[i-1] + x[i] - x[i-1]) \tag{6}$$

It can only pass relatively high frequencies because it requires large (i.e., fast) changes and tends to quickly forget its prior output values (see Fig. 3). The parameter α takes values in the interval [0;1]. Values near 1 imply that the output will decay very slowly but will also be strongly influenced by small changes in the input signal.

A constant input (i.e., an input with $(x[i] - x[i-1])$) will always lead to an output decay to zero. A small α implies that the output will decay quickly, requiring large changes in the input (i.e., $(x[i] - x[i-1])$ is large) for the output to vary considerably.

Figure 3 illustrates the concept. The y signal may be further treated by a band filter, removing small peaks and only keeping the values above a certain threshold, compatible with the ramp definition accepted.

3.2 Building a Probabilistic Ramp Representation

The detection mechanisms outlined above serve as indicator function for each time step in one scenario. When applied in a set of scenarios as a sample of the wind power pdf, we have in place a Monte Carlo process that can give as a result the probability of a specific ramp event and also an estimate of the ramping probability distribution at each time step as a function of the ramp amplitude.

The general algorithm is as follows:

- Generate a large set of N wind power scenarios, sampled with the wind power forecasting model.

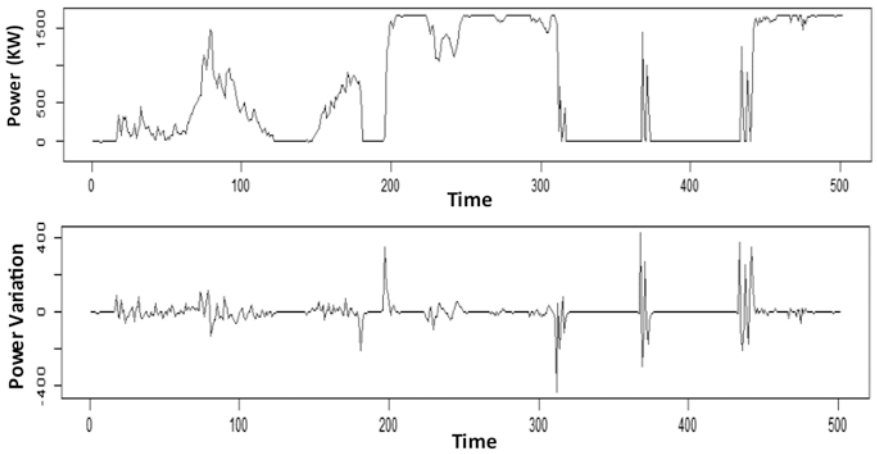

Fig. 3 *Top* wind power, *Bottom* high-pass-filtered signal ($\alpha = 0.25$)

- For each scenario, detect in each time step if there is a ramp event of each type defined.
- Count the total of ramp event detections in each time step for the whole sampled set of scenarios, associated with each ramp type.
- Based on the sample ratio of number of detected events n_i of type i over the size N of the sampled set, define probabilities for each ramp event in each time step of the forecasting horizon.

3.3 Building Cumulative Ramp Probability Diagrams

A histogram may be built by defining a set of bins $\Delta^b P$, ranging from ΔP_{ramp} to a user-specified maximum power change, and define the vote counting for each histogram bin b

$$V_k^b = \sum_{j=1}^{N} [\Delta^{bl} P < F(\Delta P_j^k) < \Delta^{bu} P] \tag{7}$$

where the lower and upper bound of the histogram bins are bl and bu, and F is the ramp definition in terms of power change.

This allows the definition of a cumulative ramp probability diagram such as in Fig. 4. From diagrams such as these, a measure of risk can be associated with the probability $p(\Delta P \geq \Delta P_r)$ of having a ramp event with a change equal or greater than P_r.

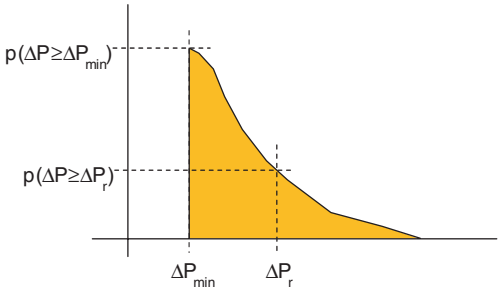

Fig. 4 A cumulative ramp probability diagram allowing risk evaluation for a ramping value ΔP_r. ΔP_{min} is the minimum acceptable power variation that does not trigger a ramp event alarm

3.4 Deciding that a Ramp Event Should be Declared

From the set of scenarios, one may thus define an empirical probability of exceeding a given threshold ΔP_{ramp}:

$$P(E_k) = \frac{1}{N}\sum_{j=1}^{N}[F(\Delta P_j^k) > \Delta P_{\text{ramp}}] \tag{8}$$

By setting a cutoff threshold *thr* on the probability $P(E)$, we may declare the occurrence of an event (ramp) at time step k if

$$P(E_k) > \text{thr} \tag{9}$$

This declaration converts the probabilistic ramp prediction into a binary choice that may lead to a decision to act and is needed in the operation context. Section 5 presents a way to define the threshold *thr* in an optimal way.

4 Application of the New Model

To verify the quality of the model, we organized an experiment built from real data from a large wind farm in the United States., in a time period of 12 weeks (21/10/2009–18/02/2010). We generated 5,000 scenarios (possible predictions of power) using Ref. [11]. The algorithm described above was run for each 24 h ahead, and cumulative ramp probability diagrams were built for windows of 3 h, counting and classifying possible ramps through the use of the high-pass filter to detect possible ramps and a band filter to eliminate small changes.

Figure 5 shows the case for one day. One can observe a point forecast, produced by the model in Ref. [13], and the actual values measured. Below, one has ramp cumulative probability diagrams, for 3-h steps, which provide information about the probability of having a ramp (given a definition) and also about the probability of the magnitude of such a ramp.

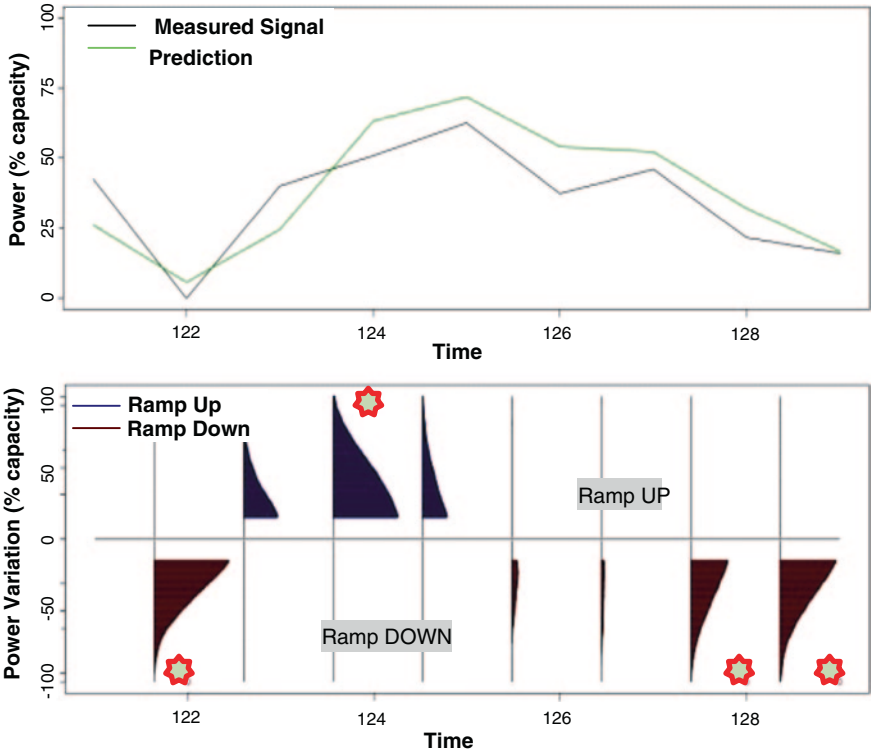

Fig. 5 *Top* actual measured wind power and the point forecast for 24 h (slightly over-forecasting in most time steps), *Bottom* cumulative probability diagrams for ramp-up (*above*) and ramp-down (*below*) events. A *star marks* intervals with a prediction/declaration for a ramp to occur

These diagrams are rotated, relative to Fig. 4, and the vertical axis is associated with a ΔP value, while the horizontal axis corresponds to the probability of having a ramp event of a magnitude equal or greater than a given power threshold. It is possible to have at the same time some probability of having either ramp-up or ramp-down, representing a variety of behavior observed in the generated wind power scenarios for the same type of occurrence.

5 Quality Analysis

Ramp event detection is a process where one may define hits (TP–true positives or TN–true negatives) and misses (FP–false positives, or false alarms, when a ramp is predicted but does not occur, and FN–false negatives or missed detections, when no ramp is predicted but occurs). The results below were obtained using a 3-h aggregation defining a ramp-up or -down of magnitude change higher than 25 % of the wind farm nominal power. This is the ΔP_{ramp} threshold value set for the time period Δt (= 3 h, in

this case). With this Δt value, definitions one, two and three lead to equal results. As for definition 4 (a moving average), the results come from setting $n_{am} = 2$. With $n_{am} = 1$, one gets almost the same results as when running definitions one, two and three.

Some widely used statistics to assess the quality of deterministic event detections defined in [0, 1] are precision (or sensitivity, or true-positive rate (TPR)), recall and specificity. *Precision* is defined as the ratio between the number of true positives and of positive forecasts. *Recall* is defined as the ratio between the number of true positives and of observed positives. *Specificity* is the fraction of true negatives, and the quantity (1–Specificity) may be called the *false-positive rate (FPR)*.

$$\text{Precision} = \frac{TP}{TP + FP};\ \text{Recall} = \frac{TP}{TP + FN};\ \text{Specificity} = \frac{TN}{TN + FP} \quad (10)$$

These concepts can be used to assess the effect of the actions resulting from probabilistic information. It is evident that in probabilistic forecasts, a new degree of freedom is introduced: a threshold to define the occurrence of the event.

A technique that may help in choosing a threshold level that optimizes event detection is the *receiver operating characteristic* (*ROC)* curve, which is a graphical plot in the plane FPR $\times$ TPR and domain [0,1] $\times$ [0,1]. This plot is achieved by changing progressively a cutoff value that defines the detection of an event—this value is associated with the probability of observing a ramp, from examining all scenarios. In this ROC domain, the main diagonal (0,0)–(1,1) defines a prediction like a random guess. The optimum corresponding to perfect discrimination is the point (0,1) where all positives are detected and no negatives are taken as (false) positives.

Figure 6 displays the ROC curves that we obtain in the classification of ramp-up events using definition 1, 4 and 5 and setting ΔP_{ramp} (amplitude of the band filter that eliminates small events) equal to 25 % of the nominal power. The model produces a better result than random guessing. The cutoff value that should be

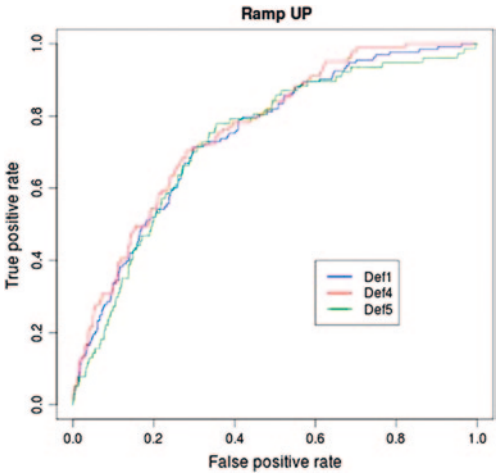

Fig. 6 ROC *curves* for definitions 1, 4 and 5

adopted depends [14] on the relative costs of missing a positive and of assuming a positive when there is none. If these costs are equal, and assuming a uniform event distribution, then the slope of TPR/FPR equals 1 and the cutoff value to be adopted, to accept or reject an alarm, should be the one that leads to the tangent to the ROC curve with slope 1 that is closest to the optimum point (0,1). This is relevant in the application of the method to wind power ramp prediction: the cot of missing a positive may be related with emergency ramping of generators or power purchases at high spot prices or load disconnection; the cost of accepting a false alarm is related with higher unit commitment costs or higher cost of operational reserve allocated.

Assume binary forecasts, where each example can be labeled using one of two classes in the set {y,n}, and a forecast can output the corresponding {Y,N}. Consider that we know the distribution of *yes* and *no* events, that is, the probabilities P(y) and P(n), and that we define the costs *cost*(Y;n) and *cost*(N;y) to be, respectively, the costs of predicting a event when no event occurs (false positive) and the cost of predicting no event when an event actually occurs (false negative). The slope of the line (a tangent line) that touches the ROC curve at the optimum operating point—a point with coordinates (FPR_0, TPR_0) that is associated with a probability threshold thr_0—is given by P(n)cost(Y;n)/P(y)cost(N;y).

If this distribution is unknown, we can estimate the distribution from the observations. The point (FPR_0, TPR_0) where the tangent line and the curve touch is the optimum operating point, in the sense that this point minimizes the expected cost given by the following expression:

$$EC = P(Y; n) \times \text{cost}(Y; n) + P(N; y) \times \text{cost}(N; y) \tag{11}$$

where P(Y;n) is the probability of predicting an event when it does not occur (probability of a false positive) and P(N;y) is the probability of predicting that an event does not occur when it really occurs (probability of a false negative).

Figure 7 presents the tangent lines and identifies the associated optimum operating point, including the optimal thr_0 associated with Eq. (9), that we get by running definition 1 and setting two error cost configurations to predict ramp-up events. In Conf. 1, we define the error costs to be *cost* (N;y) = 200, that is, the cost of a FN (cFN), and *cost* (Y;n) = 10, that is, the cost of a FP (cFP). In Conf. 2, we consider *cost* (N;y) = 10 and *cost* (Y;n) = 200.

The ROC curve is annotated with the corresponding empirical probability values, observed on the set of scenarios. The point obtained from optimizing Eq. (11) is associated with the optimal threshold thr_0 value. If the probability calculated is above thr_0, one should declare the prediction of occurrence of a ramp; if not, a prediction of no ramp. Referring to Fig. 5, this declaration was produced for the intervals marked with a star, where the probability of a ramp of magnitude above 25 % of the wind farm nominal power exceeds the optimal $thr_0 \approx 0.2$ obtained from optimizing Eq. (11) over the ROC curve.

Figure 8 plots the expected cost for a set of probability thresholds. These plots were generated by running definition 1 to identify ramp-ups. In these figures, we can easily identify the minimum expected costs that define the cutoff probability threshold corresponding to the optimum operating point.

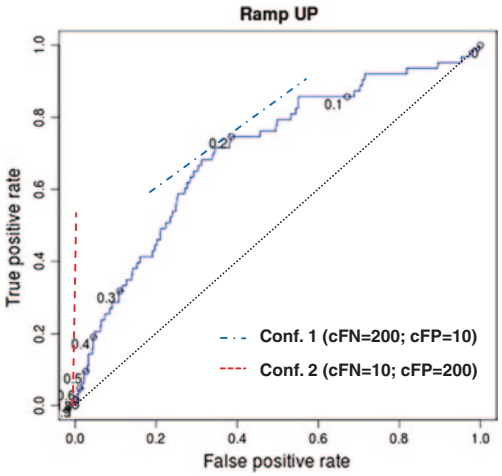

Fig. 7 ROC *curve* and *tangent lines* for definition 1 and two cost configurations

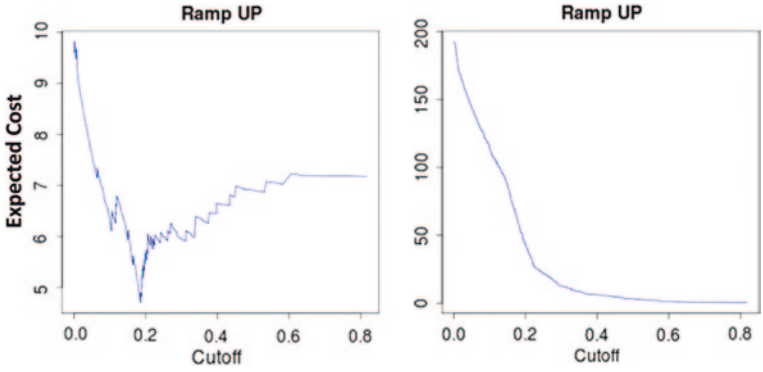

Fig. 8 Expected cost using definition 1: cFN = 200; cFP = 10, on the *left*, and cFN = 10; cFP = 200, on the *right*

Forecasters that assign a probability to each event often use the Brier Score (BS) [15], which is a score function that measures the average squared deviation between predicted probabilities and the actual outcomes. It is computed as

$$BS = \frac{1}{N}\sum_{t=1}^{N}(X_t - Y_t)^2 \tag{12}$$

where X_t is the event forecast probability; Y_t is the actual outcome (0 if not happened, 1 if happened) and N—number of forecasting instances. It is obvious that the optimum Brier Score would be of 0, for perfect sharp predictions. The Brier Score obtained in the experiment being described gave the values described in Table 1. By inspecting these results, we can see that by using

Table 1 Brier scores for the probabilistic forecasting system for both ramp types

	Ramp-up			Ramp-down		
	D1	D4	D5	D1	D4	D5
BS	0.078	0.091	0.082	0.080	0.086	0.076

Table 2 CSI comparison against a point forecast system: CSI for three ramp definitions and considering phase errors with a lag of 2 and 4 h

	Ramp-up–CSI					
	Probabilistic forecast			Point forecast		
Phase error	D1	D4	D5	D1	D4	D5
–	0.12	0.20	0.15	0.09	0.17	0.08
2	0.30	0.36	0.32	0.18	0.31	0.24
4	0.38	0.45	0.38	0.26	0.37	0.32

definition 1, we get a lower BS when detecting ramp-ups. In contrast, definitions 4 and 5 get lower BS for detection of ramp-down events.

Another useful metric is the critical success index (CSI), defined as follows:

$$\mathrm{CSI} = \frac{\mathrm{TP}}{\mathrm{TP} + \mathrm{FN} + \mathrm{FP}} \tag{12}$$

The CSI metric takes values in the interval [0;1], where 1 means correct prediction. CSI measures the fraction of observed and/or forecast events that were correctly predicted.

In Table 2, we present CSI values obtained in experiments to predict upward ramp events, for definitions 1, 4 and 5 and considering phase errors for time lags of 2 and 4 periods. The probability cutoff value is 0.3. The results for ramp-down display a similar performance. Regarding other definitions and parameters, we can say that the performance of our model improves when we consider large sizes of the time step (Δt), large aggregation windows and, obviously, consider phase error. Overall, we can say that we obtain the best results of our experiments by running the detection process for ramp definitions 4 and 5.

6 Ramp Forecasting and Unit Commitment

Figure 9 makes explicit the role of probabilistic ramp forecasting. By setting alarms at specific hours and by defining probabilities associated with ramp presence and amplitude, the model establishes risk levels for ramp events—in the form of a probability of having a ramp of a given amplitude or greater. A system operator may then decide, based on the risks he is willing to take, whether to accept a specific unit commitment or to hedge against the adverse event and plan for some extra reserve, at some cost. This also indicates how system operators may take full

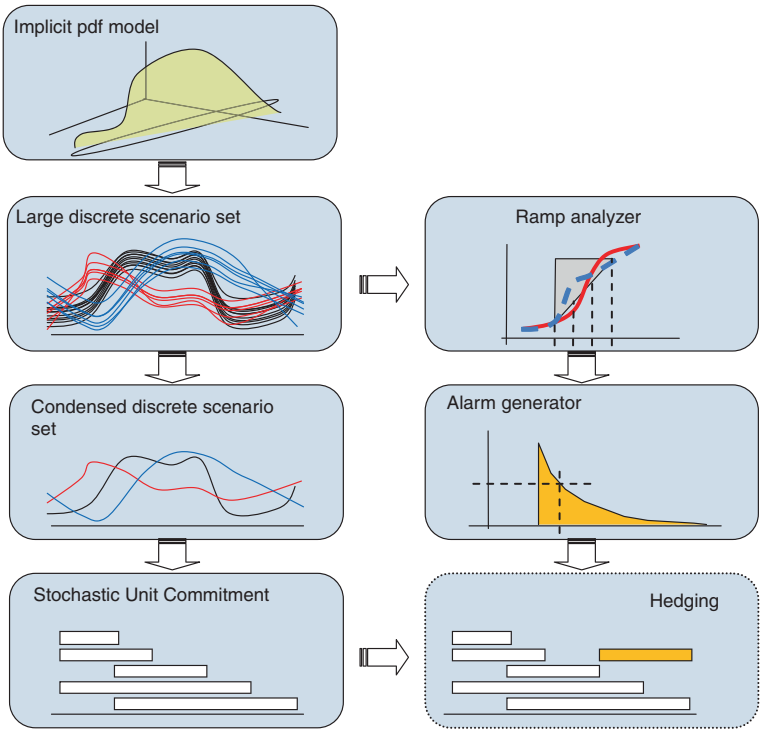

Fig. 9 Conceptual modules relating scenario generation, unit commitment and ramp event analysis

advantage of probabilistic wind power forecasting models—to adopt a stochastic model for the unit commitment exercise. However, even if a classical model is used, the reasoning about ramp risks and hedging applies.

7 Conclusions

Ramp forecasting has been recognized as a difficult exercise, related with predictions about the derivative of a time series. But, it is of the utmost importance to take into account the possibility of ramp events, especially in systems with high penetration of wind and where the remainder generation resource is dominantly of the slow thermal type, such as coal and nuclear power. The problem is somewhat less serious if the power system has significant hydro generation or gas turbines—but the system security and costs incurred in mitigating risks, that is, the cost of adopting hedging policies, are still very important.

To adequately assess costs and risks, a probabilistic approach is mandatory. This chapter brings to light a new approach to define a probabilistic model for

ramp forecasting, in a form that is useful for system operators that have to decide generation unit commitment. The output is a histogram, at every hour, indicating the probability of a ramp exceeding a certain threshold, for all magnitudes above a minimum ramp level defined. The approach does not provide dispatch decision suggestions—however, the declaration of a ramp event based on a probability threshold contributes to the decision process: it may serve as input to a hedging process, where the operator may decide to run the risk of being subject to a ramp event (e.g., in the case of a low probability for an event of a damaging magnitude) or to hedge by changing the unit commitment in an appropriate (more costly) way to avoid problems in case the event materializes.

Tests with real data from a US wind farm have proved the validity and usefulness of the approach. The experimental results, evaluated under the ROC curve concept, show clear advantages of the probabilistic forecaster over point forecasts and random guesses. It must be said that the quality of ramp forecasting depends a great deal on the quality of meteorological forecasts, translated into numerical weather models, which supply data to the general short-term wind power forecasting problem.

In sum, the work presented here, by assigning a probability to each possible ramp magnitude, is a clear step forward, providing a methodology useful to the industry.

Acknowledgments This manuscript has been created by UChicago Argonne, LLC, Operator of Argonne National Laboratory ('Argonne'). Argonne, a U.S. Department of Energy Office of Science laboratory, is operated under Contract No. DE AC02-06CH11357. The U.S. Government retains for itself, and others acting on its behalf, a paid-up non-exclusive, irrevocable worldwide license in said article to reproduce, prepare derivative works, distribute copies to the public, and perform publicly and display publicly, by or on behalf of the Government. The authors acknowledge EDP Renewables North America for providing the wind farm data used in the analysis.

The general fundamental work at INESC TEC is partially funded by the ERDF from the EU through the Programme COMPETE and by the Portuguese Government through FCT—Foundation for Science and Technology, namely under PEST-C/EEI/LA 0014/2011 and project ref. LASCA PTDC/EEA-EEL/104278/2008 and GEMS PTDC/EEA-EEL/105261/2008.

References

1. Ferreira C, Gama J, Miranda V, Botterud A (2010) A survey on wind power ramp forecasting. Report ANL/DIS 10–13, Argonne national laboratory, Dec
2. Greaves B et al (2009) Temporal forecast uncertainty for ramp events. In: Proceedings of EWEC'09, Marseille, France
3. Potter CW, Grimit E, Nijssen B (2009) Potential benefits of a dedicated probabilistic rapid ramp event forecast tool. In: Proceedings of PSCE'09, Seattle, USA
4. Freedman J, Markus M, Penc R (2008) Analysis of west texas wind plant ramp-up and ramp-down events. AWS Truewind, LLC, NY
5. Kamath C (2010) Understanding wind ramp events through analysis of historical data. In: Proceedings of IEEE PES transmission and distribution conference and exposition, LA, United States
6. Zheng H, Kusiak A (2009) Prediction of wind farm power ramp rates: a data-mining approach. J Solar Energ Eng, vol 131

7. Jørgensen JU, Mörlen C (2008) AESO wind power forecasting pilot project. Technical report, Ebberup, Denmark
8. Truewind-LLC AWS (2008) AWS Truewind's final report for the alberta forecasting pilot project. Alberta, Canada
9. Schaefer JT (1990) The critical success index as an indicator of warning skill. Weather Forec 5:570–575
10. Bossavy A, Girard R, Kariniotakis G (2010) Forecasting uncertainty related to ramps of wind power production. In: Proceedings of EWEC'10, Warsaw, Poland
11. Nielsen HA, Madsen H, Nielsen TS (2006) Using quantile regression to extend an existing wind power forecasting system with probabilistic forecasts. Wind Energ 9(1–2):95–108
12. Bessa RJ, Miranda V, Gama J (2009) Entropy and correntropy against minimum square error in offline and online three-day ahead wind power forecasting. IEEE Trans Power Sys 24(4):1657–1666, Nov
13. Juban J, Siebert N, Kariniotakis GN (2007) Probabilistic short-term wind power forecasting for the optimal management of wind generation. In: Proceedings IEEE PowerTech, Lausanne, France, pp 683–688
14. Provost F, Fawcett T (1997) Analysis and visualization of classifier performance: comparison under imprecise class and cost distributions, KDD'97, USA, pp 43–48
15. Weigel P, Liniger MA, Appenzeller C (2007) Generalization of the discrete brier and ranked probability skill scores for weighted multimodel ensemble forecasts. Mon Weather Rev 135(1):118–124

Application of Hourly Time Series Models in Day-ahead Wind Power Commitment

Suman Thapa, Rajesh Karki and Roy Billinton

1 Introduction

Wind power is regarded as the most suitable environment friendly alternative to conventional bulk power generation. Many countries around the world are rapidly installing wind farms, and several nations have already arrived at a position where a significant portion of their electric energy supply is contributed by wind power. Wind power generation is mainly dependant on the wind characteristics at the particular location and has an uncertain and random nature. Wind power, therefore, cannot be dispatched in the same way as the conventional generating units. In a wind-integrated power system, the system operator has to appropriately commit conventional generating units taking into account the wind power that may be available during the committed time period in order to satisfy the projected load with an acceptable degree of reliability. In an electric power system with low wind penetration, variations in wind power generation can be absorbed by the system through the use of the short-term reserves [1]. System operators face considerable challenges in keeping the balance between the generation and the demand with an acceptable degree of reliability when the wind power penetration is significant. Accurate wind power prediction becomes very important in determining adequate operating reserve in wind-integrated power system operation. There is a wide range of different

S. Thapa (✉) · R. Karki · R. Billinton
Power Systems Research Group, Department of Electrical and Computer Engineering, University of Saskatchewan, Saskatoon, SK, Canada
e-mail: suman.thapa@usask.ca

R. Karki
e-mail: rajesh.karki@usask.ca

R. Billinton
e-mail: roy.billinton@usask.ca

R. Billinton et al. (eds.), *Reliability and Risk Evaluation of Wind Integrated Power Systems*, Reliable and Sustainable Electric Power and Energy Systems Management,
DOI: 10.1007/978-81-322-0987-4_4, © Springer India 2013

methods for short-term wind power prediction. Reference [2] presents a chronological review of the various available techniques. The methods can be broadly categorized into two approaches known as physical and statistical approaches. The physical approach makes use of numerical weather prediction (NWP) models to predict the wind speed which is then converted into wind power using a physical wind to power conversion model [3]. Statistical methods such as the autoregressive moving average (ARMA) model [4] have also been used for short-term wind power prediction [5]. Physical models are suitable for forecasting horizons of 8–48 h, and a pure statistical model may be more suitable for a relatively shorter horizon such as 1–6 h. System operators often use a persistence model [6] for short-term prediction because of its simplicity. This model assumes that the wind condition in the next short time interval will be similar to the present or initial condition, and the system is operated assuming the wind power in the next time interval will be equal to or a fixed percentage of the current wind power generation. The uncertainty and the risks associated with such deterministic wind power commitment are, however, not considered. A novel method developed by the power system research group at the University of Saskatchewan quantifies the uncertainty of wind power generation in a short future time using a conditional probability approach [7]. References [8, 9] further extend the conditional probability approach to evaluate the risk of wind power commitment in a short future time of 1–2 h. A simplified method to commit wind power in a lead time of 1 and 2 h based upon a risk criterion known as the wind power commitment risk (WPCR) is presented in [10]. An appreciation of the available wind power a few hours ahead (1–4 h) can assist the system operator to optimize the required regulating margin. Additional knowledge of wind power availability a day-ahead can be used to assist in scheduling longer term reserves [3]. This chapter presents an investigation of the conditional probability approach in quantifying the risk of wind power commitment as the lead time is extended from 1–2 h to 24 h.

2 Wind Power Model

The basic wind power model consists of a wind speed model and a wind turbine generator (WTG) model. The wind speed in a short future time depends upon the initial time wind speed at the site. The conditional probability method can be used to assess the risk of wind power commitment utilizing the knowledge of the initial condition. It requires a large number of data points to create a valid probability distribution and an ARMA model developed for a particular wind site can be employed to simulate the required data. The hourly wind speed data at Regina, Saskatchewan in Canada, obtained from Environment Canada are used in this study. The ARMA model for the Regina wind site is reported in [11] and is presented in (1).

$$\begin{aligned} y_t &= 0.9336y_{t-1} + 0.4506y_{t-2} - 0.5545y_{t-3} + 0.111y_{t-4} \\ &\quad + \alpha_t - 0.2033\alpha_{t-1} - 0.4684\alpha_{t-2} + 0.2301\alpha_{t-3} \\ &\quad \alpha_t \in \text{NID}\ (0, 0.409423^2) \end{aligned} \tag{1}$$

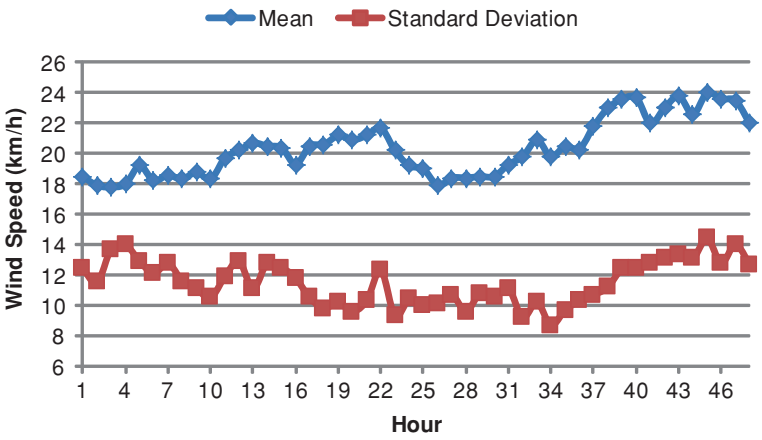

Fig. 1 Hourly mean and standard deviation (*SD*) of the wind speed at Regina (Hour 1–48)

Figure 1 presents a sample of the wind speed statistics at Regina obtained from Environment Canada. The annual hourly mean wind speed and standard deviation (SD) at Regina are 19.52 km/h and 10.99 km/h, respectively.

The wind power curve of a typical WTG is shown in Fig. 2. The power output is zero for all wind speeds less than a minimum value called the cut-in speed V_{ci}. The wind speed and power output follow a nonlinear relationship for any wind speed within the range of the cut-in and the rated speed V_r. The power output is constant at the rated capacity for all speeds greater or equal to the rated capacity. The power output is, however, zero at or above the cutout speed V_{co} as the WTG is shut down for safety reasons during such extreme wind speed conditions. The speed power relation is shown in (2).

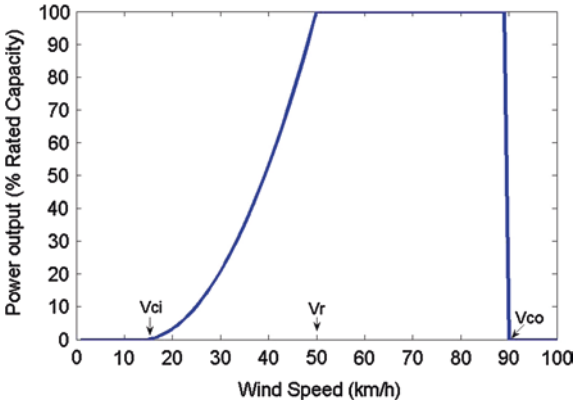

Fig. 2 Wind-power characteristics of a typical WTG with 15, 50 and 90 km/h as the cut-in, rated and cutout speed, respectively

$$\begin{aligned} P_t &= 0 \quad \text{for } V_{\text{ci}} > \text{SW}_t > V_{\text{co}} \\ &= \left(A + B \cdot \text{SW}_t + C \cdot \text{SW}_t^2\right) P_{\text{r}} \quad \text{for } V_{\text{ci}} < \text{SW}_t < V_r \\ &= P_{\text{r}} \quad \text{for } V_r < \text{SW}_t < V_{\text{co}} \end{aligned} \tag{2}$$

The A, B and C parameters of (2) are presented in [12].

3 Wind Power Commitment Risk

The wind speed in the next few hours depends on the wind speed at the present time, referred to as the initial wind condition in this study. Figure 3 presents the probability distributions of the wind speeds at Hour 12 given the three different initial conditions of 20, 25 and 30 km/h at Hour 10. The Regina wind speed ARMA model is given in (1). The probability distributions of the wind speed, conditional on the initial wind speeds, are very close to the normal distribution. It can be observed that the wind speed distribution moves toward a higher wind speed as the initial speed increases. This indicates that the short-term wind speed distribution is highly dependent on the initial wind condition.

Figure 4 considers the wind speed distribution at Hour 12 conditional on the initial wind speed of 25 km/h at Hour 10. The wind power curve described in Fig. 2 is also contained in Fig. 4 which shows that initial wind power is approximately 10 % of the rated capacity. If the wind power commitment for the lead time of two hours was made based upon a pure persistence model, the capacity value of the wind power would be assessed at 10 % of the rated capacity. The wind speed distribution, however, shows that there is a significant probability that the wind

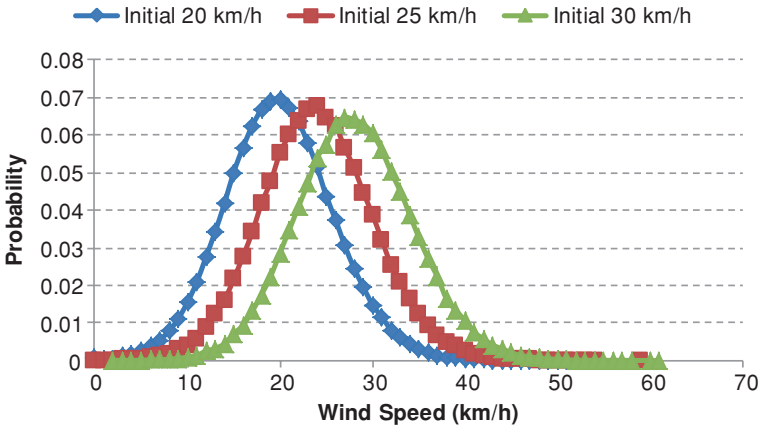

Fig. 3 Wind speed probability distributions at Hour 12 conditional on the given speeds at Hour 10

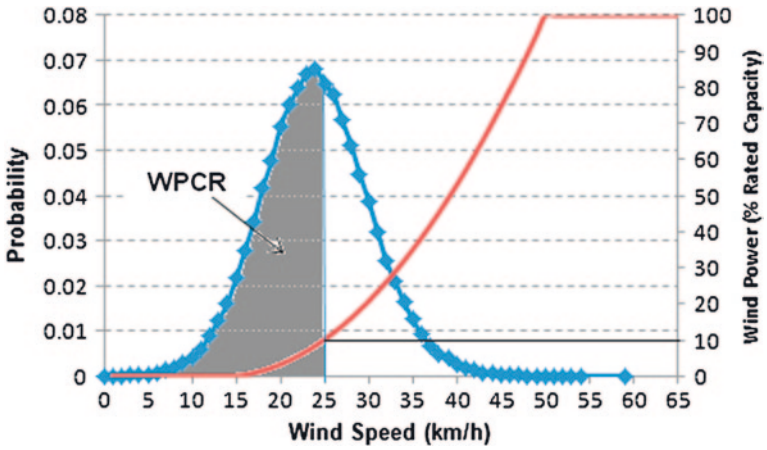

Fig. 4 Evaluation of wind power commitment risk (*WPCR*) for a lead time of 2 h

power will be less than the committed value. The shaded area in Fig. 4 gives the probability that the wind power in the lead time will be less than the committed value. This probability is designated as the WPCR [9].

It can be observed from Fig. 4 that the WPCR increases as the committed value of wind power increases. The capacity value of wind power in a short future time depends upon the initial condition and the amount of risk the system is able or prepared to accept [10].

Figure 5 shows the WPCR of committing 100 % of the initial power for the lead times of 1, 2 and 4 h corresponding to three initial conditions designated as Case A, B and C at Hour 10. The three cases corresponding to the wind speeds of 25, 30 and 34 km/h give power outputs of 10, 20 and 30 % of the rated capacity,

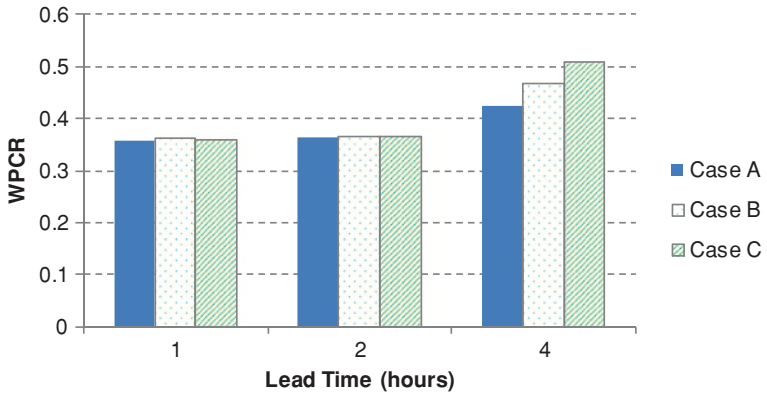

Fig. 5 WPCR of using a pure persistence model for short-term wind power commitment

Fig. 6 WPCR of committing 100 and 80 % of the initial power (lead time = 1 h)

respectively. These power output levels would be the forecast values using a pure persistence model approach. As shown in Fig. 5, the WPCR varies from 0.36 to 0.51 as the lead time increases from 1 to 4 h.

Figure 6 shows the variation in WPCR as the wind power commitment is reduced from 100 to 80 % of the initial power for a lead time of 1 h. The WPCR obviously decreases as the wind power capacity value is reduced. The studies also show that the risk associated with a deterministic commitment policy is not consistent with different initial conditions and lead times.

It might be considered desirable to have the risk maintained at a level dictated by a managerial decision. Figure 7 presents a scenario in which the capacity values

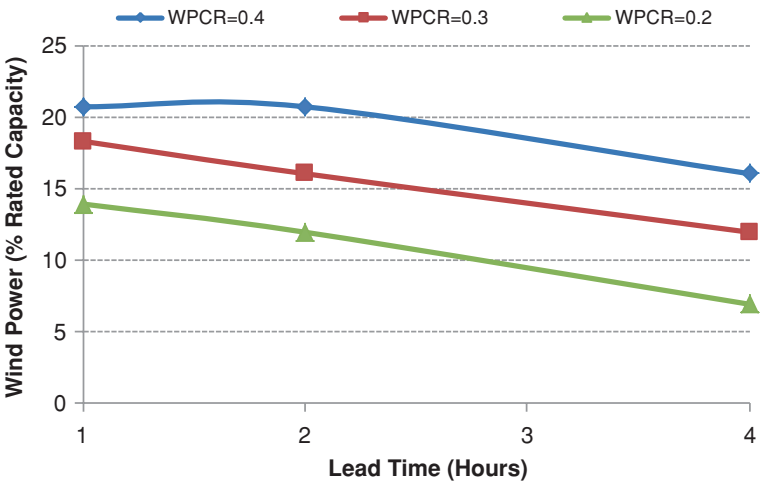

Fig. 7 WPCR constrained wind power commitment

of the wind power at the specified lead times are constrained by a WPCR criterion. The initial condition corresponds to Case B at Hour 10 where the initial wind power is 20 % of the rated capacity. It can be seen that the wind capacity value goes up as the WPCR criterion value is increased, which indicates that wind power can be assessed a higher capacity value if the system is prepared to accept a higher level of risk. It can also be seen from Fig. 7 that the wind capacity value decreases for a given WPCR criterion as the lead time increases. For example, the capacity value decreases from 14 to 7 % of the rated capacity which is 70 and 28.6 % of the initial power, respectively, as the lead time is increased from 1 to 4 h at the WPCR criterion of 0.2.

3.1 Impact of Lead Time

The studies presented in the previous sections consider short future times such as 1–4 h. This section presents a study of wind power commitment and the associated WPCR as the lead time is extended to 24 h. Figure 8 shows the statistics of the wind speed distribution with lead time for the two initial conditions at Hour 10 designated as Case A and B in the previous section. It can be seen that the mean value of the wind speed decreases, while the SD increases as the lead time is increased. The increase of the SD is an indication that the variability and, therefore, the uncertainty will increase moving into the future. The mean wind speed varies from 24.37 to 20.43 km/h for Case A, while it varies from 28.78 to 21.37 km/h for Case B as the lead time increases from 1 to 24 h. The plots of the mean wind speed show a sharp decline up to a lead time of about 10 h and then settle down as the lead time further increases. The SD on the other hand increases from 4.86 to 9.9 km/h for Case A and 5.03–10.07 km/h for Case B as the lead time increases from 1 to 24 h. The plots of the SD rise sharply up to about 10 h and become almost constant as

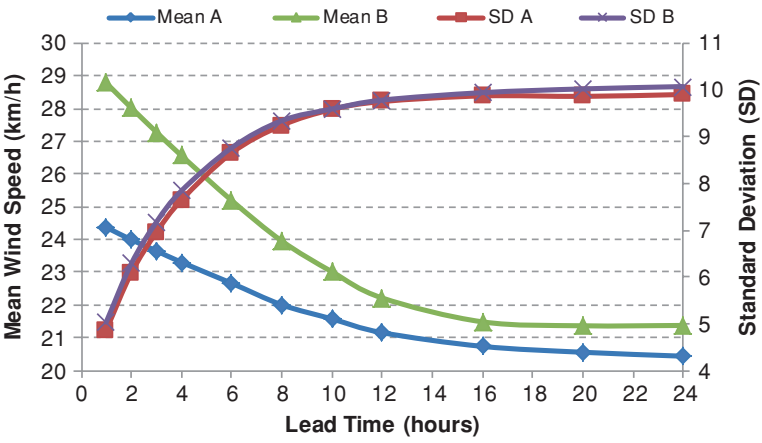

Fig. 8 Wind speed statistics conditional on two different initial conditions at Hour 10

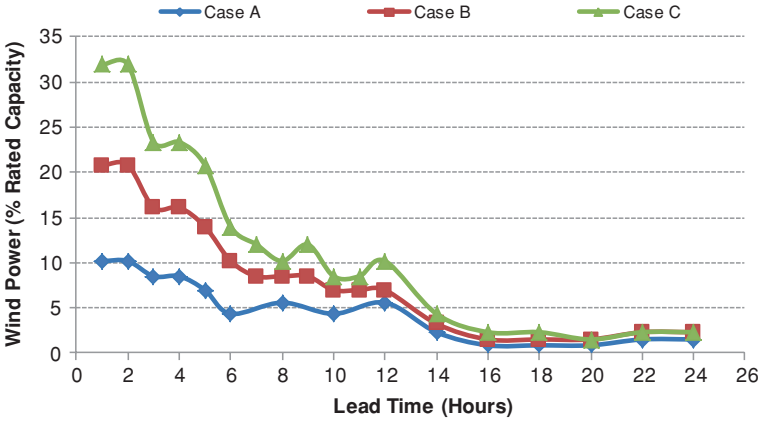

Fig. 9 Wind power commitment for three initial conditions (WPCR = 0.4)

the lead time is further increased. The two plots of mean values for the two initial conditions start some distant apart, gradually tend to converge up to a lead time of about 6 h and then maintain a spread of about 1 km/h as the lead time is further increased. The plots of the SDs are relatively close to each other for both cases at all the lead times. This indicates that the variability is quite independent of the initial conditions and is mainly dependent on the lead time.

The capacity value of wind power at a WPCR criterion of 0.4 is presented in Fig. 9 for the three initial conditions in Case A, B and C at Hour 10. The lead times considered are up to 24 h from the initial time. The capacity value of wind power as obtained from the conditional wind speed distribution varies from 10.17 to 1.5 % of the rated capacity for Case A. The capacity values similarly vary from 20.78 to 2.3 % and 31.91 to 2.3 % of the rated capacity for Case B and C, respectively. The WPCR constrained wind capacity value decreases significantly with lead time for any initial condition and reaches a relatively small value when the lead time is greater than 12 h. Figure 9 shows that the three curves for the initial conditions are significantly apart at small lead times (e.g. 1–6 h), but become close to each other at a relatively small capacity value as the lead time increases beyond 12 h. This suggests that the impact of the initial condition on a future wind capacity value decreases significantly as the lead time is increased beyond 12 h, and the impact is insignificant in day-ahead wind power commitment analysis.

3.2 Impact of WPCR Criteria

The selection of a suitable WPCR criterion is a management decision which should consider the operating strategy, types and sizes of the conventional units and the reserves that can be made available during fluctuations in wind

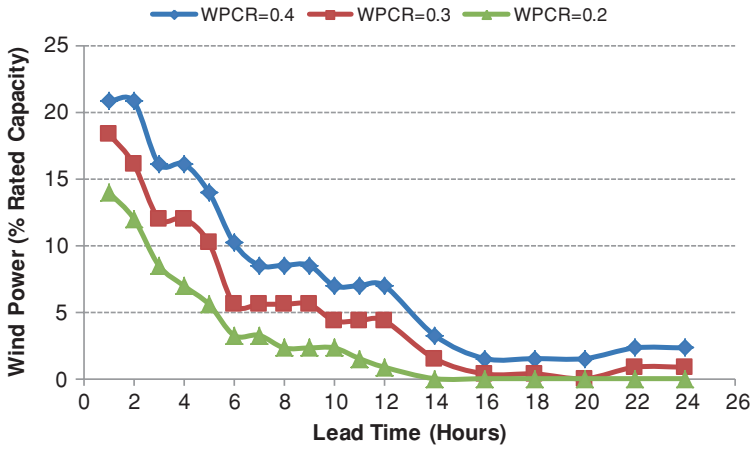

Fig. 10 Wind power commitment for three WPCR criteria (initial power = 20 % of the rated capacity)

power generation. Figure 10 presents the wind power commitment in a short future time period ranging from 1 to 24 h constrained by three WPCR criteria of 0.4, 0.3 and 0.2 given that the wind power at the initial time is 20 % of the rated capacity (Case B). The capacity value varies from 20.78 to 2.3, 18.36–0.86 and 13.97–0 % of the rated capacity, respectively, at the WPCR criteria of 0.4, 0.3 and 0.2 as the lead time increases from 1 to 24 h. Figure 10 shows how the wind power profile rises as the risk criterion increases allowing a higher capacity value of the wind power to be committed in the lead time considered. It can also be seen that the day-ahead capacity value assigned to the wind power is essentially zero at WPCR criteria of 0.3 and 0.2. A higher risk criterion of 0.4 or higher could be applied for such long horizons as there is time for the system operators to employ available means to mitigate unfavorable consequences due to low wind situations by making operating adjustments a few hours ahead.

4 Day-ahead WPCR

As noted earlier, knowledge of short-term wind power can assist the system to optimize the required regulating capacity. It is also necessary to assess the day-ahead wind power to schedule the conventional units. Physical methods employing NWP are often used to predict wind power over such a long horizon. The physical methods, however, also contain forecasting errors, and hourly models are used to mitigate the errors of wind power prediction and determine the spinning reserve requirements. It has been observed from the preceding section that

the impact of initial wind conditions on future wind capacity values decrease significantly beyond lead times of 10–12 h and have negligible impact in day-ahead wind capacity assessment. Conditional probability considerations used for short-term (i.e., 1–4 h) wind power commitment are not required for day-ahead wind power assessments, and historic wind speed statistics at the particular hour without consideration of initial wind conditions can be used to provide a probabilistic day-ahead wind capacity value.

Figure 11 presents the probability distributions of the wind speed at Hour 11 and Hour 14 which represent lead times of 1 and 4 h, respectively. The left end of the figure has the distributions shown by the solid lines without markers obtained from the hourly wind speed distributions in the ARMA model. These distributions are designated as unconditional distributions in Fig. 11 as they do not depend upon any initial conditions. The figure also shows the conditional wind speed distributions at the two lead times for the Case B and C conditions. The conditional wind speed distributions for lead times of 1 and 4 h move distinctively toward higher wind speeds as the initial conditions change from lower to higher wind speeds. The distributions for a lead time of 24 h are similarly presented in Fig. 12. Contrary to the distributions shown in Fig. 11, the probability distributions for a lead time of 24 h are very similar for both initial conditions and they are close to one obtained from the hourly wind speed probability distribution. This further illustrates that the initial conditions are significant in short-term wind power commitment but not in longer horizons such as those in day-ahead commitment. More importantly, it also indicates that the historic wind speed statistics can be directly used to assess approximate day-ahead capacity values for wind power.

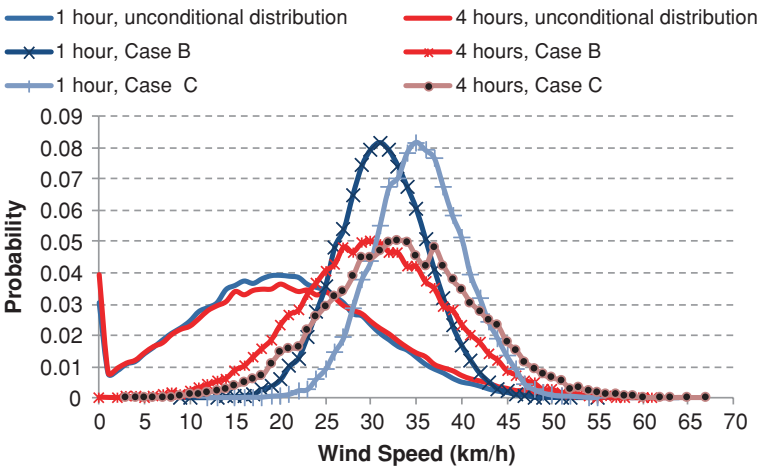

Fig. 11 Wind speed probability distribution (conditional and unconditional) for 1 and 4 h lead times

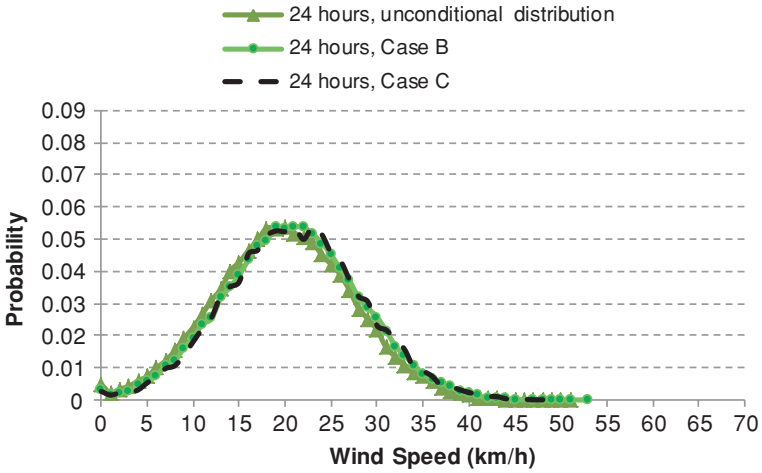

Fig. 12 Wind speed probability distributions (conditional and unconditional) for a 24 h lead time

4.1 Approximate Day-ahead WPCR

The previous section illustrates that historic wind speed statistics can be directly used to assess the day-ahead capacity value of wind power in day-ahead generation planning. Sufficient historic wind speed data are usually not available to many system operators. A simplified method requiring limited data for day-ahead wind capacity assessments could, therefore, be very useful to system operators. The probability distribution obtained from historic wind speed data collected over a large number of years, or obtained from simulated data using the appropriate ARMA model as shown in Fig. 12 can, however, be approximated by a normal distribution based on the mean wind speed and the SD for the particular hour. Figure 13 shows the cumulative wind speed probability distributions obtained from the wind speed data simulations using the ARMA model and the normal distribution using the hourly wind speed statistics at Hour 34 which is the 24 h of lead time referred to Hour 10 as the initial time. In both the methods, the negative values of the wind speed are converted to zeroes. The ordinate in Fig. 13 gives the WPCR which is the probability that the wind speed would be less than the value given in the abscissa. It can be seen that the WPCR evaluated using the two methods are approximately equal.

The simplicity of the approximate normal distribution method makes it easy to apply in system operation, and the method only requires the mean wind speed and the SD for a particular hour. The method can be used to assess the day-ahead capacity value of wind power for a selected WPCR criterion. The simplified normal distribution method has been applied to assess the capacity values of wind power for each hour of the next day. Figure 14 presents the wind power

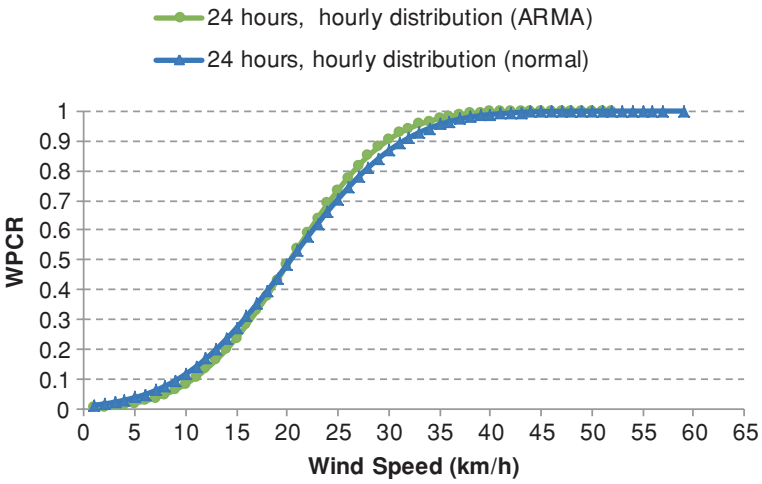

Fig. 13 Wind speed cumulative probability distributions (ARMA and normal) for a 24 h lead time

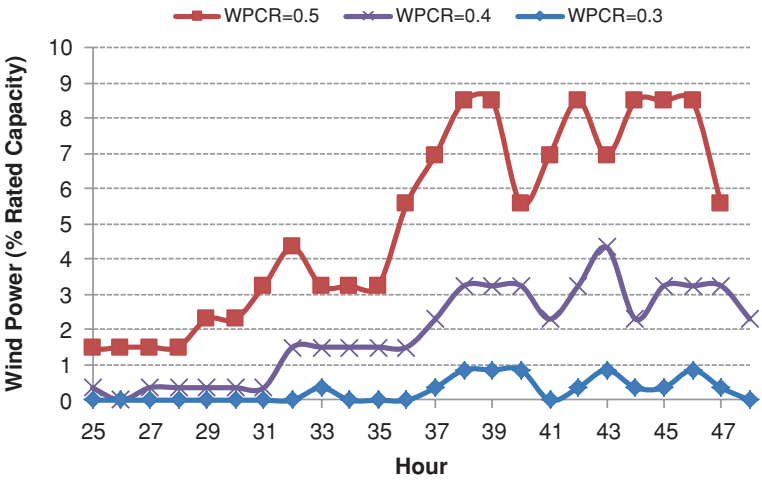

Fig. 14 Wind power commitment using the normal distribution of the historic wind speed statistic

commitment for Hour 24–48 for WPCR criteria of 0.5, 0.4 and 0.3. The capacity value varies from 1.5 to 8.5 % of the rated capacity at the WPCR of 0.5 during the hours considered with an average of approximately 5 % of the rated capacity over the time considered. The capacity value decreases to 0–4.3 % with an average of approximately 2 % of the rated capacity at the WPCR of 0.4 over the same period. It follows the same hourly trend as that shown in Fig. 1. It is also noticeable

that the wind has almost no capacity value when the WPCR criterion is reduced to 0.3. It should be noted that a low WPCR criterion such as 0.3 does not totally negate the capacity value of wind power while making a day-ahead commitment. The system operator should consider accepting a higher WPCR such as 0.5 while scheduling the units and adjust the regulating capacity later in the day employing the hourly models using the conditional probability method.

5 Conclusion

The capacity value of wind power in a short future time is driven by the initial conditions. The conditional probability approach can be used to quantify uncertainties associated with short-term wind power commitment. Risk-based methods are useful in assessing the capacity value of wind power as they allow the system operator to appropriately manage the short- and long-term system reserves. The conditional probability approach is useful in assessing the WPCR and the capacity value constrained by the WPCR criteria for short future times such as 1–4 h. The studies presented show that the impacts of initial conditions weaken as the lead time increases and initial conditions are not the driving factor when long lead times such as 24 h are considered. The historic hourly wind speed probability distributions without the consideration of any initial condition may be used to assign day-ahead capacity value to a wind farm based on a suitable WPCR criterion. The method can be simplified using a normal probability distribution of wind speeds for the particular hour based on the mean wind speed and the SD for the given hour. Sophisticated and complex methods of wind power prediction are not readily applied in practice. The approximate normal distribution method presented in this chapter can be easily applied and should be useful for day-ahead unit scheduling. The conditional hourly models may then be used for shorter term wind power commitment considering appropriate WPCR criteria.

References

1. Eriksen PB, Ackermann T, Abildgaard H, Smith P, Winter W, Rodriguez Garcia JM (2005) System operation with high wind penetration. Power Energ Mag IEEE 3:65–74
2. Costa A, Crespo A, Navarro J, Lizcano G, Madsen H, Feitosa E (2008) A review on the young history of the wind power short-term prediction. Renew Sustain Energ Rev 12(8):1725–1744
3. Ernst B (2012) Wind power prediction. In: Ackermann T (ed) Wind power in power systems, 2nd edn. Wiley, Chichester, pp 753–766
4. Box GEP, Jenkins GM (1970) Time series analysis; forecasting and control. Holden-Day, San Francisco
5. Milligan M, Schwartz M, Wan Y (2003) Statistical wind power forecasting models: results for U.S. wind farms. Nat Renew Energ Lab May 2003 Available: http://www.nrel.gov/docs/fy03osti/33956.pdf

6. Nielsen TS, Joensen A, Madsen H, Landberg L, Giebel G (1999) A new reference for wind power forecasting
7. Billinton R, Karki B, Karki R, Ramakrishna G (2009) Unit commitment risk analysis of wind integrated power systems. IEEE Trans Power Syst 24:930–939
8. Thapa S, Karki R, Billinton R (2011) Evaluation of wind power commitment risk in system operation. In: Electrical power and energy conference (EPEC), 2011 IEEE, pp 284–289
9. Karki R, Thapa S, Billinton R (2012) Operating risk analysis of wind-integrated power systems. Electr Power Compon Syst 40:399–413
10. Karki R, Thapa S, Billinton RB (2012) A simplified risk-based method for short-term wind power commitment. IEEE Trans Sustain Energ PP:1
11. Billinton R, Chen H, Ghajar R (1996) Time-series models for reliability evaluation of power systems including wind energy. Microelectron Reliab 36(9):1253–1261
12. Giorsetto P, Utsurogi KF (1983) Development of a new procedure for reliability modeling of wind turbine generators. IEEE Trans Power Apparatus Syst PAS-102:134–143

Probabilistic Guarantees for the N-1 Security of Systems with Wind Power Generation

Maria Vrakopoulou, Kostas Margellos, John Lygeros and Göran Andersson

1 Introduction

Security in power systems is an important topic of research, and it has been studied extensively over the last years. Following Refs. [1, 2], security of a power system refers to its ability to survive contingencies while avoiding any undesirable disruption of service. To quantify security, the concept of N-1 security assessment has been developed (see e.g., Ref. [3]). In this context, we consider the system to be in an N-1 secure state, if any single component outage does not lead to cascading failures. Therefore, designing the system to be N-1 secure provides a way to prevent the network from widespread blackouts, which in most cases develop as a result of cascading events [4].

Toward this objective, Refs. [5, 6] considered FACTS devices and designed their setting in an optimal way to enhance the steady state security of the system. In Ref. [7], the author used a metric different from the N-1 security criterion and proposed a model predictive control scheme to achieve a high level of security

M. Vrakopoulou (✉) · G. Andersson
Power Systems Laboratory, Department of Electrical Engineering,
ETH Zürich, Zürich, Switzerland
e-mail: vrakopoulou@eeh.ee.ethz.ch

G. Andersson
e-mail: andersson@eeh.ee.ethz.ch

K. Margellos · J. Lygeros
Automatic Control Laboratory, Department of Electrical Engineering,
ETH Zürich, Zürich, Switzerland
e-mail: margellos@control.ee.ethz.ch

J. Lygeros
e-mail: lygeros@control.ee.ethz.ch

R. Billinton et al. (eds.), *Reliability and Risk Evaluation of Wind Integrated Power Systems*, Reliable and Sustainable Electric Power and Energy Systems Management,
DOI: 10.1007/978-81-322-0987-4_5, © Springer India 2013

against large disturbances. From a market point of view, the authors of Milano et al. [8] proposed a method for incorporating contingencies and stability constraints by making use of a voltage constrained optimal power flow.

The expected increase in the installed capacity of renewable energy sources highlights the necessity of revisiting the existing N-1 security assessment methodology, so as to take into account their intermittent nature, which can have a major impact on the way power is distributed across the network. From an economic perspective, Bouffard and Galiana [9] designed a stochastic forward electricity market clearing problem, allowing for higher wind power penetration while meeting the security requirements. The authors of Grijalva et al. [10] defined a set of security metrics to capture the different aspects of a large-scale wind integration project.

In Ref. [11], the authors attempt to quantify the value of wind at different network locations by solving a security constrained unit commitment problem. In a similar setting, Wang et al. [12] formulated a stochastic unit commitment program for a combined wind–thermal system, but do not take security constraints explicitly into account in the design process. Instead, a subsequent step is performed, to measure the frequency of insecure instances. In Ref. [13], a simulation-based analysis was carried out to evaluate the N-1 security of the Finnish transmission system, in case of a simultaneous grid fault and a sudden decrease of the wind power infeed.

In this work, we propose a novel framework, which provides probabilistic guarantees when designing an N-1 secure day-ahead dispatch for the generating units in systems with high amount of fluctuating power sources. Note that, as in most of the related literature, we consider as preventive actions only the generation dispatches. Additional controls, including changes in the topology configuration, the phase shifting transformer settings, etc., are not taken into account. We integrate the security constraints, emanating from the N-1 criterion, to a DC optimal power flow program [14], and formulate a stochastic optimization problem with chance constraints, which consist a probabilistic version of the transmission capacity constraints. To transform this problem to a tractable one, we employ the so-called scenario approach [15, 16]. In Ref. [15], the authors provide a bound for the number of samples of the uncertain parameter (in this case the wind power) that one should generate to substitute the chance constraint with a number of hard constraints while maintaining the desired probabilistic guarantees. The resulting problem can be then solved easily by existing numerical tools [17].

This approach is inherently different from other stochastic optimization approaches, and it has only recently been applied to power system related problems (e.g., Refs. [18–21]). In the remainder of the chapter, it is assumed that the fluctuating power infeed consists of wind power. Typically, as proposed by Papaefthymiou and Klöckli [22], a Markov chain-based model is employed to generate wind power scenarios.

To evaluate the necessity of a robust N-1 security design, we compare our method with a benchmark approach, which assumes that the network operator determines the dispatch of the generators based only on the available wind power forecast. The performance of our method is then verified via Monte Carlo

simulations for different wind power realizations, using a modified version of the IEEE 30-bus network, retrieved from Ref. [23].

Section 2 provides the setup of the problem and information about how we treat uncertainty, whereas Sect. 3 states the resulting optimization program. In Sect. 4, we provide details regarding the scenario approach optimization technique and the Markov chain-based wind power model. Section 5 shows the obtained simulation results to illustrate the performance of our approach. Finally, Sect. 6 concludes the work and provides an outlook for open problems.

2 Problem Setup

For the analysis of the subsequent subsections, we consider a power network comprising of N_G generating units, N_L loads, N_l lines, N_b buses and N_w wind power generators. It should be noted, unless stated otherwise, that by the term line, we refer to both lines and transformers.

2.1 Power Flow Equations

As already mentioned, a DC power flow formulation is adopted [24], since it leads to a linear representation of the network, ensuring convexity of the developed optimization problem. It is based on the assumptions that

1. The voltage at every bus of the network remains constant at 1p.u.
2. The active power losses are neglected.
3. $\sin\theta_{\text{km}} \approx \theta_{\text{km}}$, where θ_{km} is the angle in radians across the branch connecting the buses k and m.

The resulting power flow equation for every line $k \to m$ is given by

$$P_f = B_f \theta \tag{1}$$

where $P_f \in \mathbb{R}^{N_l}$ is a vector containing the power flows P_{km} of each line, $\theta \in \mathbb{R}^{N_b}$ denotes the voltage angles at every bus, and $B_f \in \mathbb{R}^{N_l \times N_b}$.

The active power injection at a bus k is given by $P_k = \sum_{m \in \Omega_k} P_{\text{km}}$ where $\Omega_k = \{m \in \{1, \ldots, N_b\} | \, k \to m \ \text{is a line}\}$. In a more compact notation

$$P = B_{\text{BUS}} \theta \tag{2}$$

where $P \in \mathbb{R}^{Nb}$ is the vector of the net injections P_k, and $B_{\text{BUS}} \in \mathbb{R}^{N_b \times N_b}$ denotes the nodal admittance matrix of the network.

In the sequel, we eliminate θ from Eqs. (1), (2) so as to represent the power flows P_f as a function of the power injections P. Note that B_{BUS} is singular, with rank $N_b - 1$, hence it is not invertible, and Eq. (2) cannot be solved directly with

respect to θ. Therefore, to obtain a solution, one of the equations in Eq. (2) is removed, and the angle associated with this row is chosen as a reference angle and is set to zero. Without loss of generality, the last row of Eq. (2) is removed, that is, $\theta_{N_b} = 0$. Let then $\tilde{B}_{\text{BUS}} \in \mathbb{R}^{(N_b-1)\times(N_b-1)}$, $\tilde{\theta} \in \mathbb{R}^{N_b-1}$, $\tilde{P} \in \mathbb{R}^{N_b-1}$ denote the remaining parts of B_{BUS}, θ, and P, respectively. Then,

$$\tilde{P} = \tilde{B}_{\text{BUS}}^{-1}\tilde{\theta}. \tag{3}$$

Substituting Eqs. (3) into (2) with $\theta = [\tilde{\theta} \;\; 0]^T$, we have

$$P_f = B_f \begin{bmatrix} \tilde{B}_{\text{BUS}}^{-1}\tilde{P} \\ 0 \end{bmatrix}. \tag{4}$$

The power injection vector P can be written in a generic form as

$$P = C_G P_{\text{Gen}} + C_w P_w - C_L P_L, \tag{5}$$

where $P_{\text{Gen}} \in \mathbb{R}^{N_G}$, $P_w \in \mathbb{R}^{N_w}$ and $P_L \in \mathbb{R}^{N_L}$ denote the generating power, the wind power infeed and the load, respectively. Matrices C_G, C_w, C_L are of appropriate dimension, and their element (i, j) is "1" if generator j (respectively wind power/load) is connected to the bus i, and zero otherwise.

2.2 Dynamic Considerations

An outage or a deviation of the wind power from its forecasted value, which will lead to generation–load mismatch, will induce frequency deviations and activate the active power reserves of the system. To take this into account in our formulation, we consider that a new steady state is reached, as an effect of the secondary frequency control action. This is a reasonable assumption, since the optimization process is carried out in hourly steps, and hence frequency deviation settles again to zero due to secondary frequency reserve deployment. Therefore, we define $d \in \mathbb{R}^{N_G}$ to be a distribution vector, weighting the excess–deficit of power among the generating units participating in the frequency control. If a generator is not contributing to frequency control, the corresponding element in the d vector is zero. Let $P_{\text{mismatch}} \in \mathbb{R}$ represent the total generation–load mismatch, which may occur due to the difference between the actual wind from its forecasted value and/or as an effect of generation–load loss. Then, the new equilibrium operating point of the generators due to the secondary frequency control will be $P_{\text{Gen}} = P_G - d\,P_{\text{mismatch}}$, where $P_G \in \mathbb{R}^{N_G}$ is the generation dispatch corresponding to the forecasted wind power $P_w^f \in \mathbb{R}^{N_w}$.

Equation (5) can be then rewritten as

$$P = C_G(P_G - d\,P_{\text{mismatch}}) + C_w P_w - C_L P_L, \tag{6}$$

P_{mismatch} depends each time on the outage we consider. For the N-1 security analysis, we consider any single component outage; however, a single line outage may trip a bus, and hence more than a single load, generator or wind power outages are taken into account. In the general case, the generation–load mismatch is determined by

$$P_{\text{mismatch}} = 1_{1\times N_w}(P_w - P_w^f) - P_L^{\text{out}} + P_G^{\text{out}} + P_w^{\text{out}},$$

where $P_L^{\text{out}}, P_G^{\text{out}}, P_w^{\text{out}} \in \mathbb{R}$ represent the total load, conventional generation or wind power generation outage that may occur.

2.3 Uncertainty Handling

There are two sources of uncertainty in the formulation of the preceding sections. The first one refers to component outages, whereas the second is the uncertain wind power production P_w. Therefore, we need to specify the way these uncertainties are treated, or in other words, in which sense the dispatch we will compute is robust toward component outages and wind power fluctuations. Note that no load uncertainty is considered, although the proposed framework could be extended to include such cases as well.

For the component outages, a worst-case approach is adopted, that is, we enumerate all possible outages and design a generation schedule that is robust with respect to all these cases. Alternatively, a computational simpler problem may be achieved if only a few outages are selected according to some reliability index [25]. Following the same approach for the wind power uncertainty is not adequate, since the wind power takes values from a distribution with unbounded support. On the other hand, choosing arbitrarily some extreme values for the wind power production limits may lead to very conservative conclusions or, in an optimization context, to feasibility problems. Therefore, we follow a probabilistic approach and compute a generation schedule so that the limits of the generating units and the transmission capacity constraints are satisfied with a high probability. To achieve this, a scenario-based technique is adopted [15].

3 Problem Formulation

The main objective is to design a minimum cost day-ahead dispatch while satisfying the N-1 security constraints in a probabilistic sense. For the N-1 security analysis, we take into account any single outage involving the tripping of a line, load generator or wind power generator. Denote then by $I = \{0,1,\ldots,N_{\text{out}}\}$ the outage indices, where the index "0" corresponds to the case of no outage, and N_{out} represents the total number of outages, that is, $N_{\text{out}} = N_G + N_L + N_l + N_w$.

We introduce the superscript i to highlight the dependency of our variables and constant on the corresponding outage. Variable P_G^i denotes the remaining part of PG once one or more generators are tripped due to outage i.

We consider an optimization horizon $N_t = 24$ with hourly steps and introduce the subscript t in our notation to characterize the value of the quantities defined in the previous section for a given time instance $t = 1,\ldots, N_t$. Let C_1, $C_2 \in \mathbb{R}^{N_G}$ be generation cost vectors, and by $[C_2]$ denote a diagonal matrix with vector C_2 on the diagonal. The resulting optimization problem is given by

$$\min_{\{P_{G,t}\}_{t=1}^{N_t}} \sum_{t=1}^{N_t} \left(C_1^T P_{G,t} + P_{G,t}^T [C_2] P_{G,t} \right), \tag{7}$$

subject to

1. Deterministic constraints

These constraints correspond to case where the wind power is equal to its forecasted value.

Power balance constraints: For all $t = 1,\ldots,N_t$ and $i = 0$

$$1_{1\times N_b} \left(C_G^i P_{G,t} + C_w^i P_{w,t}^f - C_L^i P_{L,t} \right) = 0 \tag{8}$$

This constraint encodes the fact that the power balance in the network should be always satisfied when $P_{w,t} = P_{w,t}^f$. In other words, the sum of all generation dispatches of the conventional units and the total wind power production should match the total load of the system.

Generation and transmission capacity constraints: For all $t = 1,\ldots, N_t$ and all $i \in I$

$$\begin{aligned} -\tilde{P}_{\text{line}}^i \;&\leq B_f^i \begin{bmatrix} (\tilde{B}_{\text{BUS}}^i)^{-1} \tilde{P}_t^i \\ 0 \end{bmatrix} \leq \tilde{P}_{\text{line}}^i, \\ P_{\min}^i \leq P_{G,t}^i \;&- d^i P_{\text{mismatch},}^i \leq P_{\max}^i, \end{aligned} \tag{9}$$

where

$\tilde{P}_t^i = \left[C_G^i (P_{G,t}^i - d^i P_{\text{mismatch},t}^i) + C_w^i P_{w,t}^f - C_L^i P_{L,t} \right]_{n-1}$. and $[\cdot]_{\text{n}-1}$ denotes the fact that we eliminate the last row of the quantity inside the brackets. $P_{\min}^i$, $P_{\max}^i$ denote the minimum and maximum generating capacity of each unit, and $\tilde{P}_{\text{line}}^i$ denotes the line capacity limits.

2. Probabilistic constraints

Generation and transmission capacity constraints: For all $t = 1,\ldots, N_t$

$$\begin{aligned} &\mathbb{P}\,(\,P_{w,t} \in \mathbb{R}^{N_w} | - \bar{P}^i_{\text{line}} \;\leq B^i_f \begin{bmatrix} (\tilde{B}^i_{\text{BUS}})^{-1}\tilde{P}^i_t \\ 0 \end{bmatrix} \leq \bar{P}^i_{\text{line}}\,, \\ &\quad P^i_{\min} \leq P^i_{G,t} - d^i\,P^i_{\text{mismatch},} \leq P^i_{\max}, \\ &\quad \forall\; i \in I\,) \;\geq\; 1-\varepsilon, \end{aligned} \tag{10}$$

where $\tilde{P}^i_t = \left[C^i_G(P^i_{G,t} - d^i\,P^i_{\text{mismatch},t}) + C^i_w P_{w,t} - C^i_L P_{L,t}\right]_{n-1}$.

Variable d^i depends on the outage i, since in case of a generator outage, its elements are recalculated so that they sum to one. Matrices B^i_f and $\tilde{B}^i_{\text{BUS}}$ depend on the outage i, since they are both topology-related quantities. Specifically, for a line outage that does not trip a bus, $B^i_f \in \mathbb{R}^{(N_l-1)\times N_b}$ and $\tilde{B}^i_{\text{BUS}} \in \mathbb{R}^{(N_b-1)\times(N_b-1)}$, whereas for a line outage that trips a bus, $B^i_f \in \mathbb{R}^{(N_l-1)\times(N_b-1)}$ and $\tilde{B}^i_{\text{BUS}} \in \mathbb{R}^{(N_b-2)\times(N_b-2)}$. For generation or load single outages, $B^i_f = B^0_f \in \mathbb{R}^{N_l\times N_b}$ and $\tilde{B}^i_{\text{BUS}} = \tilde{B}^0_{\text{BUS}} \in \mathbb{R}^{(N_b-1)\times(N_b-1)}$.

The first constraint inside the probability consists a probabilistic version of the standard transmission capacity constraints for each outage i. It implies that the power flows remain inside the line capacity limits (encoded by $\bar{P}^i_{line}$) with probability at least 1-ε with respect to the underlying wind power distribution. If, for example, $\varepsilon = 0.1$, then constraint Eq. (10) will be satisfied with probability 0.9. The second constraint provides guarantees that the scheduled generation dispatch will not result in a new operating point outside the generation capacity limits.

Note that we are assuming here that all non-scheduled capacity is available as reserves, represented by $d^l\,P^l_{\text{mismatch},t}$, and that this is enough to cover the possible mismatch that may occur. Therefore, when an outage results in a generation–load mismatch, the power balance constraint is trivially satisfied due to Eq. (8).

The resulting problem Eqs. (7)–(10) is a stochastic program with chance constraints and a quadratic objective function. To obtain a solution to this problem, we employ the method described in the following section.

4 Wind Power Modeling and the Scenario Approach

4.1 The Scenario Approach

In the previous section, the problem of identifying a secure generation dispatch to achieve N-1 security was formulated as a stochastic program with chance constraints. The chance constraint implies that for any component outage, the lines do not get overloaded with probability at least 1-ε. To obtain a solution for this problem, we use the so-called scenario approach [15], whose authors proposed and provided a bound for the number of realizations of the uncertain parameter (in this case the wind power) that one should generate in order to substitute the probabilistic constraint with this finite number of hard constraints while offering probabilistic performance

guarantees. That way, the resulting problem can be solved efficiently using existing numerical tools [17]. Following Ref. [16], the number of uncertainty instances that should be generated to maintain these ε-type guarantees is

$$N_s \geq \frac{2}{\varepsilon}\left(\ln\frac{1}{\beta} + N_d\right), \tag{11}$$

where $\varepsilon \in (0,1)$ is the violation parameter determining the desired probability level (see (Eq. 10)). Variable N_d denotes the number of decision variables, which for this case is the number of generation dispatches (i.e. $N_d = N_G$), since the stages in the optimization problem are decoupled. Otherwise, one would have $N_d = N_G N_t$. Although this bound grows linearly with respect to N_d, we can keep the number of generated scenarios, and hence the complexity of the resulting optimization problem, relatively low, since even for large-scale networks N_d still leads to a manageable value for N_s. Parameter β characterizes our confidence regarding the obtained solution and captures the case of a bad multi-sample. In other words, with confidence at least 1- β, the solution of the problem will satisfy the chance constraint with probability at least 1-ε. Note that since β appears inside the logarithm in Eq. (11), high confidence levels could be achieved without increasing the computational burden significantly.

There are two prerequisites to employ the scenario approach. The first requires the underlying optimization program to be convex (the objective function and the formulas inside the probabilistic constraint), which by inspection of the optimization problem of Sect. 3 is satisfied. The second is that we should have a model to generate scenarios for the uncertain parameter, that is, wind power time series in our case.

By inspection of Eq. (11), the number of scenarios that need to be generated to achieve the desired probabilistic guarantees grows with the number of decision variables. Constraint Eq. (10) though, exhibits a specific structure; it is affine with respect to the uncertainty $P_{w,t}$ and there is no bilinearity between the uncertainty and the decision variables. Therefore, instead of enforcing the constraints for each of the extracted scenarios, we could a-priori evaluate the uncertainty function for the Ns samples and keep its row-wise extrema. We then require the constraints to be satisfied only for the constructed values of the uncertainty function, which implies that we only increase the number of constraints by a factor of 2 instead of N_s.

Motivated by this discussion, one can exploit the recent results of Ref. [26], and instead of using the standard scenario approach, a two-step procedure can be followed. For a given ε and β, we first compute probabilistic bounds for $P_{w,t}$, and then use them to compute the solution of the robust counterpart of Eqs. (7)–(10), which will now have hyper-rectangular uncertainty. This reformulation has been already employed in Refs. [20, 21], and allows us to provide probabilistic guarantees even for systems that are non-convex. That way mixed-integer programs, like those arising in unit commitment problems could be captured as well. We will not pursue this discussion here, however, for more details regarding this modification of the standard scenario approach the reader is referred to Ref. [26].

4.2 Wind Power Modeling

We assume that the wind power at every time instance is the sum of the forecasted wind power, as this was disclosed to the operator at the market clearing time in a day-ahead context, and a stochastic component. To model the latter one and generate different wind error realizations, motivated by Papaefthymiou and Klöckli [22], we use a Markov chain mechanism. We used normalized hourly measured wind power data, both forecasts and actual values, for the total wind power infeed of Germany over the period 2006–2011. Following Ref. [22], we discretized the error between the forecast and the actual data to "train" the transition probability matrix, which enables us to generate various wind power error realizations.

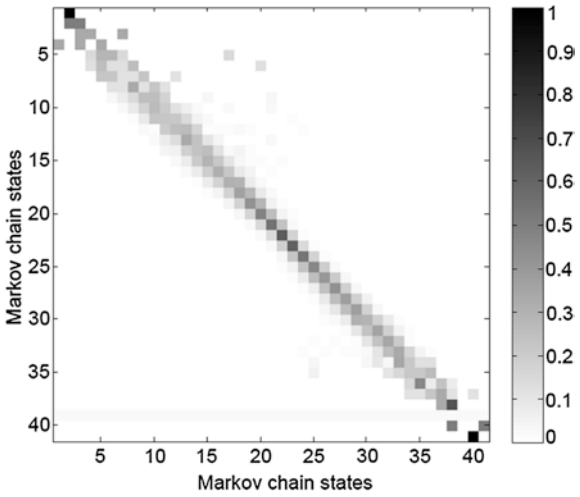

Fig. 1 Top view of the transition probability matrix for the wind power error, using a 41-state Markov chain. The color coding denotes the associated transition probability; *black* corresponds to high, whereas *white* to low probability values

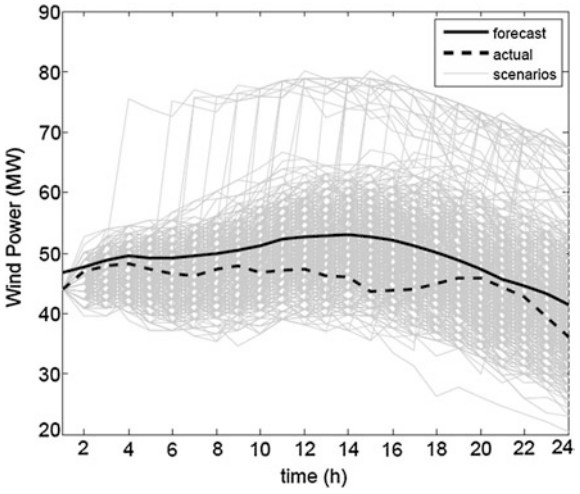

Fig. 2 Forecast (*dashed line*) and actual (*solid black line*) wind power, and 10,000 wind power scenarios (*solid gray lines*) based on different error realizations, initialized with the actual wind power

Figure 1 shows the resulting transition probability matrix, when a 41-state Markov chain is constructed. As noted in Ref. [22], the block triangular structure of the state transition matrix suggests that the wind power error is strongly correlated in time. For a single day of the simulated data, Fig. 2 shows the forecast (solid black line) and the actual (dashed line) wind power, and also 10,000 wind power trajectories (solid gray line), generated by the Markov chain-based model, starting at the real wind power value measured at the initial time.

5 Simulation Results

In this section, we evaluate the performance of our approach by applying it to a modified version of the IEEE 30-bus network Ref. [23], which includes a wind power generator connected at bus 22. A single line diagram of the system is given in Fig. 3, whereas all numerical values for the network data and the cost vectors are retrieved from Ref. [23]. It includes $N_b = 30$ buses, $N_G = 6$ generators, $N_l = 41$ lines and $N_w = 1$ wind power generator. To quantify in terms of probability the improvement afforded by the proposed method, we compare it with what we will refer to as a benchmark approach. The benchmark approach involves solving a deterministic variant of the problem defined in Sect. 3, where only the day-ahead forecast is considered. The system operator would then

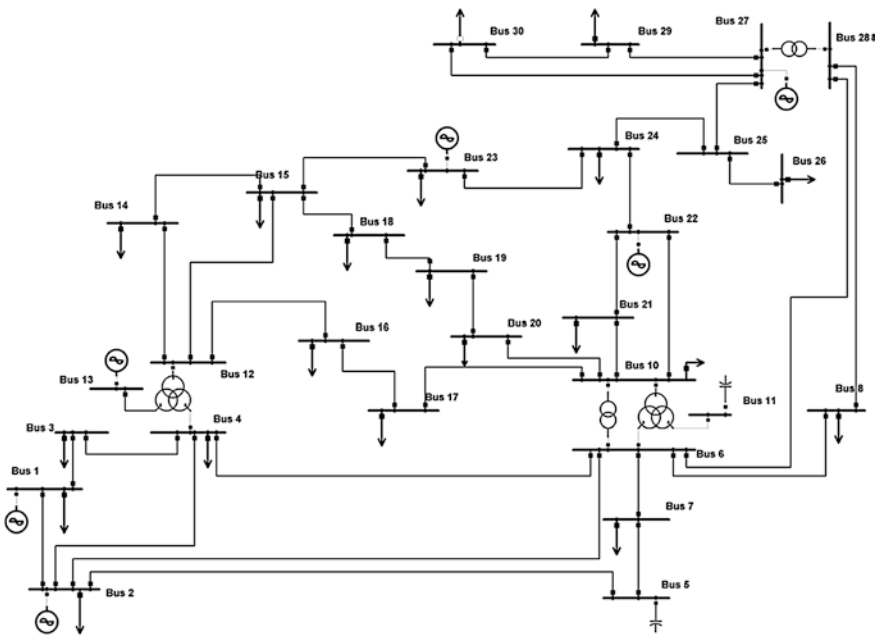

Fig. 3 IEEE 30-bus network with a wind power generator connected to bus 22

run a standard N-1 security routine (i.e., solve Eqs. (7)–(10)) with $\varepsilon = 0$ and $P_{w,t} = P^{f}_{w,t}$ for all $t = 1,\ldots,N_t$). For the robust implementation of our algorithm, the stochastic program Eqs. (7)–(10) were solved using the scenario approach, with $\varepsilon = 0.1$ and $\beta = 10^{-4}$. To compute the numerical solution of the problem, both for the probabilistically robust day-ahead dispatch and the benchmark approach, the solver CPLEX [17] was used via the MATLAB® interface YALMIP [27].

We used the forecast of a single day from the wind power dataset, depicted (together with the 200 scenarios, generated by our Markov chain model and initialized 16 h ahead at the market clearing time) in Fig. 4b. As shown in Fig. 4a, four different profiles, representing how the total load in the system changes over the day, are considered. For each case in Fig. 4a, both the benchmark forecast-based approach and our robust technique are applied. Each dispatch was then tested against 10,000 wind power realizations (not including the 200 scenarios used for the optimization process), representing the potential "actual" wind infeed, and the number of insecure incidents was recorded. With the term insecurity, we refer to the case where after the contingency analysis that was performed, one or more of the lines got overloaded (i.e., the deterministic version of constraint Eq. (10), for $P_{w,t}$ being the "actual" wind power, was violated), for at least one of the N_{out} outages.

Figure 4c, d show the probability of insecure cases, computed as the ratio between the number of identified insecurities over the 10,000 test cases. By inspection of Fig. 4c, d, we can easily deduce that the forecast-based dispatch leads to significantly more line overloadings compared to the proposed robust solution. It is also apparent that the magnitude of the load plays an important role on the frequency of security critical cases. In general, at the time of the day where the load is high, the lines operate closer to their limits, and hence it is more likely to end up with a constraint violation in our contingency check. Note that the load profile L_1 (red) is high over the entire day, leading to an increased number of insecure encounters. From a network perspective, the contingency analysis revealed that lines $10 \rightarrow 22$, $21 \rightarrow 22$, $22 \rightarrow 24$ are the most critical ones in the sense that they are more frequently overloaded in case of an outage. Note that bus 22 is the one where the wind power generator is connected to.

It should be also mentioned that the robust dispatch leads to a much lower number of constraint violations compared to its ε-type theoretical guarantees, confirming that the bound on the number of necessary scenarios proposed by Calafiore and Campi [15] is indeed conservative. Nevertheless, in case tighter guarantees are required, ε could be reduced resulting in a higher value for N_s, without an unaffordable increase in the computational overhead, reducing ε ten-fold requires one to extract ten times more scenarios, leading to a still very much tractable optimization problem.

To further test our algorithm, we considered the load profile L_2 and applied both our robust approach and the benchmark method to compute the generation dispatch for 90 different days of the 2007 data. In a post-processing phase, a contingency analysis was carried out, using the actual wind realization (extracted

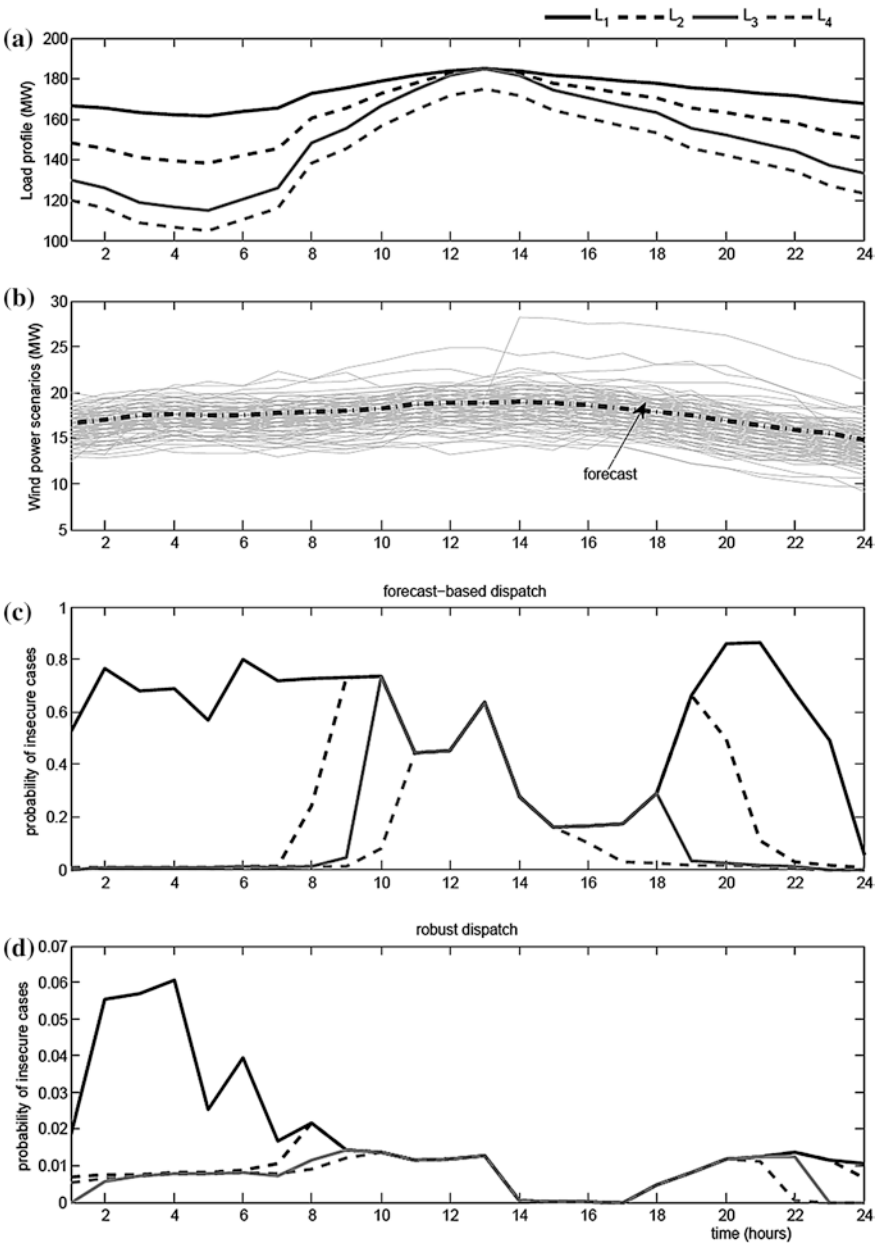

Fig. 4 **a** Four different daily load profiles. **b** Forecast wind power (*black dotted line*) and the generated scenarios (*gray*), based on different error realizations, that were used to construct the robust generation dispatch. **c** Probability of insecure instances estimated by evaluating the generation dispatch and generated by solving a deterministic problem considering only the forecast against 10,000 wind power realizations. The line type corresponds to the different load profiles of Fig. 4a. **d** Probability of insecure instances estimated by evaluating the robust generation dispatch and generated by our proposed methodology against 10,000 wind power realizations

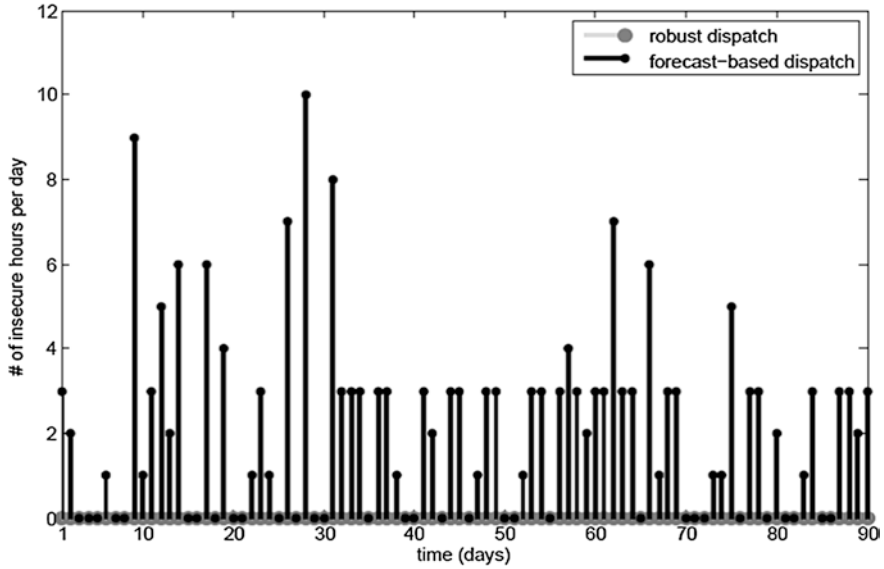

Fig. 5 Number of insecure hours per day for the forecast-based and the proposed robust dispatches, encountered by the contingency analysis using the actual wind power scenarios for 90 days

from the real data) for each day. The obtained results are depicted in Fig. 5. The "red" lines correspond to the case where the forecast-based approach is used and show the total number of hours per day where the system is not N-1 secure. In contrast to our method, which achieves secure operation for all days, the forecast-based approach leads very frequently to insecure incidents. It should be noted that the cases where a low number of insecurities are recorded correspond to situations where the forecasted wind power is very close to its actual value. Day 26 of Fig. 5 corresponds to the day analyzed in Fig. 4 for different load profiles. The average value of line overloadings per day was 2 % of the line capacity limits, high enough to require a preventive action by the system operator. As expected, the daily cost of the proposed solution is higher than the benchmark one, due to presence of additional constraints. However, a maximum difference of 0.6 % was encountered, implying that only small adjustments were needed to design a secure day-ahead dispatch. This additional cost could be thought of as a price to pay for security in networks with high penetration of renewable energy sources (in addition to the cost of reserves).

6 Concluding Remarks

In this chapter, a new methodology for generating a probabilistically robust generation dispatch so as to ensure that the system is N-1 secure under wind uncertainty is proposed. To obtain a solution to this problem, a stochastic chance constrained

optimization program was developed and was solved using the scenario approach. The efficiency of the proposed scheme was evaluated in terms of Monte Carlo simulations on the IEEE 30-bus network and was compared against the solution corresponding to the deterministic variant of the problem.

In this work, no reserve scheduling was considered, and it was assumed that the reserves are bounded by the generating capacity of each unit. In Refs. [20, 21], the current approach was combined with a mechanism for scheduling the reserves (i.e., optimizing also over the distribution vectors). For a more realistic study, apart from the dispatch of the generators additional control inputs could be considered (e.g., topological configuration changes) to provide more freedom when designing an N-1 secure system. An additional research direction is to substitute the underline DC power flow with a convex AC power flow relaxation and investigate the potential of decentralizing developed algorithm.

It should be also noted that increasing the wind power penetration in the network will lead to feasibility problems. Our proposed framework could be used though to provide an indication of the maximum possible wind power infeed, or as a guideline for where to place wind generation or new lines to achieve a secure system.

References

1. Kundur P, Paserba J, Ajjarapu V, Andersson G, Bose A, Canizares C, Hatziargyriou N, Hill D, Stankovic A, Taylor C, Cutsem TV, Vittal V (2004) Definition and classification of power system stability. IEEE Trans Power Syst 19(3):1387–1401
2. Morison K, Kundur P, Wang L (1986) Critical issues for successful online security assessment. In: Savulescu S (ed) Critical issues for successful online security assessment. Springer, New York, pp 147–166
3. Stott B, Alsac O, Monticelli A (1987) Security analysis and optimization. In: Proceedings of the IEEE, vol 75(12). pp 1623–1644
4. Andersson G, Donalek P, Farmer R, Hatziargyriou N, Kamwa I, Kundur P, Martins N, Paserba J, Purbeik P, Sanchez-Gasca J, Schulz R, Stankovic A, Taylor C, Vittal V (2005) Causes of the 2003 major grid blackouts in North America and Europe, and recommended means to improve system dynamic performance. IEEE Trans Power Syst 20(4):1922–1928
5. Hug-Glanzmann G (2008) Coordinated power flow control to enhance steady-state security in power systems, Ph.D. Thesis, ETH Zürich, Nr. 17586
6. Hug-Glanzmann G, Andersson G (2009) N-1 security in optimal power flow control applied to limited areas. IET Gener Transm Distrib 3(2):206–215
7. Zima M (2006) Contributions to security of electric power systems, Ph.D. Thesis, ETH Zürich, Nr. 16492
8. Milano F, Canizares C, Invernizzi M (2005) Voltage stability constrained OPF market models considering N-1 contingency criteria. Electr Power Syst Res 74(1):27–36
9. Bouffard F, Galiana F (2008) Stochastic security for operations planning with significant wind power generation. IEEE Trans Power Syst 23(2):306–316
10. Grijalva S, Dahman S, Patten K, Visnesky A Jr (2007) Large-scale integration of wind generation including network temporal security analysis. IEEE Trans Energy Convers 22(1):181–188
11. Hamidi V, Li F, Yao L (2008) The effect of wind farms location on value of wind by considering security. Power and energy society general meeting–conversion and delivery of electrical energy in the 21st century, pp 1–6

12. Wang Y, Xia Q, Kang C (2011) A novel security stochastic unit commitment for wind-thermal system operation. In: International conference on electric utility deregulation and restructuring and power technologies, vol 1, pp 386–393
13. Ahola A, Haarla L, Matilainen J, Lemström B (2009) Wind power and the (N-1) security of the Finnish transmission grid–a simulation study. In: European wind energy conference and exhibition, EWEC, Elsevier, Europe, pp 1–10
14. Stott B, Jardim J, Alsac O (2009) DC power flow revisited. IEEE Trans Power Syst 24(3):1290–1300
15. Calafiore G, Campi MC (2006) The scenario approach to robust control design. IEEE Trans Autom Control 51(5):742–753
16. Campi MC, Garatti S, Prandini M (2009) The scenario approach for systems and control design. Annu Rev Control 33(1):149–157
17. ILOG.SA (2008) CPLEX11.0 user's manual. Technical report, France
18. Vrakopoulou M, Margellos K, Lygeros J, Andersson G (2012) Probabilistic guarantees for the N-1 security of systems with wind power generation. In: International conference on probabilistic methods applied to power systems, pp 853–863
19. Margellos K, Haring T, Hohayem P, Schubiger M, Lygeros J, Andersson G (2012) A robust reserve scheduling technique for power systems with high wind penetration. In: International conference on probabilistic methods applied to power systems, pp 870–875
20. Vrakopoulou M, Margellos K, Lygeros J, Andersson G (2012) A probabilistic framework for security constrained reserve scheduling of networks with wind power generation. In: IEEE international energy conference and exhibitionpp, pp 508–513
21. Vrakopoulou M, Margellos K, Lygeros J, Andersson G A (2012) probabilistic framework for reserve scheduling and N-1 security assessment of systems with high wind power penetration. In: Submitted to IEEE PES Transactions on Power Systems
22. Papaefthymiou G, Klöckli B (2008) MCMC for wind power simulation. IEEE Trans Energy Convers 23(1):234–240
23. Zimmerman RD, Murillo-Sanchez CE, Thomas RJ (2011) MATPOWER: Steady-state operations, planning, and analysis tools for power systems research and education. IEEE Trans Power Syst 26(1):12–19
24. Andersson G (2012) Power system analysis, lecture notes. ETH Zürich, Zürich
25. Yang F, Meliopoulos A, Kokkinides G, Stefopoulos G (2006) Security–constrained adequacy evaluation of bulk power system reliability. In: International conference on probabilistic methods applied to power systems 2006:1–8
26. Margellos K, Goulart P, Lygeros J (2012) On the road between robust optimization and the scenario approach for chance constrained optimization problems. In: Submitted to IEEE Transactions on Automatic Control
27. Löfberg J (2005) YALMIP: a toolbox for modeling and optimization in MATLAB", IEEE. In: International symposium on computer aided control systems design, pp 284–289

Adequacy and Security Measures in Integrated Intermittent Renewable Generation Systems

Wijarn Wangdee, Roy Billinton and Wenyuan Li

1 Introduction

Substantial integration of intermittent renewable energy resources such as wind generation in electric power systems dictates the need to investigate the system reliability implications when adding large amounts of highly variable capacity that differ considerably from conventional generation sources. In order to accomplish this, utilizing a systematic approach to effectively capture the overall reliability measures of a system containing large amounts of intermittent renewable energy sources is required.

In general, power system reliability can be subdivided into the two fundamental aspects:system adequacy and system security [1]. System adequacy relates to the existence of sufficient facilities within the system to satisfy the consumer demand load whereas system security relates to the ability of the system to respond to disturbances arising within that system. Wind power generation can provide capacity contribution to the overall system reserve from both adequacy and security standpoints [2]. This chapter applies system well-being analysis [3–11] to encapsulate both generation adequacy and security concerns in order that meaningful comparisons of the overall reliability impacts of intermittent renewable energy sources and conventional

W. Wangdee (✉) · W. Li
BC Hydro and Power Authority, Vancouver, BC, Canada
e-mail: wijarn.wangdee@bchydro.com

W. Li
e-mail: wen.yuan.li@bchydro.com

R. Billinton
Power System Research Group, Department of Electrical and Computer Engineering, University of Saskatchewan, Saskatoon, Canada
e-mail: roy.billinton@usask.ca

R. Billinton et al. (eds.), *Reliability and Risk Evaluation of Wind Integrated Power Systems*, Reliable and Sustainable Electric Power and Energy Systems Management,
DOI: 10.1007/978-81-322-0987-4_6, © Springer India 2013

generation can be assessed. A deterministic security criterion of the loss of the largest online generating unit, which is widely used by many Canadian electric utilities [6, 12], is considered in the study as a security measure for contingency reserve in system operation. The healthy state probability index is used as a security benchmark to indicate the operational reliability, and the at-risk state probability index, which is a loss of load probability (LOLP) indicator, is used as the adequacy criterion to indicate the long-term planning reliability. A sequential Monte Carlo simulation technique was utilized in the study in this chapter as this technique is ideally suited to the chronological analysis of intermittent resources such as wind power. The sequential simulation approach also provides accurate frequency and duration assessments of the system reliability indices [13, 14]. An auto-regressive moving average (ARMA) time series model was utilized to simulate hourly wind speeds [15]. Historical wind speeds from actual multiple wind farms were used in the studies. The study results are demonstrated using two test systems designated as the Roy Billinton Test System (RBTS) [16] and IEEE-RTS [17].

It should be noted that there are various types of intermittent renewable energy sources such as wind, solar, run-of-river hydro, tidal and wave generators, etc. The basic study methodology used in this chapter can also be applied to consider these intermittent renewable sources. This chapter is focused on the application to wind power generation and uses its intermittent and diffuse nature to illustrate the characteristics of intermittent renewable energy sources that behave quite differently from conventional generating sources.

2 Wind Power Generation Model

The wind generation model fundamentally consists of two main parts designated as the wind speed model and the wind farm model. These two parts are briefly described as follows.

2.1 Wind Speed Modeling

An important requirement in incorporating wind power generation in power system reliability analysis using sequential Monte Carlo simulation is to realistically simulate the hourly wind speed in a chronological manner. Wind speed varies with time and geographical site and at a specific hour is influenced by the wind speeds of the immediate previous hours. Wind speed models, therefore, have unique characteristics that are highly dependent on site locations. An ARMA time series model [15] was used to simulate hourly wind speeds of specified wind farm sites. Hourly wind speed time data from 2004 to 2006 (3 year time series) obtained from National Renewable Energy Laboratory [18] were used in the ARMA model development. Wind speed data for the three selected locations used in the study are shown in

Table 1 Wind speed data at the three different sites

Wind farm sites (name)	Site M1	Site M2	Site O1
Mean wind speed (m/s)	9.10	8.38	10.03
Standard deviation (m/s)	5.50	4.48	5.20
Geographical location	Mountain	Mountain	Offshore
Correlation w.r.t. Site M1	1.00	0.85	0.05

Table 1. Wind speed correlation was applied when considering the multiple-wind-farm scenarios in the study, that is, a three-wind-farm scenario considers the wind speed correlation among Sites M1, M2 and O1 as noted in Table 1.

2.2 Wind Farm Modeling

The power output characteristics of a wind turbine generator (WTG) basically differ from those of conventional generating units. The wind speed has a major influence on the power output. There is a nonlinear relationship between the power output of the WTG and the wind speed. Instead of using a single wind turbine power curve, an entire wind farm power curve (aggregation of multiple wind turbines) was utilized in this study to represent the operational parameters of the combined individual WTG units located in that wind farm. The wind farm power curve for Site M1 is shown in Fig. 1. The hourly power output of the wind farm can be obtained from the simulated hourly wind speed using Eq. (1).

$$P\left(\mathrm{SW}_t\right) = \begin{cases} 0 & 0 \le \mathrm{SW}_t < 3 \\ \left(A + B \times \mathrm{SW}_t + C \times \mathrm{SW}_t^2 + D \times \mathrm{SW}_t^3\right) \times P_r & 3 \le \mathrm{SW}_t < 16 \\ P_r & 16 \le \mathrm{SW}_t < 25 \\ (E + F \times \mathrm{SW}_t) \times P_r & 25 \le \mathrm{SW}_t < 28 \\ 0 & \mathrm{SW}_t \ge 28 \end{cases} \tag{1}$$

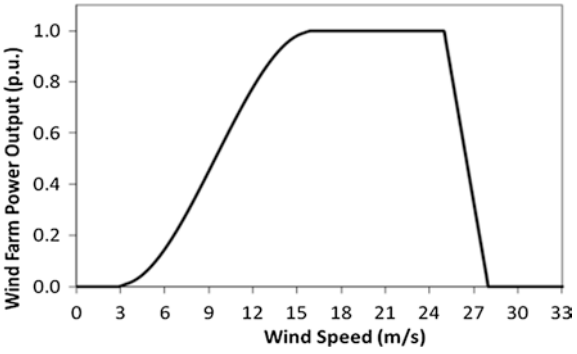

Fig. 1 Wind farm power curve for Site M1

where P_r and SW_t are the rated power output of the WTG and the hourly simulated wind speed, respectively. The constants *A, B, C, D, E* and *F* were obtained using curve-fitting analysis of the historical wind farm power output information. The *A, B, C, D, E* and *F* values for Site M1 are 0.1829, −0.1268, 0.0255, –0.0009, 9.3130 and –0.3326, respectively. Wind farm power curves and associated parameters for Sites M2 and O1 were derived in a similar manner. The WTG units used in the study are assumed to have rated capacities from 0.2 to 2 MW for the RBTS and assumed to have rated capacities from 1 to 4 MW for the IEEE-RTS. The failure rates and average repair times for all WTG units are 2 failures/year and 44 h, respectively.

3 Study Systems and Methodology

3.1 Study Systems

The RBTS [16] and the IEEE Reliability Test System (IEEE-RTS) [17] were used in the study. The RBTS is a six-bus system composed of 11 generating units. The system peak load is 185 MW, and the total generation is 240 MW. The capacity of the largest unit in the RBTS is 40 MW. The IEEE-RTS is a 24-bus system consisting of 32 generating units. The system peak load is 2,850 MW, and the total generation is 3,405 MW. The capacity of the largest unit in the IEEE-RTS is 400 MW. Sequential simulation was used in this study, and therefore, the detailed load characteristics considering different customer types at individual load buses can be incorporated in the system coincident load. The individual bus load models were developed using a bottom-up approach [19], which recognizes the individual customer sector characteristics at each bus, and therefore, the system coincident peak and chronological load curves differ from those described in [16, 17] in which all the load buses are modeled using the same chronological load profile as the entire system load profile.

3.2 Study Methodology

Well-being analysis was utilized in this study, and the fundamental model is shown in Fig. 2. The system well-being method offers a combined framework that incorporates both deterministic and probabilistic considerations. The combined deterministic and probabilistic perception occurs through the definition of the system operating states [6]. The system well-being designated by the accepted deterministic criteria is categorized as being healthy, marginal and at-risk states. A system operates in the healthy state when it has enough capacity reserve to meet a deterministic criterion such as the loss of the largest online generating unit. In the marginal state, the system is not in any trouble but does not have sufficient margin to meet the specified deterministic criterion. The system is in the at-risk state if the load exceeds the available capacity. The probability of being in the at-risk state is the traditional LOLP.

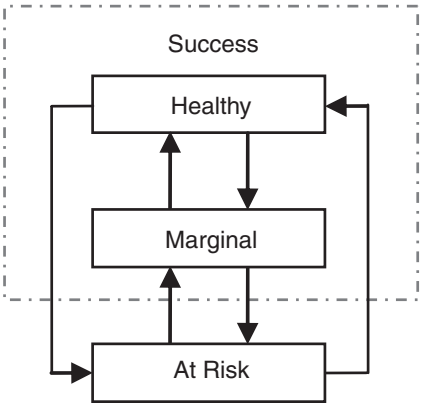

Fig. 2 System well-being analysis framework

In the system well-being analysis presented in this chapter, the amount of generation capacity reserve required is determined by the capacity of the largest operating (online) unit at a particular point in time. This implies that the capacity of the largest available generating unit may not be the same under different generation system states. Throughout the total period of study, the generating capacity reserve is compared against the capacity of the largest operating unit at each particular hour to determine the health, margin and at-risk states. The details of the methodology of system well-being analysis applied to the generation system reliability evaluation can be found in [3, 8].

The system well-being analysis framework can provide comprehensive knowledge on what the degree of system vulnerability might be under a particular system condition. It gives system engineers and risk managers with a quantitative interpretation of the degree of system security (N-1, healthy) and insecurity (marginal) in addition to the traditional risk measure.

The degree of system well-being can be quantified in the form of the probabilities, frequencies and durations of the healthy, marginal and at-risk states defined as follows:

P_H *Healthy state probability* (*/year*)
P_M *Marginal state probability* (*/year*)
P_R *At-risk state probability* (*/year*)
F_H *Healthy state frequency* (*occurrences/year*)
F_M *Marginal state frequency* (*occurrences/year*)
F_R *At-risk state frequency* (*occurrences/year*)
D_H *Healthy state duration* (*hours/occurrence*)
D_M *Marginal state duration (hours/occurrence)*
D_R *At-risk state duration* (*hours/occurrence*)

In this chapter, the at-risk state probability (P_R) and the healthy state probability (P_H) indices, respectively, are used as the reference points to measure the same system adequacy and security.

4 RBTS Study Results

4.1 Adequacy-Based Comparison

Table 2 presents the system well-being indices of the original RBTS and the modified RBTS in which the three scenarios are considered: (1) adding a conventional generating unit, (2) adding three wind farms, (3) replacing an existing conventional generating unit by the three wind farms. The results shown in Table 2 were obtained on the basis of maintaining the same adequacy level ($P_R = 0.00043$ or 3.76 h/year). Adding new generation to the system while maintaining the system load at the original level will result in system reliability improvement (i.e., P_R reduced). In order to preserve the reliability level at the reference point (either P_R-based or P_H-based), the system load has to be scaled up to a certain level when adding new generation so that the system reliability can be maintained at the same level as that in the original system with the 1.0 per unit load level. As shown in Table 2, the system load levels in Cases A1 and A2 were scaled up to the 1.1156 per unit load level when adding the conventional unit and when adding the wind farms capacities, respectively. The increased load associated with adding the new generation is considered as the effective load-carrying capability. In order to provide a reasonable comparison between the conventional generation addition scenario (Case A1) and the wind generation addition scenario (Case A2), the system loads in both cases have been scaled up to the same level (i.e., 1.1156 p.u.), which implies that the effective load-carrying capability obtained from adding a 20-MW conventional unit is the same as that provided by adding 3 × 21.2 MW wind farms.

A similar approach was applied in other case studies associated with adding new generation discussed later in this chapter where the system load is scaled up in order that the specified reliability can be maintained at a similar level to that in the original system.

Table 2 Well-being indices of the RBTS for different generation scenarios based on the specified adequacy level

Index	Base case	Case A1	Case A2	Case A3
P_H	0.98456	0.98511	0.98053	0.98054
P_M	0.01501	0.01445	0.01904	0.01903
P_R	***0.00043***	***0.00043***	***0.00043***	***0.00043***
F_H	25.1	22.4	35.3	33.5
F_M	25.8	23.1	36.1	34.3
F_R	0.8	0.7	1.0	1.0
D_H	403.2	456.3	267.4	285.2
D_M	5.1	5.4	4.6	4.8
D_R	4.6	4.8	3.6	3.8

Base case: Original system without wind power generation
Case A1: Add a 20-MW conventional unit @ 1.1156 p.u. load level
Case A2: Add 3 × 21.2 MW wind farms @ 1.1156 p.u. load level
Case A3: Replace a 20-MW conv. unit by 3 × 21.0 MW wind farms

It should be noted that the amount of wind power capacity required in the case of adding wind generation (Case A2) and that required in the case of replacing an existing conventional unit by wind generation (Case A3) for maintaining the same system reliability is not necessarily equal. In this particular example, they are very close as the difference is masked due to sufficient total generation capacities in the RBTS. The difference in the two similar cases for the IEEE-RTS in the next section will, however, be larger.

The results in Table 2 show that when maintaining the system adequacy level at P_R of 0.00043, the P_H of Cases A2 and A3 associated with wind power generation is lower than the Base Case P_H. This outcome indicates that the system security level is not retained by adding only wind generation to maintain the specified adequacy level. Table 2 also shows that the frequency indices (F_H, F_M and F_R) increase for Cases A2 and A3 compared to those in the Base Case and that the system states are more dynamic when integrating wind power generation as there are more movements between the healthy and marginal states compared to the Base Case. In other words, the system containing wind generation can move more frequently to the marginal state where the system is still adequate but not as secure as before. As a result of the increase in system state movements, the average residence time in each system state decreases. This conclusion is, however, not true for Case A1 when adding a conventional unit in which F_H, F_M and F_R slightly decrease resulting in a slightly increase in the average residence time in each system state. In addition, the P_H of Case A1 is slightly higher than the Base Case P_H. This indicates that the system security level can be retained (even further improved) when adding conventional generation to maintain the specified adequacy level.

4.2 Security-Based Comparison

In Table 3, the system security level is maintained ($P_H = 0.98456$) in all the cases. Under this condition, the system requires more wind power generation capacity in Cases S2 and S3 compared to the adequacy-based cases shown in Table 2.

When integrating wind power generation to the system (Cases S2 and S3), P_R decreases whereas P_M increases. This implies that while maintaining the same security level for the cases containing wind power generation, there is probability movement from the at-risk state (where the system is inadequate and insecure) to the marginal state (where the system is adequate but not secure) leading to an improvement in system adequacy compared to the Base Case. This is beneficial from the long-term capacity planning viewpoint. However, F_H and F_M for Cases S2 and S3 shown in Table 3 are still greater than those of the Base Case, which implies that system operation performance is still adversely influenced by wind power integration since it leads to more frequent movements from the healthy state to the marginal state where the system is insecure. The D_H of Cases S2 and S3 shown in Table 3 increases compared to those in Table 2, which implies that the average duration for the system to reside in the healthy state is improved

Table 3 Well-being indices of the RBTS for different generation scenarios based on the specified security level

Index	Base case	Case S1	Case S2	Case S3
P_H	***0.98456***	***0.98456***	***0.98456***	***0.98456***
P_M	0.01501	0.01500	0.01510	0.01512
P_R	0.00043	0.00044	0.00034	0.00032
F_H	25.1	24.8	30.6	27.8
F_M	25.8	25.6	31.4	28.3
F_R	0.8	0.8	0.8	0.8
D_H	403.2	404.3	312.5	350.8
D_M	5.1	5.1	4.2	4.6
D_R	4.6	4.5	3.4	3.6

Base case: Original system without wind power generation
Case S1: Add a 20-MW conventional unit @ 1.1193 p.u. load level
Case S2: Add 3 × 27.2 MW wind farms @ 1.1193 p.u. load level
Case S3: Replace a 20-MW conv. unit by 3 × 27.0 MW wind farms

(staying longer per visit). However, the D_H of Cases S2 and S3 are still shorter than those of the Base Case due to the increased frequency of movements between the healthy and marginal states. This indicates that the frequency and duration indices of the RBTS could still be unfavorably affected by wind generation integration even though both system adequacy (P_R) and security (P_H) levels are well maintained.

Table 3 also indicates that all the indices of Case S1 are very similar to those of the Base Case, which implies that the adding conventional generation does not adversely affect the system reliability from either adequacy or security standpoints.

4.3 System Well-Being Index Probability Distributions

The results shown in Tables 2 and 3 are based on the average or expected values of the well-being indices. One advantage when utilizing sequential Monte Carlo simulation in system well-being analysis is the ability to provide system well-being index probability distributions associated with the expected values. The system well-being index probability distributions, which provide a pictorial representation of the annual variability of the indices, are illustrated in this section. The probability distributions of the overall system well-being indices in Tables 2 and 3 are graphically presented in Figs. 3 and 4, respectively. Reliability index probability distributions are normally expressed as histograms using discrete intervals (bins). The probability distributions shown in this chapter are, however, presented using approximate continuous distributions for illustration purposes rather than histograms, which facilitate comparisons among the various scenario results on the same axis. In order to differentiate the expected values of the system well-being indices described in Sect. 3 B from the representation of the system well-being

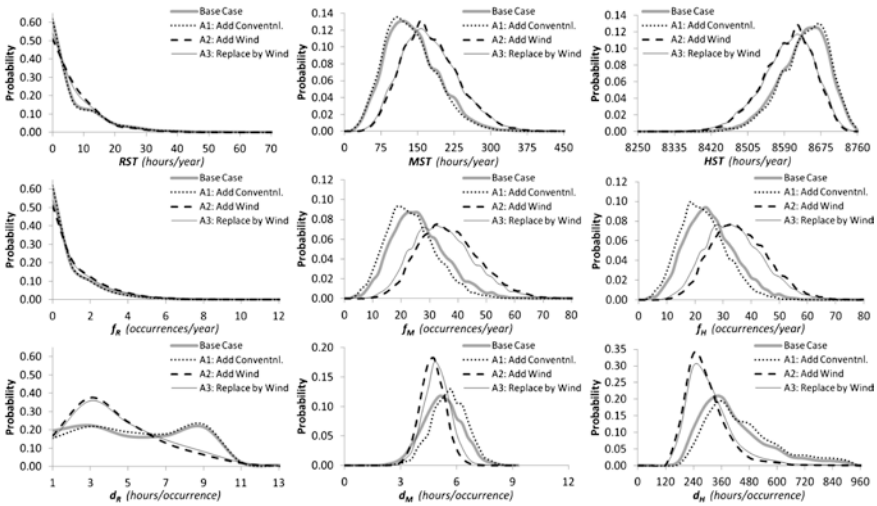

Fig. 3 System well-being index probability distributions of the RBTS associated with different generation scenarios while maintaining the specified adequacy level, $P_R = 0.00043$

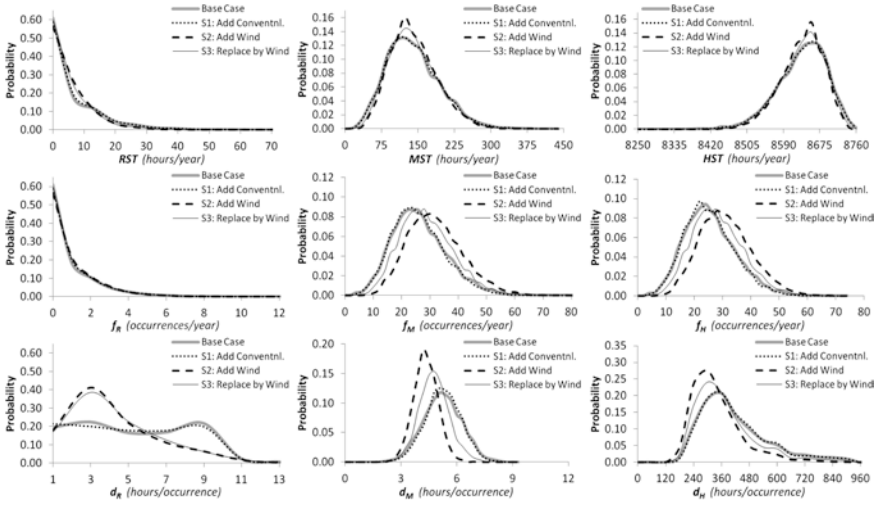

Fig. 4 System well-being index probability distributions of the RBTS associated with different generation scenarios while maintaining the specified security level, $P_H = 0.98456$

index probability distributions, the symbols used to represent the annual variability (probability distribution) of the system well-being indices are as follows:

HST	*Annual healthy state time* (*hours/year*)
MST	*Annual marginal state time* (*hours/year*)
RST	*Annual at-risk state time* (*hours/year*)
f_H	*Annual healthy state frequency* (*occurrence/year*)

f_M *Annual marginal state frequency* (*occurrence/year*)
f_R *Annual at-risk state frequency* (*occurrence/year*)
d_H *Annual healthy state duration* (*hours/occurrence*)
d_M *Annual marginal state duration* (*hours/occurrence*)
d_R *Annual at-risk state duration* (*hours/occurrence*)

Note that the *HST*, *MST* and *RST* indices were obtained by multiplying the relevant state probability by 8,760 in order to present the indices in a form of the state time in hours per year.

Figure 3 indicates that although the expected values of P_R for all the four cases are the same ($P_R = 0.00043$), their probability distribution profiles are different. The *RST* distribution profiles of the Base Case and Case A1 (adding conventional generation) are very similar, but different from those of Cases A2 and A3, which have wind power integration. It is interesting to note that the probability of having $RST = 0$ (no loss of load) for the system with wind power integration is reduced compared to the Base Case. In other words, the integrated wind power system will be more likely to encounter the loss of load situation ($RST > 0$) in each year than the system with no wind power integration. For example, the probability of having $RST = 0$ for the Base Case is greater than 0.60 whereas that for Cases A2 and A3 is only about 0.50. As previously mentioned, the system security level is not retained in the integrated wind power system while maintaining the specified adequacy level. Figure 3 clearly shows that the *HST* distribution profiles of Cases A2 and A3 shift to the left compared to that of the Base Case. Figure 3 also shows that the f_H distribution profiles of the systems containing wind power generation (Cases A2 and A3) have more dispersion and, therefore, more uncertainty with lower predicted probability of occurrence compared to those of the Base Case.

In Fig. 4, where the four generation scenarios are considered based on the same expected system security level ($P_H = 0.98456$), the *HST* distribution profiles of the four cases are quite similar. The f_H distribution profiles of the four cases also have a similar degree of dispersion. It is interesting to note that even though the expected values of P_R for the systems with wind power integration (Cases S2 and S3) are lower than that of the Base Case, the probabilities of having $RST = 0$ for Cases S2 and S3 are now closer to the Base Case than those shown in Fig. 3. This means that the integrated wind power system could increase the likelihood of having the no loss of load situation ($RST = 0$) in each year, to be similar to the system without wind power integration, by designing the system to maintain the system security level instead of solely designing it to maintain the system adequacy level.

5 IEEE-RTS Study Results

The IEEE-RTS Base Case is not as secure (or not as healthy) as the RBTS Base Case from a system operation viewpoint, because the P_H of the IEEE-RTS is lower than that of the RBTS. This indicates that there is a greater chance for

the IEEE-RTS to reside in states that are inadequate (P_R) and/or insecure (P_M) compared to the RBTS. The fundamental reasons are that the IEEE-RTS is a more generation deficient system than the RBTS and the forced outage rate of the largest generating unit in the IEEE-RTS is much greater than that of the largest generating unit in the RBTS.

5.1 Adequacy-Based Comparison

Table 4 presents the system well-being indices of the original IEEE-RTS and the modified IEEE-RTS cases based on maintaining the same adequacy level ($P_R = 0.00355$ or 31.10 h/year).

The results in Table 4 indicate that although P_R for all the cases are the same, the P_H values of Cases A2 and A3 containing wind power generation are both lower than the P_H of the Base Case, which indicates that the system security level cannot be retained when integrating wind generation to maintain the specified adequacy level. The F_R values of Cases A2 and A3 are quite similar to the Base Case value, but F_H and F_M of Cases A2 and A3 are greater than those of the Base Case, which indicates that there are more frequent movements between the healthy and marginal states for the system containing wind generation. The increase in system state movements results in a decrease in the average residence time in each system state. This is, however, not the case when adding conventional generation (Case A1) where F_H, F_M, F_R as well as D_H, D_M, D_R are relatively similar to those of the Base Case. In addition, the P_H of Case A1 is slightly higher than the P_H of the Base Case. This implies that the system security level can also be retained (even further improved) when adding conventional generation to maintain the specified adequacy level.

Table 4 Well-being indices of the IEEE-RTS for different generation scenarios based on the specified adequacy level

Index	Base case	Case A1	Case A2	Case A3
P_H	0.95961	0.96053	0.94183	0.94022
P_M	0.03684	0.03592	0.05462	0.05623
P_R	***0.00355***	***0.00355***	***0.00355***	***0.00355***
F_H	76.4	76.7	100.3	100.2
F_M	80.1	79.9	106.5	106.8
F_R	8.2	8.3	8.2	8.1
D_H	120.5	119.9	87.0	87.0
D_M	4.0	3.9	4.5	4.6
D_R	3.5	3.5	3.5	3.6

Base case: Original system without wind power generation
Case A1: Add a 155-MW conventional unit @ 1.0575 p.u. load level
Case A2: Add 3 × 139 MW wind farms @ 1.0575 p.u. load level
Case A3: Replace a 155-MW conv. unit by 3 × 133 MW wind farms

5.2 Security-Based Comparison

When the system is held at the same security level ($P_H = 0.95961$) as shown in Table 5, the P_R values of Cases S2 and S3 are lower while the P_M are greater than that of the Base Case, which indicates that the system containing wind generation is more adequate than the Base Case, as there is probability movement from the at-risk state to the marginal state resulting in a lower risk of load curtailment. The F_H, F_M and D_H values for Cases S2 and S3 are relatively similar to those of the Base Case, whereas there is an improvement in F_R in Cases S2 and S3 compared to the Base Case. It should be noted, however, that the amount of wind generation required under the security-based consideration (Table 5) is significantly increased compared to the amount of wind generation required under the adequacy-based consideration (Table 4). This implies that the system security level of the IEEE-RTS can be more critically affected by wind power integration than that of the RBTS if only the adequacy-based consideration is used to maintain the system reliability.

5.3 System Well-Being Index Probability Distributions

The probability distributions of the system well-being indices given in Tables 4 and 5 are graphically presented in Figs. 5 and 6, respectively. Figure 5 shows the system well-being index probability distributions for the four generation scenarios of the IEEE-RTS obtained on the basis of maintaining the same expected value of system adequacy level ($P_R = 0.00355$). The probability of having $RST = 0$ for the IEEE-RTS with and without wind power integration are quite similar. The *HST* distribution profiles for the wind power integration scenarios (Cases A2 and A3) shift

Table 5 Well-being indices of the IEEE-RTS for different generation scenarios based on the specified security level

Index	Base case	Case S1	Case S2	Case S3
P_H	***0.95961***	***0.95961***	***0.95961***	***0.95961***
P_M	0.03684	0.03673	0.03815	0.03825
P_R	0.00355	0.00366	0.00224	0.00214
F_H	76.4	78.5	77.0	75.4
F_M	80.1	81.7	81.2	79.8
F_R	8.2	8.6	5.6	5.3
D_H	120.5	116.9	117.1	119.8
D_M	4.0	3.9	4.1	4.2
D_R	3.5	3.5	3.3	3.3

Base case: Original system without wind power generation
Case S1: Add a 155-MW conventional unit @ 1.0592 p.u. load level
Case S2: Add 3 × 233 MW wind farms @ 1.0592 p.u. load level
Case S3: Replace a 155-MW conv. unit by 3 × 227 MW wind farms

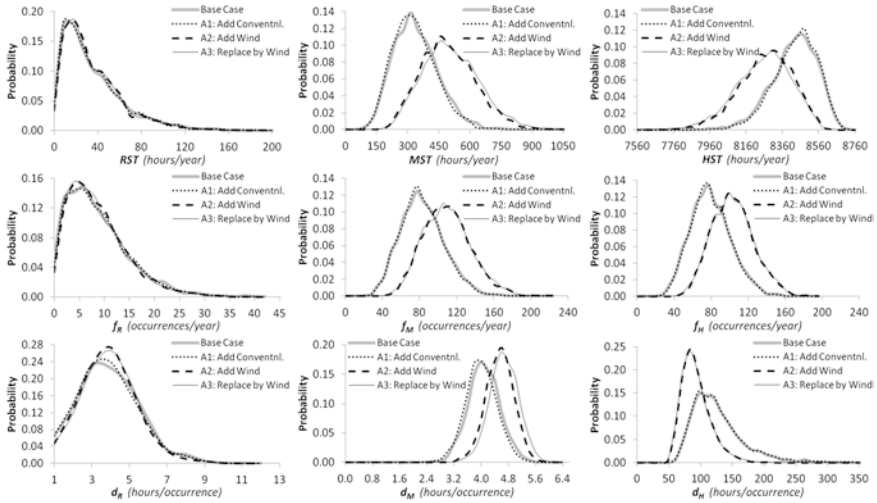

Fig. 5 System well-being index probability distributions of the IEEE-RTS associated with different generation scenarios while maintaining the specified adequacy level, $P_R = 0.00355$

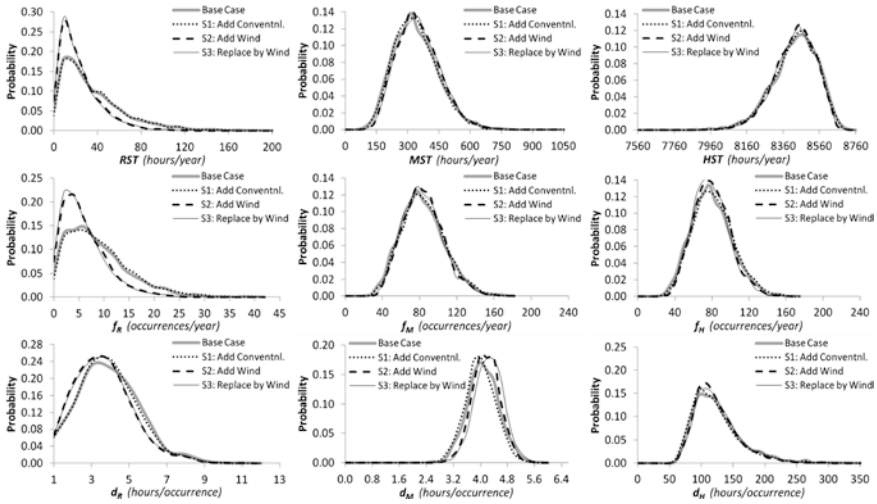

Fig. 6 System well-being index probability distributions of the IEEE-RTS associated with different generation scenarios while maintaining the specified security level, $P_H = 0.95961$

to the left and have more dispersion compared to those for the cases without wind power integration (Base Case and Case A1).

In Fig. 6, where the four generation scenarios are evaluated based on the same expected system security level ($P_H = 0.95961$), the *HST* distribution profiles of the four cases are quite similar. The *RST* distribution profiles for the system with wind

power integration (Cases S2 and S3) obviously shift to the left, which indicates a considerable improvement on the system adequacy. Nonetheless, the probability of having $RST = 0$ (no loss of load situation) in each year for the system with a large amount of wind power integration does not improve, even with significant wind power integration, compared to the cases without wind power integration. It should be emphasized that the probability distribution profiles of Case A1 (adding conventional generation) shown in Figs. 5 and 6 are very similar to those of the Base Case.

6 Conclusions

This chapter investigates the reliability impacts of an intermittent renewable energy resource, in this case wind power generation, from both generation adequacy and security perspectives. The system well-being analysis approach was utilized in the studies to provide quantitative knowledge from both reliability perspectives. The results based on the RBTS and IEEE-RTS indicate that the system adequacy and security levels can be well maintained when adding conventional generating units. This is, however, not the case for the wind generation integrations where the system security level could deteriorate considerably due to wind generation integration, even though the specified system adequacy level can be maintained to satisfy the long-term capacity planning reserve requirement. The degree of security degradation is, however, system dependent. The impact of wind generation integration from both system adequacy and security standpoints should be investigated and comprehended in order that the system reliability from both long-term planning and operational points of view are not compromised.

References

1. Billinton R, Allan RN (1996) Reliability evaluation of power systems, 2nd edn. Plenum Press, New York
2. Wangdee W and Billinton R (2012) Probing the intermittent energy resource contributions from generation adequacy and security perspectives. IEEE Trans Power Syst 27(4):2306–2313
3. Billinton R, Fotuhi-Firuzabad M (1994) Basic framework for generating system operating health analysis. IEEE Trans Power Syst 9(3):1610–1617
4. Billinton R, Fotuhi-Firuzabad M, Aboreshaid S (1997) Power system health analysis. Reliab Eng Syst Saf 55(1):1–8
5. Billinton R, Fotuhi-Firuzabad M (1996) Reserve capacity assessment in small isolated electric power generating systems. Power Eng J 10(2):73–80
6. Billinton R, Karki R (1999) Capacity reserve assessment using system well-being analysis. IEEE Trans Power Syst 14(2):433–438
7. Billinton R, Karki R (1999) Application of Monte Carlo simulation to generating system well-being analysis. IEEE Trans Power Syst 14(3):1172–1177
8. Bagen (2005) Reliability and cost/worth evaluation of generating systems utilizing wind and solar energy, Ph.D. thesis. University of Saskatchewan, Canada, [Online]. Available: http://library.usask.ca/theses/available/etd-08242005-211402/unrestricted/ Bagen_PhD_Thesis.pdf

9. Billinton R, Lian G (1994) Composite power system health analysis using a security constrained adequacy evaluation procedure. IEEE Trans Power Syst 9(2):936–941
10. da Silva AML, de Resende LC, Manso LAF, Billinton R (2004) Well-being analysis for composite generation and transmission systems. IEEE Trans Power Syst 19(4):1763–1770
11. Wangdee W, Billinton R (2006) Bulk electric system well-being analysis using sequential Monte Carlo simulation. IEEE Trans Power Syst 21(1):188–193
12. GE Energy Project Team (2006) Final report to: Ontario power authority (OPA), independent electricity system operator (IESO), Canadian wind energy association (CanWEA) for Ontario wind integration study. [Online]. Available: http://www.uwig.org/OPA-Report-200610-1.pdf
13. Billinton R, Li W (1994) Reliability assessment of electrical power systems using Monte Carlo methods. Plenum Publishing, New York
14. Billinton R, Wangdee W (2005) Impact of utilizing sequential and non-sequential simulation techniques in bulk electric system reliability assessment. Proc Inst Elect Eng Gen Transm Distrib 152(5):623–628
15. Billinton R, Chen H, Ghajar R (1996) Time-series models for reliability evaluation of power systems including wind energy. Microelectron Reliab 36(9):1253–1261
16. Billinton R et al (1989) A reliability test system for educational purposes - basic data. IEEE Trans Power Syst 4(3):1238–1244
17. IEEE Task Force (1979) IEEE reliability test system. IEEE Trans Power App Syst PAS-98(6):2047–2054
18. Wind Integration Datasets: Western wind dataset. National renewable energy laboratory (NREL). [Online]. Available: http://www.nrel.gov/wind/integrationdatasets/western/methodology.html
19. Sankarakrishnan A, Billinton R (1995) Sequential Monte Carlo simulation for composite power system reliability analysis with time varying loads. IEEE Trans Power Syst 10(3):1540–1545

Representation of Wind and Load Correlation in Non-Sequential Monte Carlo Reliability Evaluation

Carmen L. T. Borges and Julio A. S. Dias

1 Introduction

Probabilistic reliability evaluation of power systems can be performed by two distinct representations of the system: state space and chronological simulation. In the state space representation, the system states are randomly sampled by non-sequential Monte Carlo simulation (MCS). In the chronological representation, the states are sequentially sampled to simulate system operation by sequential MCS.

Sequential MCS tends to produce more accurate results in the presence of time-varying elements, such as load curves and wind generation, because the time series are explicitly represented, and therefore, the correlation and statistical dependency between them are preserved. Some papers are based on this approach [1–3]. However, sequential MCS has a high computational cost and can become prohibitive for practical large systems.

Non-sequential MCS has a much lower computational cost, but the representation of time-varying elements is not straightforward. Usually, non-sequential MCS-based models do not consider the statistical dependence between time series because the system states are obtained by sampling the state space based on the hypothesis that the events are independent. However, disregarding the statistical dependency may lead to incorrect reliability indices since the occurrence of load shedding depends on the states of the time-varying generation and the time-varying load. By considering that there is

C. L. T. Borges (✉)
Electrical Engineering Department, Federal University of Rio de Janeiro, Rio de Janeiro, Brazil
e-mail: carmen@nacad.ufrj.br

J. A. S. Dias
PSR, Rio de Janeiro, Brazil
e-mail: alberto@psr-inc.com

R. Billinton et al. (eds.), *Reliability and Risk Evaluation of Wind Integrated Power Systems*, Reliable and Sustainable Electric Power and Energy Systems Management,
DOI: 10.1007/978-81-322-0987-4_7, © Springer India 2013

no correlation between them may conduct to a sampled state that does not represent an actual state of the system. In general terms, the independent approach produces precise results if all time-varying elements are fully correlated or are totally uncorrelated. Since this cannot be known in advance, the representation of the actual correlation between the time-varying elements is necessary to produce accurate indices.

Therefore, this chapter proposes a model for considering the correlation between any numbers of time series in non-sequential MCS. The correlation may occur between wind generations located at different sites, wind generation and system time-varying load, individual buses time-varying loads, etc. The consideration of correlation in non-sequential simulations has been applied to systems with at most two wind series [4] or without consideration of time-varying load [5]. The proposed model may be applied to any reliability study (generating system, composite system, etc.) where several time series are present. The results shown in this chapter are for generating system reliability evaluation, and the accuracy of the calculated indices is demonstrated by the comparison with those obtained by sequential MCS.

2 Reliability Evaluation by Non-Sequential MCS

The calculation of the reliability indices in non-sequential MCS can be summarized by evaluating Eq. (1):

$$\overline{E}(F) = \frac{1}{N}\sum_{i=1}^{N} F\left(\underline{x}^i\right) \tag{1}$$

where N is the number of simulated states, F is the test function for calculating the indices for each system state $\underline{x}^{\mathrm{i}}$, and $\overline{E}(F)$is the estimate of the annual reliability indices.

The system states are obtained by combining the states of all its components, which are obtained by sampling the cumulative probability distribution function of the operating states of each component. For a system with m components, a system state can be represented by the random vector $\underline{x} = [x_1, x_2,\ldots, x_{\mathrm{k}},\ldots, x_m]$ where x_k represents the state of the k-th component.

The models usually used by non-sequential MCS assume that the states of the components are statistically independent, and therefore, defining $P(x_k)$ as the probability of occurrence associated with the k-th component, the probability of the i-th system state $P(\underline{x}^i)$ may be calculated by

$$P\left(\underline{x}^i\right) = p_i = \prod_{k=1}^{m} P\left(x_k\right). \tag{2}$$

Sampling the component state is done by applying the inverse transformation method to the cumulative distribution function (CDF) of the component, by generating a random number U_k uniformly distributed between [0,1], so that the state of a component modeled by n states is given by

$$x_k = \begin{cases} 1 & \text{if } 0 \le U_k < P_1 \\ 2 & \text{if } P_1 \le U_k < P_2 \\ \vdots & \vdots \\ n & \text{if } P_{n-1} \le U_k \le 1. \end{cases} \tag{3}$$

However, power systems are not only composed by components that may be accurately represented by independent random variables (transmission lines, transformers, generators, etc.) but also by time-varying elements (wind, loads, etc.) that are represented by time series. These time-varying elements can be statistically correlated, and therefore, the consideration of statistical independence becomes invalid. Therefore, an appropriate approach is required for a correct representation of the correlation between them in non-sequential MCS.

3 Representation of Correlated Time-Varying Elements

3.1 Two Elements

Consider, at first, two different time-varying elements which could be two series of wind, for example, and assume that random variable x_1 represents the state of the first element, and x_2 represents the state of the second. Equation (2) can be rewritten by separating the terms related to the two variables:

$$p_i = P(x_1, x_2) \cdot \prod_{k=3}^{m} P(x_k). \tag{4}$$

If x_1 and x_2 are not statistically independent, $P(x_1, x_2)$ can be more generally written as

$$P(x_1, x_2) = P(x_1 | x_2) \cdot P(x_2). \tag{5}$$

Therefore, the probability of the i-th state of the system can be written as

$$p_i = P(x_1 | x_2) \cdot P(x_2) \cdot \prod_{k=3}^{m} P(x_k). \tag{6}$$

In the proposed model, the states sampling process is adapted to be able to incorporate the conditional probability present in (6). This is done after obtaining a distribution function for the conditional probability $P(x_1 | x_2.)$, as will be described later.

Considering, for simplicity, that the two variables have the same number of states n, the conditional probability distribution function will consist of n distinct distributions like

$$P\left(x_1|x_2.\right) = \begin{cases} P\left(x_1|x_2 = 1.\right) & \text{if } x_2 = 1 \\ P\left(x_1|x_2 = 2.\right) & \text{if } x_2 = 2 \\ \vdots & \vdots \\ P\left(x_1|x_2 = n.\right) & \text{if } x_2 = \text{n.} \end{cases} \tag{7}$$

The model, therefore, represents the two correlated variables by a vector of probability distributions of variable x_1 associated with a single probability function of variable x_2, where each element in the array is the distribution associated with one state of x_2. Figure 1 illustrates this representation for an example with $n = 5$.

The conceptual algorithm for sampling a state considering two dependent variables is given by

1. Sample the state of x_2 from its CDF P(x_2), as Eq. (3);
2. Select the appropriate distribution $P\left(x_1|x_2\right)$ according to the sampled state of x_2 as Eq. (7);
3. Sample the state of x_1 by applying the inverse transformation method to the distribution $P\left(x_1|x_2\right)$ selected;
4. Sample the states of the independent components x_k, as Eq. (3).

3.2 Three or More Elements

This model can be extended for the consideration of several statistically dependent time-varying elements. For the particular case of three dependent variables, it can be written based on the chain rule:

$$P\left(x_1, x_2, x_3\right) = P\left(x_1|x_2, x_3.\right) \cdot P\left(x_2|x_3.\right) \cdot P\left(x_3\right). \tag{8}$$

And therefore, the probability of the i-th state of the system can be written as

$$p_i = P\left(x_1|x_2, x_3.\right) \cdot P\left(x_2|x_3.\right) \cdot P\left(x_3\right) \cdot \prod_{k=4}^{m} P\left(x_k\right). \tag{9}$$

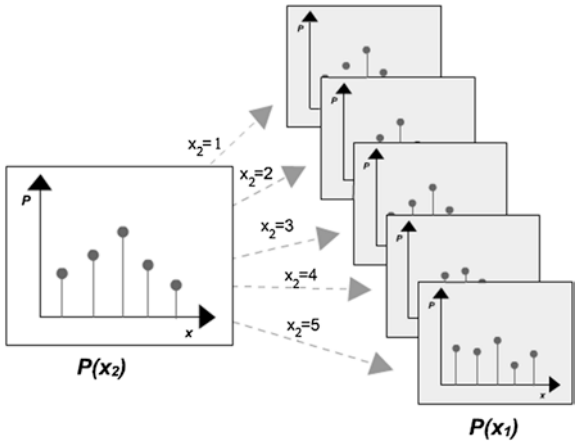

Fig. 1 Model for two correlated variables

Similarly to the case of two dependent variables, the following conditional probability distribution functions can be defined for three dependent variables:

$$P\left(x_2|x_3.\right) = \begin{cases} P\left(x_2|x_3 = 1.\right) & \text{if } x_3 = 1 \\ P\left(x_2|x_3 = 2.\right) & \text{if } x_3 = 2 \\ \vdots & \vdots \\ P\left(x_2|x_3 = n.\right) & \text{if } x_3 = \text{n} \end{cases} \tag{10}$$

$$P\left(x_1|x_2., x_3\right) = \begin{cases} P\left(x_1|x_2 = 1., x_3 = 1\right) & \text{if } x_2 = 1;\ x_3 = 1 \\ P\left(x_1|x_2 = 2., x_3 = 1\right) & \text{if } x_2 = 2;\ x_3 = 1 \\ P\left(x_1|x_2 = 1., x_3 = 2\right) & \text{if } x_2 = 1;\ x_3 = 2 \\ P\left(x_1|x_2 = 2., x_3 = 2\right) & \text{if } x_2 = 2;\ x_3 = 2 \\ \vdots & \vdots \\ P\left(x_1|x_2 = n., x_3 = n\right) & \text{if } x_2 = n;\ x_3 = n \end{cases} \tag{11}$$

Therefore, the model represents the three correlated variables by a chain of vectors of probability distributions, similarly to the way done for two variables.

The conceptual algorithm for sampling a system state considering three dependent variables becomes

1. Sample the state of x_3 from its CDF P(x_3), as Eq. (3);
2. Select the appropriate distribution $P\left(x_2|x_3\right)$ according to the sampled state of x_3, as Eq. (10);
3. Sample the value of x_2 by applying the inverse transformation method to the distribution $P\left(x_2|x_3\right)$ selected;
4. Select the appropriate distribution $P\left(x_1|x_2, x_3\right)$ according to the sampled states of x_2 and x_3, as Eq. (11);
5. Sample the value of x_1 by applying the inverse transformation method to the distribution $P\left(x_1|x_2,\ x_3\right)$ selected;
6. Sample the states of the independent components $x_{k,}$ as Eq. (3).

4 Obtaining Conditional Probability Distribution Functions

The conditional probability distribution functions are obtained by a recursive algorithm that depends on the number of dependent variables. For the case of three dependent variables, for example, $P(x_3)$, $P\left(x_2|x_3.\right)$ and $P\left(x_1|x_2,.\ x_3\right)$ are obtained from the respective time series by the following conceptual algorithm:

1. Choose n the number of states to represent x_1, x_2 and x_3;
2. Cluster the time series of x_1, x_2 and x_3 into n states using the k-means algorithm [6];
3. Obtain the probability distribution function of x_3 $P(x_3)$;
4. Fix the first state of $x_3(k = 1)$;

5. For this state of x_3, calculate the probability of occurrence of each state of x_2, thereby obtaining $P(x_2|x_3 = k.)$;
6. Fix the first state of x_2 ($j = 1$);
7. For these states of x_3 and x_2, calculate the probability of occurrence of each state of x_1, thereby obtaining $P(x_1|x_2 = j, x_3 = k.)$;
8. Repeat step 7 for $j = 2 \rightarrow n$;
9. Repeat steps from 5 to 8 for $k = 2 \rightarrow n$.

5 Results

To evaluate the model proposed in this chapter, two systems are used. The first is a small test system composed only of time-varying elements, while the second is a RTS [7]-based generation system containing conventional generation and time-varying elements (wind and load).

5.1 Test System

In order to evaluate the model accuracy, a system composed of wind generation and time-varying load is used, as shown in Fig. 2.

The generation system consists of two wind power plants that are chosen from three different plant models, whose characteristics are presented in Table 1.

The characteristics of the wind turbines A, B and C as well as the wind time series Southeast, South and Northeast are described in [8]. The frequency distributions of the three wind time series are shown in Fig. 3.

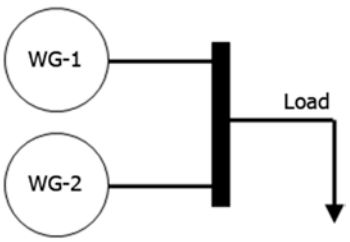

Fig. 2 Test system

Table 1 Wind power plants characteristics

Characteristics	WP-I	WP-II	WP-III
Installed capacity	75 MW	125 MW	55 MW
No. of turbines	50 × 1.5 MW	50 × 2.5 MW	50 × 1.1 MW
Turbine type	A	B	C
Wind time series	Southeast (Wind1)	South (Wind2)	Northeast (Wind3)
Average wind speed	6.59 m/s	7.0 m/s	7.58 m/s
Capacity factor	0.34	0.21	0.30

The system load is represented by the time series *Load* described in [7], and the average annual system load is 4.65 MW, as shown in Fig. 4.

The simulations are performed using the computational model *RelSim* [9], based on object-oriented modeling (OOM) and composed by a system of classes

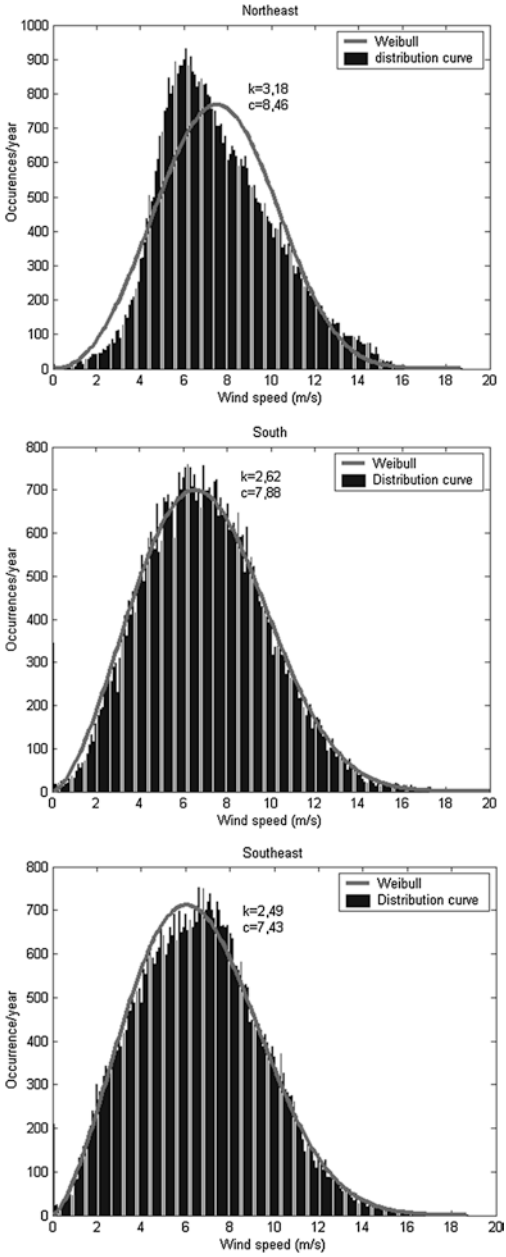

Fig. 3 Frequency distribution of the three wind time series

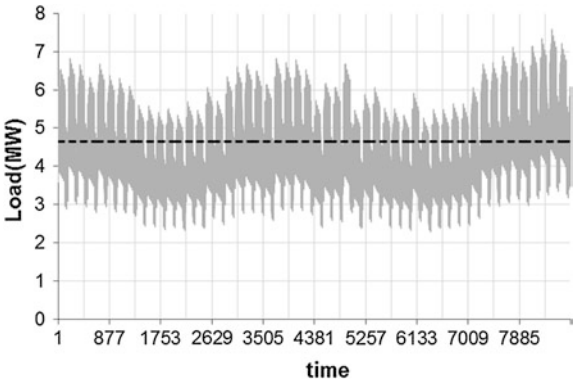

Fig. 4 System load curve

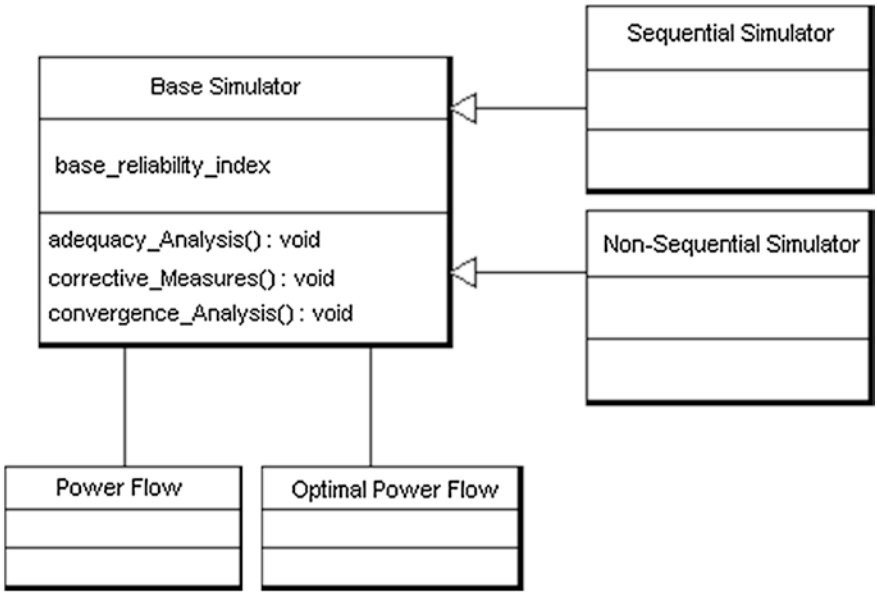

Fig. 5 Structure of *RelSim* computational model

that allows the description of the whole structure of a power system. Two basic types of simulators are implemented for composite reliability evaluation: the sequential simulator and the non-sequential simulator, as shown in Fig. 5.

Table 2 presents the correlations between the time series of the variables *Wind1*, *Wind2*, *Wind3* and *Load.* It can be observed that the largest correlations occur between *Wind2* and *Wind3* and between *Wind1* and L*oad*.

Table 2 Correlation between time series

Time series	Correlation
Wind1 × Wind2	0.042
Wind1 × Wind3	0.054
Wind2 × Wind3	0.135
Wind1 × Load	0.172
Wind2 × Load	0.125
Wind3 × Load	0.337

5.2 Variable Wind and Constant Load

In this first analysis, the load is kept constant at a fixed value. The objective of this analysis is to observe only the influence of the correlation between winds in the reliability indices. Seven different load conditions are simulated, from 0.5 to 2 pu of the average load value, for the three scenarios obtained by combination between the three wind power plants (WP-I and WP-II, WP-I and WP-III, WP-II and WP-III).

The first scenario consists of the generation system composed of wind power plants I and II. Tables 3, 4 present the values obtained for the loss of load probability (LOLP) and expected power not supplied (EPNS) indices. The second column of each table shows the values obtained by sequential MCS, which are used as reference for the calculation of the errors. The third column contains the values obtained, considering that the time-varying variables are independent, while the fourth column contains the values obtained using the proposed model.

Table 3 LOLP—scenario WP-I and WP-II

Load (pu)	Sequential simulation (pu)	Independent variables (pu)	Proposed model (pu)	Error to sequential (%)	
				Independent	Proposed
0.50	0.072	0.071	0.072	2.2	0.1
0.75	0.072	0.071	0.072	2.2	0.1
1.00	0.072	0.071	0.072	2.2	0.1
1.25	0.072	0.071	0.072	2.2	0.1
1.50	0.114	0.111	0.113	2.4	0.2
1.75	0.159	0.151	0.159	5.1	0.1
2.00	0.159	0.151	0.159	5.1	0.1

Table 4 EPNS—scenario WP-I and WP-II

Load (pu)	Sequential simulation (MW)	Independent variables (MW)	Proposed model (MW)	Error to sequential (%)	
				Independent	Proposed
0.50	0.033	0.032	0.033	2.1	0.0
0.75	0.157	0.154	0.157	2.2	0.0
1.00	0.281	0.275	0.281	2.2	0.0
1.25	0.406	0.397	0.406	2.2	0.0
1.50	0.598	0.585	0.597	2.2	0.1
1.75	0.795	0.778	0.795	2.2	0.1
2.00	1.068	1.035	1.068	3.1	0.0

The results show errors between 2.1 and 5.1 % for the indices obtained considering independent variables. The indices obtained by the proposed model, on the other hand, present very low errors, varying from 0 to 0.2 % at most. The difference between the results obtained by the two approaches is more visible to the larger load profiles, 1.75 and 2.00 pu, especially for the LOLP index. In this scenario, since the correlation between the time series is small, the error of the independent approach might be considered acceptable for some load profiles.

The second scenario consists of the generation system composed of wind power plants I and III. The errors observed for this scenario considering independent variables are lower than in the first scenario, varying from 0.1 to 2.1 % for LOLP and from 0 to 1.6 % for EPNS. This fact is expected since the correlation between these two wind series is even smaller than the correlation of two series of the first scenario. The results obtained by the proposed model are once again better than those obtained by the independent one, the largest error being 0.6 % for LOLP and 0.5 % for EPNS.

The third scenario consists of the generation system composed of wind power plants II and III. Table 5 shows the values obtained for the LOLP index, Table 6 for the EPNS index, and Fig. 6 shows a plot of the errors, where *IND_LOLP* and *IND_EPNS* correspond to the errors obtained by the independent variables approach, while *PROP_LOLP* and *PROP_EPNS* correspond to the errors obtained by the proposed model.

The errors observed in this scenario are quite high for the independent approach, reaching 15 %. This fact is justified by the existence of a higher correlation between the series of wind 2 and 3. In this case, the variables cannot be considered independent, and therefore, the independent model cannot correctly represent the behavior of the system. The results obtained by the proposed model, however, show that it perfectly captures the dependence between the variables, with all indices calculated with an error smaller than 0.5 %.

5.3 Variable Wind and Variable Load

In this analysis, the load curve is considered, thus adding another time-varying element to the two wind series of the wind power plants. The same load conditions

Table 5 LOLP—scenario WP-II and WP-III

Load (pu)	Sequential simulation (pu)	Independent variables (pu)	Proposed model (pu)	Error to sequential (%)	
				Independent	Proposed
0.50	0.000	0.000	0.000	0.0	0.0
0.75	0.075	0.065	0.075	14.0	0.5
1.00	0.075	0.065	0.075	14.0	0.5
1.25	0.149	0.127	0.150	15.0	0.2
1.50	0.149	0.127	0.150	15.0	0.2
1.75	0.193	0.171	0.194	11.7	0.3
2.00	0.230	0.206	0.231	10.3	0.2

Table 6 EPNS—scenario WP-II and WP-III

Load (pu)	Sequential simulation (MW)	Independent variables (MW)	Proposed model (MW)	Error to sequential (%)	
				Independent	Proposed
0.50	0.000	0.000	0.000	0.0	0.0
0.75	0.113	0.098	0.113	14.0	0.4
1.00	0.242	0.209	0.241	14.0	0.5
1.25	0.463	0.396	0.462	14.4	0.2
1.50	0.720	0.615	0.719	14.6	0.1
1.75	0.992	0.849	0.992	14.5	0.0
2.00	1.366	1.182	1.366	13.5	0.0

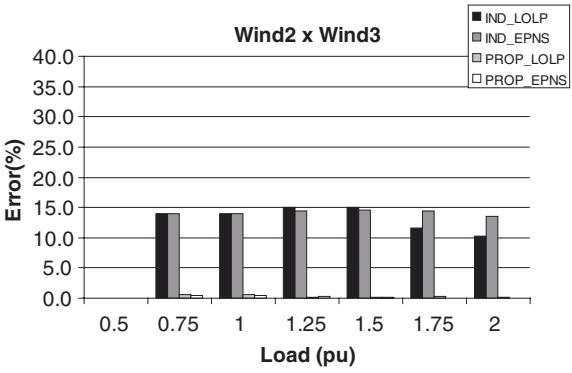

Fig. 6 Errors—WP-II and WP-III and constant load

for the three scenarios of combination of wind power plants are simulated. The results for the first scenario are shown in Tables 7, 8 and in Fig. 7.

It can be seen that the errors of the indices obtained by the proposed model are all smaller than 4.4 %, except for the load curve of 0.5 pu where the error reached 9.4 % for LOLP. This fact is due to the very low load profile, what makes the system reliability indices very small and, therefore, any difference between values represents a significant percentage. The errors of the independent approach for the low load profiles, however, are much higher than those of the proposed model indicating the higher accuracy of the last, while for the other load profiles the error level is of the same order.

Based on the difference between the LOLP index calculated by the proposed model and the independent approach, one might think that the dependence between variables does not affect significantly the accuracy of the reliability indices. However, observing the values of the EPNS index calculated by both approaches, it can be noticed that the errors for the independent one are extremely high, indicating that the dependence between variables strongly affects the value of the expected energy not supplied. Therefore, the independent approach is inadequate and might not be used.

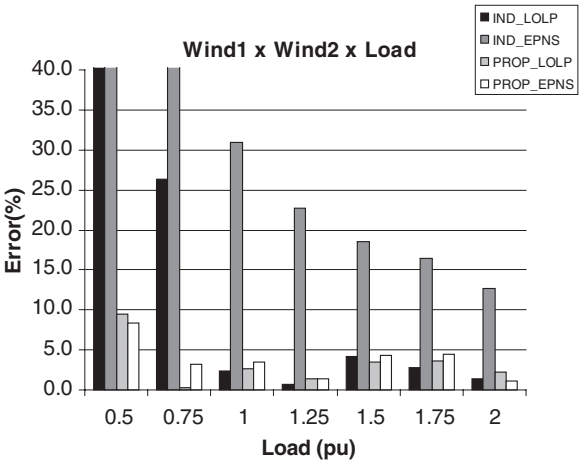

Fig. 7 Errors—WP-I and WP-II and variable load

Table 7 LOLP—scenario WP-I and WP-II and variable load

Load (pu)	Sequential simulation (pu)	Independent variables (pu)	Proposed model (pu)	Error to sequential (%)	
				Independent	Proposed
0.50	0.005	0.009	0.006	77.4	9.4
0.75	0.041	0.052	0.041	26.3	0.2
1.00	0.066	0.068	0.065	2.4	2.7
1.25	0.072	0.072	0.073	0.7	1.4
1.50	0.076	0.079	0.073	4.2	3.4
1.75	0.082	0.084	0.079	2.8	3.6
2.00	0.096	0.098	0.094	1.5	2.3

Table 8 EPNS—scenario WP-I and WP-II and variable load

Load (pu)	Sequential simulation (MW)	Independent variables (MW)	Proposed model (MW)	Error to sequential (%)	
				Independent	Proposed
0.50	0.001	0.002	0.001	58.3	8.3
0.75	0.032	0.046	0.031	44.8	3.2
1.00	0.093	0.121	0.089	31.0	3.5
1.25	0.168	0.206	0.170	22.7	1.4
1.50	0.248	0.294	0.237	18.6	4.4
1.75	0.336	0.391	0.321	16.5	4.4
2.00	0.437	0.492	0.432	12.7	1.1

For the second scenario, the indices obtained by the proposed model are much better than those obtained by the independent approach. Table 9 shows the results for the EPNS index which is the most sensitive to the time series correlation, while Fig. 8 shows the errors for the two indices calculated.

Table 9 EPNS—scenario WP-I and WP-III and variable load

Load (pu)	Sequential simulation (MW)	Independent variables (MW)	Proposed model (MW)	Error to sequential (%)	
				Independent	Proposed
0.50	0.000	0.000	0.000	0.0	0.0
0.75	0.006	0.019	0.006	203.1	0.0
1.00	0.031	0.066	0.032	109.2	2.2
1.25	0.076	0.128	0.072	69.3	4.6
1.50	0.134	0.211	0.140	57.9	5.0
1.75	0.204	0.310	0.212	52.2	4.1
2.00	0.291	0.428	0.305	47.5	4.8

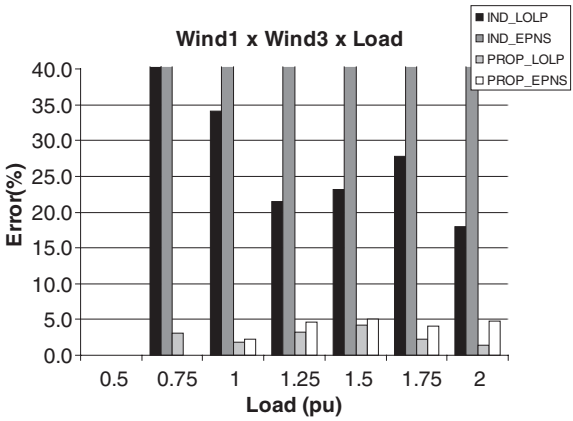

Fig. 8 Errors—WP-I and WP-III and variable load

The maximum error observed for the proposed model is 4.2 % for LOLP and 5.0 % for EPNS, whereas the errors of the independent approach vary from 18 to 158 % for LOLP and from 47.5 to 203 % for EPNS, what is completely unacceptable.

The results for the third scenario are presented in Table 10 for the EPNS index, and the errors for both indices are shown in Fig. 9. All errors for the proposed model are smaller than 4 % except for the 0.75 pu load level due again to the low

Table 10 EPNS—scenario WP-II and WP-III and variable load

Load (pu)	Sequential simulation (MW)	Independent variables (MW)	Proposed model (MW)	Error to sequential (%)	
				Independent	Proposed
0.50	0.000	0.000	0.000	0.0	0.0
0.75	0.008	0.021	0.010	157.3	22.0
1.00	0.043	0.072	0.044	68.0	3.5
1.25	0.109	0.138	0.110	26.9	0.7
1.50	0.197	0.230	0.198	16.6	0.3
1.75	0.302	0.339	0.296	12.4	1.9
2.00	0.424	0.464	0.408	9.4	4.0

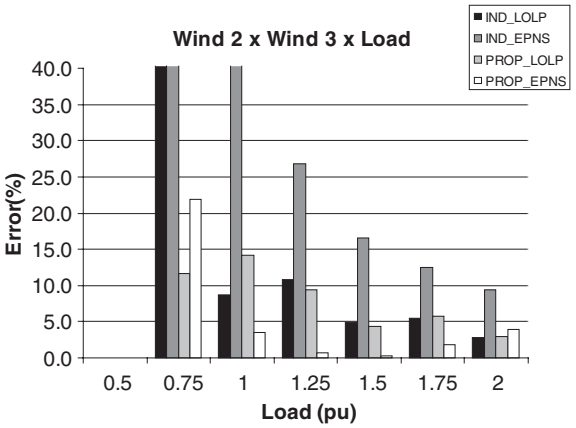

Fig. 9 Errors—WP-II and WP-III and variable load

value of the indices calculated. However, the errors for the independent approach are again very high, confirming its inadequacy to capture the influence of multiple correlated variables on the reliability indices.

5.4 Modified RTS Generating System

In order to evaluate the model performance at a more complex system, a modified RTS is used where the original generation, composed of thermal, hydro and nuclear units with installed capacity of 3,405 MW, is enlarged by two wind power plants chosen from the three plant models of Table 1. The original load curve is increased by 10 % with an average annual load is 1,862 MW. All the simulations are done for a maximum coefficient of variation (α) of 3 % for both reliability indices.

In the first scenario, wind power plants I and II are added and the results are shown in Table 11.

The errors of the proposed model are 0.0 and 2.9 % for LOLP and EPNS, respectively, whereas the correspondent errors of the independent approach are 24.0 and 26.3 %. These results confirm that the proposed model can accurately represent the dependence between time and varying elements also in the presence of independent components.

Table 11 MRTS—scenario WP-I and WP-II and variable load

Index	Sequential simulation	Independent variables	Proposed model	Error to sequential (%)	
				Independent	Proposed
LOLP (α)	0.354 % (0.021)	0.439 % (0.022)	0.354 % (0.022)	24.0	0.0
EPNS (α)	513 Kw (0.03)	648 kW (0.03)	498 kW (0.03)	26.3	2.9
No. of states	18,536,160	521,007	585,401		

Table 12 MRTS—scenario WP-I and WP-III and variable load

Index	Sequential simulation	Independent variables	Proposed model	Error to sequential (%)	
				Independent	Proposed
LOLP (α)	0.395 % (0.021)	0.519 % (0.022)	0.402 % (0.022)	31.4	1.8
EPNS (α)	564 kW (0.03)	755 kW (0.03)	568 kW (0.03)	33.9	0.7
No. of states	19,543,560	409,801	511,701		

The computational effort of the three simulation approaches can also be seen in Table 11. The proposed model requires 31.66 times less states adequacy analysis than the sequential simulation and only an additional effort of 12 % in relation to the independent approach.

In the second scenario, wind power plants I and III are added and the results are shown in Table 12. The errors of the proposed model are 1.8 and 0.7 % for LOLP and EPNS, respectively, whereas the correspondent errors of the independent approach are 31.4 and 33.9 %. It is interesting to compare the errors of the first and second scenarios of the MRTS with those of the small test system, where the same trend of increasing errors of the independent model can be observed. As a general conclusion, these errors are completely unacceptable.

In terms of computational effort, the proposed model requires 38.19 times less adequacy analysis than the sequential simulation and an additional effort of 25 % in relation to the independent approach.

6 Conclusion

The results showed that the proposed model can correctly represent the effect of the statistical dependence between time-varying elements with about 30 times less processing time than the sequential simulation and only 12–25 % more effort than the independent approach. However, the independent approach may be very inaccurate when the time series correlation is significant and in some cases fails very badly. Therefore, the model proposed represents a good alternative to correctly represent multiple wind power plants and the load curve in non-sequential simulations with an acceptable processing time.

References

1. Billinton R, Chen H, Chajar R (1996) A sequential simulation technique for adequacy evaluation of generating systems including wind energy. IEEE Trans Energy Convers 11(4):728–734
2. Wangdee W, Billinton R (2006) Considering load-carrying capability and wind speed correlation of WECS in generation adequacy assessment. IEEE Trans Energy Convers 21(3):734–741
3. Xie K, Billinton R (2009) Considering wind speed correlation of WECS in reliability evaluation using the time-shifting technique. Electr Power Syst Res 79:687–693
4. Billinton R, Gao Y, Karki R (2009) Composite generation and transmission system reliability evaluation incorporating two wind energy facilities considering wind speed correlation. IEEE Trans Power Syst 24(3):1375–1382

5. Vallée F, Lobry J, Deblecker O (2007) Impact of the wind geographical correlation level for reliability studies. IEEE Trans Power Syst 22(4):2232–2239
6. Jain AK, Dubes RC (1988) Algorithms for clustering data. Prentice-Hall, Inc, New Jersey
7. IEEE RTS (1999) Task force of APM subcommittee. IEEE Reliab Test Syst 1996 IEEE PAS 14(3):1010–1020
8. Leite AP, Borges CLT, Falcão DM (2006) Probabilistic wind farms generation model for reliability studies applied to Brazilian sites. IEEE Trans Power Syst 21(4):1493–1501
9. Dias JA, Borges CLT (2010) Object oriented model for composite reliability evaluation including time varying load and wind generation. In: Proceedings of the 11th IEEE international conference on probabilistic methods applied to power systems (PMAPS)

Composite Reliability Assessment of Power Systems with Large Penetration of Renewable Sources

Armando M. Leite da Silva, Luiz Antônio F. Manso, Silvan A. Flávio, Mauro A. da Rosa and Leonidas C. Resende

1 Introduction

The constant increase in oil prices and the concern over the reduction of gas emissions causing the greenhouse effect favor the creation of policies to encourage the production of energy through renewable sources. The recent restructuring of the electricity sector has introduced new concepts such as power market, transmission open access, cogeneration, independent production, etc., which enabled the decentralized energy generation, strengthening such policies. Thus, non-conventional energy sources, namely wind power, mini-hydro, solar, and cogeneration (e.g., biomass), start having a significant contribution in the energy production matrix [1, 2]. However, if the

A. M. Leite da Silva (✉) · S. A. Flávio
Institute of Electrical Systems and Energy,
Federal University of Itajubá, UNIFEI,
Itajubá 37.500-903, MG, Brazil
e-mail: am.leitedasilva@gmail.com

S. A. Flávio
e-mail: silvanflavio@yahoo.com.br

L. A. F. Manso · L. C. Resende
Electrical Engineering Department,
Federal University of São João del-Rei, UFSJ,
São João del-Rei 36.307-440, MG, Brazil
e-mail: lmanso@ufsj.edu.br

L. C. Resende
e-mail: leonidas@ufsj.edu.br

M. A. da Rosa
Power System Unit, INESC Tech,
4200-465 Porto, Portugal
e-mail: marosa@inescporto.pt

R. Billinton et al. (eds.), *Reliability and Risk Evaluation of Wind Integrated Power Systems*, Reliable and Sustainable Electric Power and Energy Systems Management,
DOI: 10.1007/978-81-322-0987-4_8, © Springer India 2013

volatility of the available capacity from such sources is not properly considered, the decisions taken in power systems expansion and/or operation planning can severely endanger the reliability of the power supply. Thus, systems planners and operators will require new computational tools capable of coping with these characteristics, in addition to the recent power system market implementation in a deregulated environment.

Several works to evaluate the reliability of power systems with high penetration of renewable sources have been proposed in the literature [3–21]. Most of these works deal with generating capacity reliability assessment (both static adequacy and operating reserve) and/or with small isolated power systems. In general, some of these methods propose simplified models or represent energy constraints through clustered data. Therefore, there is a need to develop more detailed models and tools, which are able to evaluate, in an accurate and efficient way, the composite generation and transmission reliability under this new context. The concern is not only to represent an important structural change, but also the need to consider a large number of new random variables and complexities arising from the floating capacity of the renewable sources.

This chapter presents an application of non-sequential Monte Carlo simulation (MCS) to evaluate the main reliability indices of composite generation and transmission systems, considering renewable energy sources. The idea is to study the behavior of the reliability indices, when a major portion of the energy sources are renewable, comprising mainly hydro, mini-hydro, wind, and solar sources. Moreover, the production of renewable power will be calculated based on hourly/monthly series (different for each region/basin) of wind speed, solar radiation, and water inflow. The proposed non-sequential MCS will be validated against the chronological MCS through several case studies with variants of the IEEE Reliability Test System (RTS) [22, 23]. Finally, an application to a real power system (the Portuguese network [13]) will demonstrate the feasibility of the proposed methodology.

2 Composite Reliability Assessment

2.1 Basic Concepts

For generation and transmission systems, the estimates of loss of load indices are obtained through composite reliability assessment algorithms, based on two distinct representations: state space and chronological modeling. Usually, state-space-based algorithms follow three major steps [24]:

(a) Select a system state (i.e., load level, equipment availability, energy availability, etc.);
(b) Analyze the performance of the selected state (i.e., check if the available generating units and circuits are able to satisfy the associated load without violating any operating limits; if necessary, activate corrective measures such as generation redispatch, load curtailment, etc.);
(c) Estimate reliability indices (i.e., loss of load indices, etc.); if the accuracy of the estimates are acceptable, stop; otherwise, go back to step (a).

State enumeration and non-sequential MCS methods are examples of state-space-based algorithms, where Markov models [25, 26] are used for both equipment and load state transitions. Therefore, states are selected and evaluated without considering any chronological connection. The necessary steps to evaluate reliability indices considering the chronological representation (sequential MCS) are conceptually the same described for the state-space representation [27–29]. The basic difference is how system states are selected; that is, step (a) of algorithm. In this case, the sequential approach moves chronologically through system states, while the non-sequential approach randomly selects system states. The sequential simulation can, therefore, perceive all chronological aspects and, hence, is able to correctly represent renewable energy sources and their natural uncertainties, due to hydrologic inflow sequences, wind speed, and solar radiation variations, etc. However, the chronological modeling implies that two consecutive state samples differ from each other in only one state component. Therefore, this method requires a more substantial computational effort than the other approach.

Recently, the non-sequential MCS was improved receiving some features as non-aggregate Markov load models [29] and a new process for estimating frequency and duration indices, named *one-step forward state transition* [30]. These features gave the non-sequential MCS the necessary flexibility to accurately represent renewable sources and they will be used in this work. This special non-sequential MCS tool is similar to the quasi-sequential MCS proposed in [31] to deal with generating capacity reliability assessment. The only restrictions of these tools are the limitations to compute reliability worth-related indices and probability distributions as discussed in [32].

2.2 Traditional Composite Reliability Indices

In this chapter, loss of load indices are estimated by flexible non-sequential simulation techniques, as the mean over N-sampled system state values X^k of the test function $F(X^k)$:

$$\tilde{E}[F] = \frac{1}{N}\sum_{k=1}^{N} F(X^k), \tag{1}$$

All the basic reliability indices can be obtained by Eq. (1), depending on the definition of the test function F. The estimate uncertainty is given by the variance of the estimator:

$$V\left(\tilde{E}[F]\right) = V(F)/N, \tag{2}$$

where $V(F)$ is the variance of the test function. This uncertainty is usually represented as the coefficient of variation:

$$\beta = \sqrt{V\left(\tilde{E}\left[F\right]\right)} \Big/ \tilde{E}\left[F\right], \tag{3}$$

The traditional reliability indices to assess composite generation and transmission adequacy are as follows:

- LOLP—loss of load probability;
- LOLE—loss of load expectation (h/year);
- EPNS—expected power not supplied (MW);
- EENS—expected energy not supplied (MWh/year);
- LOLF—loss of load frequency (occ./year);
- LOLD—loss of load duration (h).

All these indices are obtained from the statistics of the MCS process as follows. For instance, non-sequential simulation can easily provide unbiased estimates for the loss of load probability (LOLP) and expected power not supplied (EPNS) indices. In this case, the test functions F_{LOLP} and F_{EPNS} are given by [29]:

$$F_{\mathrm{LOLP}}(x^k) = \begin{cases} 0 & \text{if } x^k \in X_S \\ 1 & \text{if } x^k \in X_F \end{cases} \tag{4}$$

and,

$$F_{\mathrm{EPNS}}(x^k) = \begin{cases} 0 & \text{if } x^k \in X_S \\ \Delta P_k & \text{if } x^k \in X_F \end{cases} \tag{5}$$

where $X = X_S \cup X_F$ is the set of all possible states x (i.e., the state space), divided into two subspaces X_S of success states and X_F of failures states; ΔP_k is the amount of curtailed power at the failure state x^k. The period of analysis, for example, $T = 8{,}760$ or 8,736 h for annualized values, can be established and, thus, LOLE and EENS indices are obtained by: LOLE = LOLP × T and EENS = EPNS × T.

Non-sequential simulation can also provide unbiased estimates for the LOLF and LOLD indices. In this case, the test function F_{LOLF} is given by [30]:

$$F_{\mathrm{LOLF}}(x^k) = \begin{cases} 0 & \text{if } x^k \in X_S \\ \lambda_k^{\mathrm{out}} & \text{if } x^k \in X_F \text{ and } \mathrm{x}^m \in X_S \\ 0 & \text{if } x^k \in X_F \text{ and } \mathrm{x}^m \in X_F \end{cases} \tag{6}$$

and,

$$\mathrm{LOLD} = \mathrm{LOLP}/\mathrm{LOLF} \tag{7}$$

where λ_k^{out} is the summation of all the transition rates between failure state x^k and any state directly connected to it. The state x^m is a state reached from x^k in one transition. The proposed estimating process must simulate only one

possible transition from failure state x^k to a neighbor state x^m. That is the reason why this process is named the one-step forward state transition [30]. This process to estimate LOLF index is a very efficient approach to reduce computational effort. Moreover, it does not assume any coherent behavior in the system. This process makes it possible the modeling of time-varying loads by non-sequential techniques, which can be extended to model fluctuations in generating capacities.

2.3 Complementary Indices

Loss of Load Cost

Other indices may also be evaluated during the simulation process and among the most interesting ones is the loss of load cost (LOLC). Besides providing a relatively easy figure for discussions, that is, dollars instead of probabilities, kWh, occurrences, etc., per year, these indices can be directly included into the objective function to be minimized, according to the least-cost planning approach. Reliability worth is a relevant issue in power systems planning, and operation, and many publications have been dedicated to this subject, for example, [5, 7, 8, 13, 15, 26, 29, 32].

Another set of interesting indices can be obtained by the well-being framework [30], which classifies the operating states into three groups: healthy, marginal, and at-risk (or failure). To identify these states, the power system is submitted to a prespecified deterministic criterion. The details of this framework and the way the corresponding indices are evaluated can be found in [30].

Relative and Conditioned Contributions

Composite reliability programs can be used to assess the relative contribution of generation and transmission outages to overall system reliability [24]. Let, the LOLP, EPNS, and LOLF be expressed as a general system reliability index (RI) as follows:

$$\mathrm{RI} = \mathrm{RI}_G + \mathrm{RI}_T + \mathrm{RI}_C \tag{8}$$

where RI_G represents the contribution of generation outages (G), which are severe enough to lead to load curtailment, even if there are no limitations in transmission capacity; RI_T represents the contribution of transmission outages (T), which are severe enough to lead to load curtailment, even if the full generation capacity is available; RI_C represents the composite problems (C), that is, the combined effects of simultaneous generation and transmission failures plus the impact of generation failures with transmission restrictions on the system.

It can be seen from the above definitions that RI_G corresponds to the values calculated by a "pure" generation reliability program; in turn, RI_T corresponds

to the values calculated by a "pure" transmission reliability evaluation program; and finally, the "composite" index RI_C measures the degree of interaction between generation and transmission in the system [24]. Usually, a composite reliability tool can assess within a single-run both RI and RI_G indices and, therefore, the influence of the transmission equipment can be evaluated through the index:

$$RI_{T\&C} = RI - RI_G \tag{9}$$

Composite reliability programs can also be used to assess the conditioned contribution of generation and transmission outages to overall system reliability. For instance, $RI_{[G/T\_UP]}$ represents the system indices obtained by a composite reliability evaluation tool, where only the unavailabilities of generators are sampled; all transmission equipment are completely reliable (i.e., at the up state), but their capacities are fully considered. Similarly, $RI_{[T/G\_UP]}$ represents the system indices obtained by a composite reliability evaluation tool, where only the unavailabilities of transmission are sampled; all generation equipment are completely reliable (up state), obviously their capacities must be considered. Observe that the $RI_{[T/G\_UP]}$ index is an unbiased estimate for RI_T and, therefore, RI_C can be evaluated as "$RI_{T\&C} - RI_T$." The latter value is an approximation since $RI_{[T/G\_UP]}$ is obtained from a separated simulation.

Area and Load Point Indices

Area and load point or bus reliability indices provide information on the spatial distribution of steady-state reliability and help identify "problem" areas and buses, which may need to be reinforced. The same previous set of system indices can be evaluated at the area or bus level. Obviously, to ensure the convergence of bus reliability indices will be more difficult, since these events are naturally rarer than area or system reliability indices.

Chronological Power Flow Indices

In order to obtain the amount of wind energy spilled for systems with high penetration of wind energy sources, the chronological power flow (CPF) algorithm was recently proposed [20]. It consists in a MCS-based chronological process, performing load-flow assessments throughout the study period, for example, one year or 8,760 h. Thus, through (10), the expected wind energy spilled (EWES) is estimated for both cases: without transmission restrictions, that is, under single-bus dispatch ($EWES_G$) and with transmission restrictions ($EWES_{G\&T}$):

$$EWES = \frac{1}{NY} \sum_{k=1}^{NY} WES_k, \tag{10}$$

where WES_k is the amount of WES in year k and NY the number of simulated years. The estimation of (10) can also be carried out through a special non-sequential or

quasi-sequential MCS, based on the same methodology to be used in this chapter. The corresponding models will be described in the next subsection.

2.4 System Modeling

In this work, the network performance will be evaluated by a DC linear model. Therefore, DC power flow and/or optimal power flow (OPF) algorithms will be used together with the following models.

Load and Renewable Source Capacity

The proposed method uses a non-aggregate Markov load model with 8,760 states, sequentially connected in the same chronological order as they appear in the hourly load curve. The main idea is to keep some chronological representation in the Markov load model [29, 31]. Since the load will remain, on average, one hour at each state, therefore, state h corresponds, on average, to hour h in the actual chronological sequence. To select the load level, the composite reliability assessment tool may sample a state/hour h from a uniform distribution $U_{[1,\ 8760]}$ (special non-sequential MCS) or just follow hour-by-hour the load curve (quasi-sequential MCS).

In order to explain this model, Fig. 1 shows a sampled state h and the next state $h + 1$, where $L_h(A_m)$ represents the load level at state h in area m and λ_L is the load transition rate. Therefore, if a load transition occurs, the load level in all areas will be changed from L_h to L_{h+1}. Note that the load in a certain area may be increasing, while, at the same time, it may be decreasing in a different area. If the load is followed hour-by-hour by the simulation process, other time-dependent phenomena can be tracked as well.

The volatility of the available capacity from renewable sources can be modeled by historical yearly series [14, 31]. All of these series can be converted into non-aggregate Markov models. Thus, load states will be chronological connected with

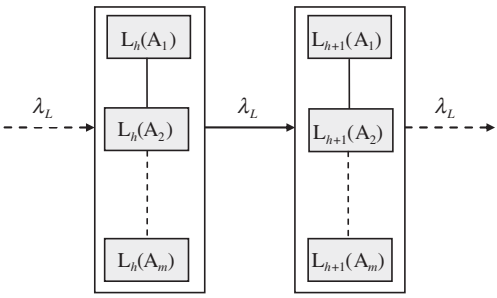

Fig. 1 Multi-level non-aggregated Markovian load model

the maximum capacity of each renewable source through h hour. These models allow to observe the complementarities between renewable and non-renewable sources and to evaluate the impact of transmission network on the reliability indices.

Thermal and Hydro units

A two-state Markov model is used for modeling the up/down cycle of all thermal and hydro generating units. They are specified through their failure (λ) and repair (μ) rates. Figure 2a shows the well-known two-state Markov model. The generating capacity of the thermal units is fixed and pre-specified. However, the capacities of the hydro units will be defined for each month, according to the corresponding hydrological series. These series are defined for each hydraulic basin based on historical data and aim at capturing the historical inflows, reservoir volumes, and type of operation. Mathematical polynomials convert the storage volumes into momentary power capacities [7, 8, 10, 14].

Wind and Solar Generating Stations

Usually, in wind or photovoltaic (PV) solar generating station, there are several generating units/cells and they will be grouped into an equivalent multi-state Markov model, as shown in Fig. 2b. Only two stochastic parameters are necessary: unit failure and repair rates. Parameter N represents the number of generating units of the renewable model. If C is the unit capacity, the amount of power associated with the kth state is given by $C_k = (N - k) \times C$, $k = 0,\ldots, N$. The cumulative probability P_k (from 0 to k) associated with this state can be easily calculated.

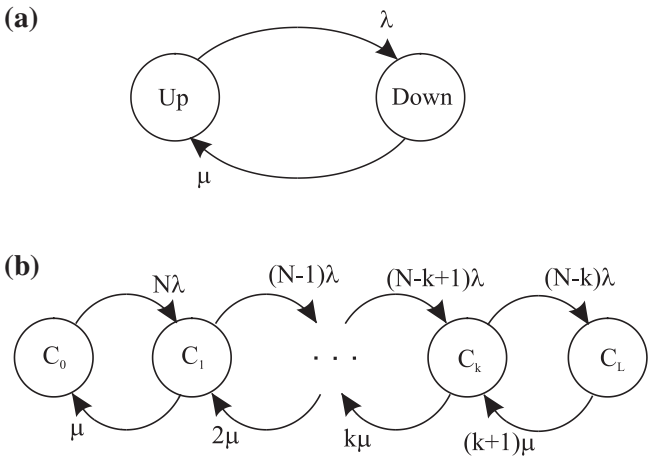

Fig. 2 (**a**) Two-state (**b**) Multi-state Markov models

In order to reduce the number of these states during the non-sequential MCS, a simple truncation process sets the desired order of accuracy. Therefore, instead of $N + 1$ states, a much smaller number up to the capacity C_L will limit this model; for example, $1 - P_L \leq$ tolerance. The productions of the renewable generating units will be defined for each hour, according to the hourly primary energy series for each geographic region. In a wind generating station, the series try to capture the wind speed and power conversion characteristics. Similarly, in a PV and concentrating solar generating stations, the series try to capture the irradiation and power conversion characteristics.

Mini-Hydro Units

Mini-hydro units are modeled similarly to the hydro generating units, but in order to simplify the modeling process, they are grouped into multi-state-units. Due to the lack of specific data in relation to the hydrological basin where they are located, only one average series per year is used to model the capacity variations with time.

Cogeneration Units

Co-generating units are modeled similarly to the thermal units, but like in the previous case, they are clustered as well. Also, an hourly utilization factor is specified, which models the actual co-generation power used by the system. This factor varies during the year following the tariff attractiveness and/or the industry production cycle [8].

2.5 Computational Procedure

The proposed algorithm to assess composite reliability indices in systems with large penetration of renewable sources is structured as follows:

1. Read all the information regarding generation and transmission parameters, hourly load levels, hydrological, wind, and solar series, and maintenance schemes. Besides that, the following parameters must be defined: (a) maximum sample size $N_{\max}$; (b) coefficient of variation β;
2. Set $N = 1$ and $h = 1$, where N represents the sample counter and h the load vector hour index;
3. Sample the hydrological, wind, solar, and co-generation series according to their probabilities of occurrence;
4. Evaluate the actual capacity of the generating units during hour h, from the sampled hydro, wind, etc. series;

5. Sample the state of each generating and transmission equipment based on their own stochastic up/down model, accounting for the maintenance scheme;
6. Evaluate all corresponding test functions F, that is, (4), (5), and (6), associated with the performance of state x_k, $(k = h)$, by means of DC power flow and/or OPF algorithms;
7. Estimate all indices and their related coefficients of variation. If any interruption criterion is met (β or $N_{\max}$), stop the simulation; otherwise, go to *Step* 8;
8. Set $N = N + 1$ and $h = h + 1$. If $h = T + 1$, set $h = 1$ and return to *Step* 3, otherwise, go to *Step* 4.

The primary idea of the previous quasi-sequential MCS is to keep tracking the load model on hourly bases, so that one can capture the time dependence of the generating capacities of renewable sources (e.g., hydro, wind, and solar units). The proposed algorithm is conceptually similar to the pseudo-chronological MCS [29], although much simpler. It incorporates some features of the one-step forward state transition [30], but it does not have the ability to calculate the distribution functions associated with the reliability indices, as in the case of the chronological MCS [29]. Moreover, the evaluation of LOLC indices can also be calculated but not with the same accuracy of the pseudo- or full-chronological MCS.

In the previous simplified computational procedure, the load states are sequentially selected, that is, hour-by-hour, which characterizes the quasi-sequential MCS. However, the load state (i.e., hour h) could also have been sampled after *step* 3, and, therefore, *step* 8 would be properly modified by disregarding the counting process "$h = h + 1$." In this case, a special or flexible non-sequential MCS is characterized.

Both MCS-based algorithms provide unbiased reliability index estimations. Moreover, they properly allow the representation of maintenance schedules under hour/monthly bases.

3 Applications to the IEEE Standard System

The proposed method is applied to the RTS96-RES (i.e., renewable sources) system. It consists of a modified version of the IEEE RTS 1996 [23], with high penetration of the renewable sources. The original hourly load curve [22] is used in all simulations. The convergence criterion of the MCS is to have a $\beta \leq 5$ %, for all indices. All computations are performed in a Pentium Core 2 Duo 2.0 GHz.

3.1 Characteristics of the RTS96-RES

The original system (RTS96) has 900 MW of hydroelectric sources, representing 9 % of the total installed capacity (10,215 MW). In order to build a new configuration with high penetration of renewable sources, 3,150 MW of thermal sources, presented in Table 1 (31 % of the total installed capacity), are selected to be replaced

Table 1 Thermal sources replaced by wind and new hydro sources

Bus	RTS96			RTS96-RES			
	No. of units	Capacity (MW)		Type	No. of units	Capacity (MW)	
		Per unit	Total			Per unit	Total
101	2	76	152	WIN[a]	319	2.5	797.5
102	2	76	152	HYD	2	84.0	168.0
113	3	197	591	HYD	3	212.0	636.0
115	1	155	155	WIN	325	2.5	812.5
201	2	76	152	WIN	181	2.5	452.5
202	2	76	152	HYD	2	80.0	160.0
213	3	197	591	HYD	3	253.0	759.0
215	1	155	155	WIN	184	2.5	460.0
301	2	76	152	WIN	285	2.5	712.5
302	2	76	152	HYD	2	96.0	192.0
313	3	197	591	HYD	3	352	1056.0
315	1	155	155	WIN	290	2.5	725.0
Total (MW)			3,150	Total (MW)			6,931.0

[a] Each wind unit has $\lambda = 4$ f/year and $\mu = (1/90)$ r/h

by wind and new hydro generators. In order to maintain a correspondence between the thermal and the effective wind power capacity, the number of wind units and new hydro units was obtained based on some statistics from the wind and hydrological series [20]. The total installed capacity of the RTS96-RES is 13,996 MW, which represents an increase of 37 % in relation to the RTS96. Figure 3 shows Area 1 with the new changes. The other two areas are similar. The new changes also include the addition of circuits 901 (101–102), 903 (101–105), 909 (105–110), and 980 (301–302). These network reinforcements were obtained by the CPF algorithm proposed in [20] in order to reduce the $EWES_{G\&T}$ index from 132.230 to 17.017 GWh/year. Therefore, the final RTS96-RES provides a robust system configuration.

To represent the volatility of renewable sources, each area of the RTS96-RES system, which corresponds to an IEEE reliability test system [22], is considered as a distinct geographic region. For the wind sources, five series, based on actual historical series from the Netherlands [33], are used, with 8,736 hourly levels, for each area of the system.

The application of the proposed methodology is described in the next subsections, through four case studies considering two wind scenarios. To illustrate the variability of these series in each area of the system, Fig. 4 shows the mean values of the wind generator output powers, in per unit, based on the five collected series, which make up Scenario 1. In the case of hydrological sources, five series are also considered, with 12 monthly levels for each plant or reservoir [7, 8]. Scenario 2 is a variant of Scenario 1 in which the wind in the October–March period is increased by a factor of 20 %, and the April–September period is decreased by 80 % (see Fig. 5). Also during the October–March months, the series of Areas 1 and 3, whose peak production occurs at the diurnal period, are shifted 12 h later in the day.

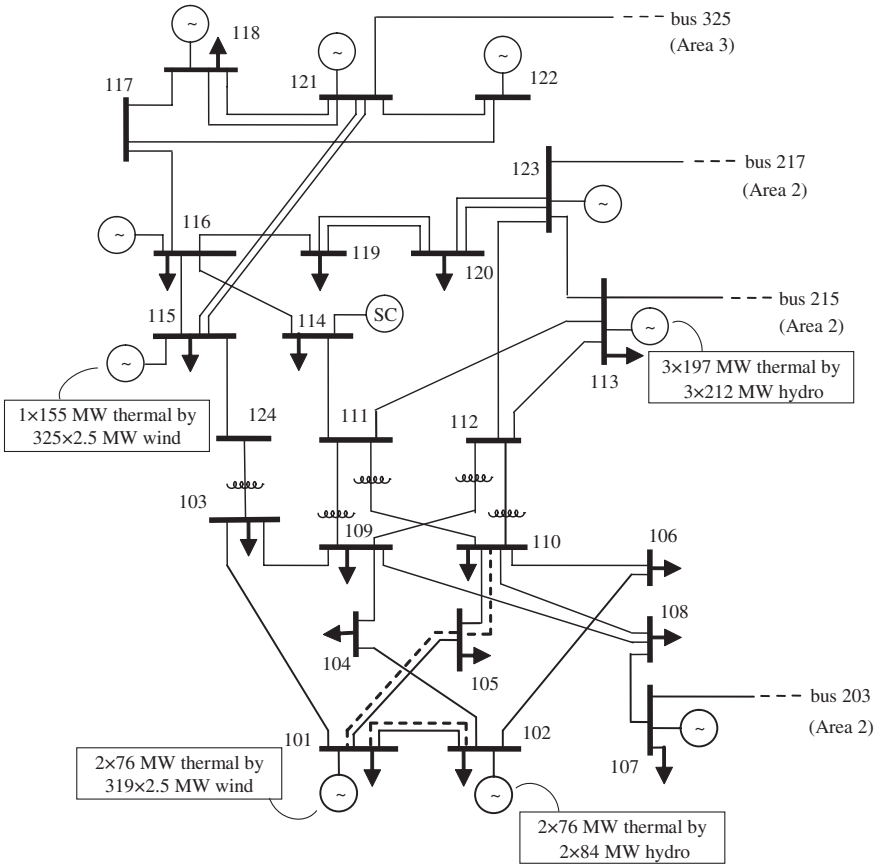

Fig. 3 IEEE RTS96-RES—Area 1 single-line diagram

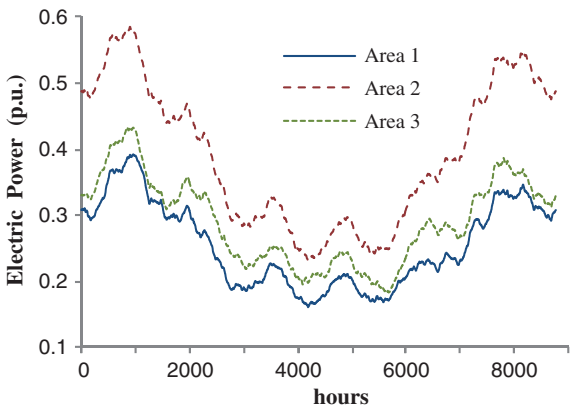

Fig. 4 Moving average yearly curve of the output from wind generators—Scenario 1

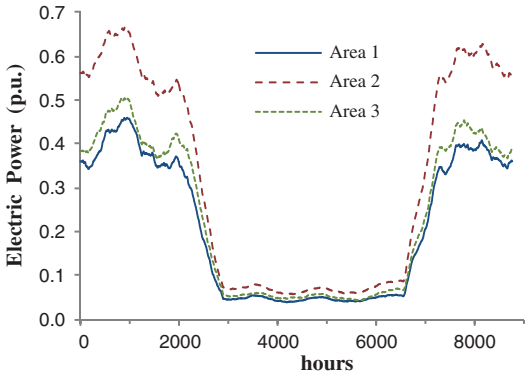

Fig. 5 Moving average yearly curve of the output from wind generators—scenario 2

Thus, in this scenario, the wind conditions are stronger during the winter period (October–March) and also during the evening/morning hours from 6 p.m. to 6 a.m.

The studies carried out with this system can be divided into four cases described in Sects. 3.3–3.6. However, before presenting these case studies, it is necessary to validate the proposed non-sequential MCS-based method.

3.2 Validation of the Proposed Method

In order to validate the proposed method, the RTS96-RES with wind Scenario 1 is evaluated by both MCS tools: the sequential/chronological algorithm (SEQ-MCS) and the proposed flexible quasi-sequential/non-sequential (NSEQ-MCS) algorithm. Table 2 presents the traditional composite reliability indices for this system configuration. One can notice that the differences are within the uncertainty margin ($\beta \leq 5$ %), which confirms the validity of the proposed methodology. The sequential MCS algorithm took 116 min to evaluate approximately 310×10^6 states, distributed in 14,106 years. On the other hand, the non-sequential MCS algorithm evaluated approximately 38×10^6 states, in 14 min, presenting a speed-up of 8.3 times in relation to the sequential MCS. Thus, from this point on, only the proposed flexible non-sequential MCS algorithm is used to evaluate all cases studied.

Table 2 Composite indices for RTS96-RES with wind scenario 1: validation of non-sequential MCS

Algorithm	LOLE (h/year)	EENS (MWh/year)	LOLF (occ./year)	LOLD (h)
Seq-MCS	0.652	130.834	0.223	2.922
NSeq-MCS	0.661	126.325	0.239	2.759

Table 3 Case 1: reliability indices—scenario 1

Indices	RI	RI_G	$RI_{T\&C}$	RI_T	RI_C
LOLE (h/year)	0.661	0.618	0.043	0.032	0.011
EENS (MWh/year)	126.325	123.024	3.301	2.654	0.647
LOLF (occ./year)	0.239	0.203	0.036	0.005	0.031

3.3 Case 1: RTS96-RES with Scenario 1

In Case 1, only hydro and wind sources are used to replace thermal sources. Scenario 1 is utilized for the hourly wind power series. Table 3 shows the complete set of reliability indices obtained with the proposed non-sequential MCS method. The LOLE index for the system is 0.661 h per year (LOLP $= 7.54 \times 10^{-5}$), which characterizes a very good performance from the reliability point of view. From this amount, 0.618 h/year refers to generation problems, and, thus, the direct or indirect influence of the transmission (i.e., $\text{LOLE}_{T\&C} = 0.043$ h/year) is very small; circa 7 %. The EENS index for the system is 126.3 MWh per year and the LOLF index is 0.239 occurrences per year. As previously stated, the proposed MCS tool took 14 min of CPU time.

3.4 Case 2: RTS96-RES with Scenario 2

In Case 2, again, only hydro and wind sources are used to replace thermal sources. Scenario 2 (Fig. 5) is employed for the wind power series. Table 4 shows the reliability indices obtained with the proposed non-sequential MCS method. The EENS index is 66.3 MWh/year, which is again a very good performance from the reliability point of view. From this amount, 62.9 MWh/year is due to generation problems, and, thus, the direct or indirect influence of the transmission (i.e., $\text{EENS}_{T\&C} \cong 3.4$ MWh/year) is very small; circa 5 % of the total. The EENS due to only transmission failures is 2.65 MWh/year and, therefore, the composite fraction is 0.74 MWh/year. This is indeed an estimated value since the conditioned indices are obtained from two extra runs with the proposed flexible non-sequential MCS algorithm. All these reliability indices indicate the large dominance of generation problems, though their consequences on the overall system are very small.

In relation to Case 1, one can observe a slight improvement in performance due to the fact that the wind became stronger during the winter, when the load

Table 4 Case 2: reliability indices—scenario 2

Indices	RI	RI_G	$RI_{T\&C}$	RI_T	RI_C
LOLE (h/year)	0.380	0.338	0.042	0.032	0.010
EENS (MWh/year)	66.289	62.894	3.395	2.654	0.741
LOLF (occ./year)	0.139	0.118	0.021	0.005	0.016

Table 5 Addition of solar and co-generation power sources

Type	Bus	No. of units	Capacity (MW)	
			Per unit	Total
Co-generation[a]	104	3	10	30
Solar[b]	106	4	20	80
Co-generation	204	3	30	30
Solar	206	4	20	80
Co-generation	304	3	30	30
Solar	306	4	20	80

[a] Each co-generation unit has $\lambda = 10$ f/year and $\mu = (1/90)$ r/h
[b] Each solar unit has $\lambda = 6$ f/year and $\mu = (1/90)$ r/h

Table 6 Case 3: reliability indices—scenario 1 and additional sources

Indices	RI	RI_G	$RI_{T\&C}$	RI_T	RI_C
LOLE (h/year)	0.461	0.425	0.036	0.032	0.004
EENS (MWh/year)	87.133	84.878	2.255	2.231	0.024
LOLF (occ./year)	0.190	0.147	0.043	0.005	0.038

curve is more intense. The proposed MCS tool took 23 min of CPU time, and circa 65×10^6 states were analyzed.

3.5 Case 3: RTS96-RES with Scenario 1—Additional Solar Power and Co-generation Power Sources

Case 3 is similar to Case 1, but an additional generation capacity is added to the system, as shown in Table 5. Table 6 shows the complete set of reliability indices obtained with the proposed non-sequential MCS method. The EENS index is 87.1 MWh/year, which is again a high-quality performance from the reliability point of view. From this amount, 84.9 MWh/year is due to generation problems, and, thus, the influence of the transmission (i.e., $EENS_{T\&C} \cong 2.3$ MWh/year) is very small. The addition of generating capacity slightly improves the system reliability performance as compared with Case 1. The proposed MCS tool took 18 min of CPU time, and circa 48×10^6 states were analyzed.

3.6 Case 4: RTS96-RES with Scenario 1, Additional Power Sources and Stressed Transmission Network

In Case 4, Scenario 1 is used together with the additional generation defined in Case 3. However, in order to stress the transmission network, all loads and generating capacities are doubled. Table 7 shows the complete set of reliability indices obtained with the proposed non-sequential MCS method. The LOLE index is now

Table 7 Case 4: reliability indices—scenario 1, additional sources, and stressed transmission network

Indices	RI	RI_G	$RI_{T\&C}$	RI_T	RI_C
LOLE (h/year)	12.278	0.394	11.884	7.101	4.783
EENS (MWh/year)	692.786	164.475	528.311	136.725	391.586
LOLF (occ./year)	4.197	0.104	4.093	2.311	1.782

12.28 h/year (LOLP $= 1.40 \times 10^{-3}$), which characterizes a significant decrease in the system reliability performance. From this amount, only 0.39 h/year refers to generation problems and, thus, the total influence of the transmission (i.e., $LOLE_{T\&C} = 11.88$ h/year) is very dominant now; circa 97 %. In relation to the unsupplied energy, $EENS_{[G/T\_UP]}$–$EENS_G = 552.10$–$164.48 = 387.76$ MWh/year shows the influence of the transmission capacity restrictions on the system, when generating unit failures occur. The influence of pure transmission failures is $EENS_T = 136.73$ MWh/year and of composite problems is $EENS_C = 391.59$ MWh/year. All previous values show the dominance of composite problems on the system performance. The proposed MCS tool spent one minute of CPU time, and circa 2×10^6 states were analyzed.

Finally, observe that if failure events are rare, as in Case 2 (LOLP $= 4.33 \times 10^{-5}$), the CPU time becomes high (23 min). Conversely, if the failures are frequent, as in Case 4 (LOLP $= 1.40 \times 10^{-3}$), the CPU time decreases (1 min). This performance can be greatly improved by using importance sampling and cross-entropy concepts as demonstrated in [34] and [35].

4 Applications to the Portuguese System

The cases presented in this section are based on planned configurations by the Portuguese Transmission System Operator (REN–Redes Energéticas Nacionais). The Transmission Network Development and Investment Plan entitled as "PDIRT 2009–2014 (2019)" is available in [36] and represents the groundwork to the 2020 configuration used in this reliability study. A complete description about data collection and the 2020 configuration supplied by REN can be found in [13].

4.1 Portuguese System Scenarios

Two different scenarios of the Portuguese system, entitled "Business-as-Usual" (BAU) and "High Renewables" (HiRES) for the 2020 horizon, were considered to explore the reliability impact of the integration of renewable sources on the Portuguese network. A study entitled as "Base" that considers all historical hydrological and wind series will be performed for both scenarios. Moreover, some specific conditions will be considered as follows: (1) the driest hydrological series (H); (2) an extremely pessimistic (zero) wind production (ZW); (3) an extremely

pessimistic wind production combined with the driest hydro condition (ZW_H). A brief description of BAU and HiRES scenarios is provided as follows.

BAU Scenario

The generation system capacity consists of 29.2 GW divided into three main components in the total Portuguese production: special regime (43.0 %), which includes renewable technologies; hydro power plants (30.5 %), with large and mini-hydro technologies; and thermal power plants (26.5 %), with several technologies. In 2020, there will be 49 hydropower plants in Portugal. In this study, 6 hydrological basins were considered, referring to 16 years of monthly hydrological conditions (1990–2005) [13]. A chronological load model with 8,760 levels for each hour of the year is used, with a peak of 13.5 GW. There will be about 3,750 wind turbines (units) in the system. Bearing the wind series in mind, Portugal was divided into 7 regions, and the average per unit value (capacity factor) remains around 0.26.

The transmission system consists of 836 circuit branches with four different voltage levels (63, 150, 220, and 400 kV), including 299 power transformers. There are 573 buses in this system including 102 load buses and 227 generating buses. It is important to emphasize that a great share of renewable production is connected to the 63 kV level, even though a small part of the wind farms may be connected to the 220 and 400 kV. In general, the hydro and thermal technologies are connected to the 220 and 400 kV, especially those power plants with a higher capacity for the energy production.

HiRES Scenario

In this scenario, renewable resources will be increased and the same generation capacity of BAU will remain for the hydro and thermal technologies. The same transmission circuits used before will be kept. This second scenario consists of 30.8 GW divided as Ssecial regime (45.8 %), which has increased in wind, photovoltaic and concentrating solar power capacity, consequently, mitigating the participation of hydro (29.0 %) and thermal power plants (25.2 %) in the total Portuguese production. The same chronological load model with 8,760 points representing each hour of the year is used, considering the same peak load on 13.5 GW. As mentioned before, the "HiRES" scenario will be submitted to the same conditions described previously; that is, H, ZW, and ZW_H. The aim is to compare the performance of the Portuguese system under the HiRES and BAU scenarios.

4.2 Composite Reliability Analysis

In the studies that follow, $\beta = 5$ % is set for the EENS and LOLF indices. Also, no maintenance activity will be scheduled with both BAU and HiRES scenarios, although the proposed methodology is capable of coping with that.

Reliability Performance of the BAU Scenario

Table 8 shows that, for the BAU "Base" case, the LOLE index is 0.768 h/year and the EENS index is 39.85 MWh/year. The failure events have occurred with a LOLF of 0.356 occ./year, which can be interpreted as 1 failure every 2.8 years. All indices revealed that the BAU scenario assessed through the "Base" case is very robust, with a LOLE lower than 1 h per year.

As stated previously, the "H" study explores the BAU configuration under a poor hydrological condition. As shown in Table 8, the risk level of the BAU scenario under this constraint slightly increases in relation to the "Base" case. The LOLE index is 0.842 h/year (the EENS index is now 55.64 MWh/year), which represents an increase of 10 % on the risk level for the overall system in relation to the "Base" case.

The "ZW" study explores the BAU scenario under a very aggressive condition, where all wind production is considered to be zero in the entire Portuguese system. The BAU configuration decreases its installed capacity circa 7,500 MW, and, consequently, impacts on the system risk level. The LOLE index increases to 12.324 h/year and the EENS index to 3,946.01 MWh/year. This result shows the importance of the wind production for the future of the Portuguese system.

Finally, "ZW_H" combines the zero wind condition described before with the poorest hydrological series. As expected, this combination revealed that the risk increases in relation to the "Base" study and to all others conditions studied. The LOLE index goes up to 15.564 h/year and the EENS index to 5,276.18 MWh/year. Thus, the analyzed configuration can be considered unacceptable for the Portuguese system. Clearly, it is very unlikely that this combination will happen and only represents an illustrative result, so that it is possible to see the limits of the BAU scenario in this study. Different scenarios involving the BAU configuration were also explored [13].

Reliability Performance of the HiRES Scenario

The main difference between BAU and HiRES scenarios is the quantity of the renewable production that is added to the Portuguese system. The HiRES scenario consists of 1,000 MW more in wind turbines, performing 8,500 MW of

Table 8 Composite reliability indices: BAU scenario

Case	LOLP	LOLE (h/year)	EENS (MWh/year)	LOLF (occ./year)
Base	8.760×10^{-5}	0.768	39.85	0.356
H	9.616×10^{-5}	0.842	55.64	0.423
ZW	1.407×10^{-3}	12.324	3,946.01	6.632
ZW_H	1.777×10^{-3}	15.564	5,276.18	7.922

wind installed capacity, 450 MW more in solar photovoltaic, performing 700 MW of the solar photovoltaic installed capacity, and 117 MW more in concentrating solar power, performing 300 MW of installed capacity. These additional capacities are equally distributed at the same buses of the BAU network configuration. It is important to highlight that both hydro and thermal capacity were not added nor the transmission system was expanded.

As the capacity of the Portuguese generating system increases, a better performance in comparison with the previous evaluation emerges. Table 9 shows that the HiRES "Base" case presents a LOLE index equals to 0.666 h/year and the EENS index is 13.30 MWh/year. The LOLF index is 0.292 occ./year and can be interpreted as one failure every 3.4 years, approximately. The average duration of each event is 2.28 h. These indices revealed that the HiRES scenario under the "Base" case can also be considered as a robust configuration, with a LOLE index lower than 1 h per year.

The "H" study explores the HiRES scenario under the poorest hydrological condition. In this case, the HiRES performance is similar to the previous "Base" case, with a slight deterioration for the composite reliability indices. The "ZW" study proposes a very aggressive condition for the HiRES configuration, where all wind production is considered to be zero in the entire Portuguese system. Consequently, the HiRES configuration decreases its installed capacity circa 8,500 MW, which, in turn, increases the system risk levels. The LOLE index increases to 5.305 h/year and the EENS index increases to 1,387.13 MWh/year. Similarly to what happens with BAU under "ZW" study, in the HiRES configuration the wind capacity, is significantly reduced, thus showing how this technology is important to the future of the Portuguese energy matrix.

The "ZW_H" case combines the previous zero wind condition with the poorest hydro case. As expected, this combination revealed that the risk level increases in relation to the "Base" case and all other studied conditions. The LOLE index increases to 6.862 h/year and the EENS index to 1,902.20 MWh/year. Under these conditions, HiRES is definitely better than the BAU configuration, although it might be considered improper for the Portuguese system. In conclusion, the increased diversity in renewable resources is always welcome, allowing for a more robust composite reliability performance.

Finally, the efficiency of the proposed composite reliability method can be demonstrated for the "Base" case with the BAU scenario: 1.6 h of CPU time against 7.4 h of a chronological MCS-based algorithm.

Table 9 Composite reliability indices: HiRES scenario

Case	LOLP	LOLE (h/year)	EENS (MWh/year)	LOLF (occ./year)
Base	7.607×10^{-5}	0.666	13.30	0.292
H	7.937×10^{-5}	0.695	17.06	0.311
ZW	6.056×10^{-4}	5.305	1,387.13	3.020
ZW_H	7.833×10^{-4}	6.862	1,902.20	3.919

5 Conclusions

This chapter presented a new methodology to evaluate composite reliability indices in power systems with high participation of renewable energy sources. Based on a flexible non-sequential Monte Carlo simulation (MCS) algorithm, which considers non-aggregate Markov models and a process for estimating frequency and duration indices named one-step forward state transition, the proposed methodology is able to cope with the volatility of renewable power sources.

Several case studies using modified configurations of the IEEE reliability test system 1996 and also a real network were carried out. The results based on various reliability indices indicated that the greater participation of renewable sources might make the restrictions imposed by the transmission network more critical. Thus, the reliability assessment algorithms of composite generation and transmission systems should be viewed as an essential tool for the decision-making process in activities related to planning or operation of new power systems, which will have an increasingly more significant participation of renewable sources.

Finally, the proposed method proved to be very accurate and efficient from the computational point of view.

Acknowledgments This work was partially supported by the following Brazilian research institutions: CNPq, CAPES, FAPEMIG, and INERGE. The authors would like to thank Prof. Warlley Salles (Federal University of São João del-Rei, MG, Brazil), Prof. Manuel Matos and Mr. Ricardo Ferreira (INESC Tec, Porto, Portugal), and also Dr. Reinaldo González-Fernández (Itaipu Binational, Paraguay) for important discussions.

References

1. Presidency Conclusions of the Brussels European Council (2007). Reference DOC/07/1. Accessible on http://www.eppgroup.eu/Press/pfocus/docs/March07.pdf
2. CAISO (2007) Integration of renewable resources. Available at http://www.caiso.com/1ca5/1ca5a7a026270.pdf
3. Billinton R, Chen H, Ghajar R (1996) A sequential simulation technique for adequacy evaluation of generating systems including wind energy. IEEE Trans Energy Convers 11(4):728–734
4. Billinton R, Karki R (2001) Capacity expansion of small isolated power systems using PV and wind energy. IEEE Trans Power Syst 16(4):892–897
5. Billinton R, Wangdee W (2007) Reliability-based transmission reinforcement planning associated with large-scale wind farms. IEEE Trans Power Syst 22(1):34–41
6. Wangdee W, Billinton R (2007) Reliability assessment of bulk electric systems containing large wind farms. Int J Elect Power Energy Syst 29(10):759–766, Dec
7. Leite da Silva AM, Manso LAF, Sales WS, Resende LC, Aguiar MJQ, Matos MA, Peças Lopes JA, Miranda V (2007) Application of Monte Carlo simulation to generating system well-being analysis considering renewable sources. Eur Trans Electr Power 17:387–400, July/Aug
8. Matos MA, Peças Lopes JA, Rosa MA, Ferreira R, Leite da Silva AM, Sales WS, Resende LC, Manso LAF (2008) Dealing with intermittent generation in the long-term evaluation of system adequacy and operational reserve requirements in the Iberian Peninsula. In: Proceedings of 2008 session CIGRÉ—international conference, Paris, France, paper C1-304, 24–29 Aug 2008
9. Lingfeng W, Singh C (2008) Population-based intelligent search in reliability evaluation of generation systems with wind power penetration. IEEE Trans Power Syst 23(3):1336–1345

10. Matos MA, Peças Lopes JA, Rosa MA, Ferreira R, Leite da Silva AM, Sales WS, Resende LC, Manso LAF (2009) Probabilistic evaluation of reserve requirements of generating systems with renewable power sources: The Portuguese and Spanish cases. Int J Electr Power Energy Syst 31(9):562–569
11. Billinton R, Yi G, Karki R (2009) Composite system adequacy assessment incorporating large-scale wind energy conversion systems considering wind speed correlation. IEEE Trans Power Syst 24(3):1375–1382
12. Liang W, Jeongje P, Jaeseok C, El-Keib AA, Shahidehpour M, Billinton R (2009) A probabilistic reliability evaluation of a power system including solar/photovoltaic cell generator. IEEE PES general meeting, Calgary, Alberta, Canada, 26−30 July 2009
13. INESC Porto and DIEE Italy—Univ of Cagliari (2009) Study on the impact of large renewable deployment on European electricity higher voltage systems—Final report (vols I—Steady state analysis and II—Reliability evaluation). Institute of the Joint Research Centre (JCR-IE), Oct 2009
14. Leite da Silva AM, Sales WS, Manso LAF, Billinton R (2010) Long-term probabilistic evaluation of operating reserve requirements with renewable sources. IEEE Trans Power Syst 25(1):106–116
15. LF Rocha, Borges CLT (2010) Probabilistic generation and interruption costs and other economic aspects related to distributed generation integration. IEEE PES GM, Minneapolis, MN, USA 25–29 July 2010
16. Flávio SA, Manso LAF, Resende LC, Sales WS, Leite da Silva AM (2011) Reliability of generation and transmission systems with large penetration of renewable sources. In: Proceedings CIGRÉ international symposium on assessing and improving power system security, reliability and performance in light of changing energy sources, Recife, Brazil, 2011
17. Ding Y, Wang P, Goel L, Loh PC, Wu Q (2011) Long-term reserve expansion of power systems with high wind power penetration using universal generating function methods. IEEE Trans Power Syst 26(2):766–774
18. Shu Z, Jirutitijaroen P (2011) Latin hypercube sampling techniques for power systems reliability analysis with renewable energy sources. IEEE Trans Power Syst 26(4):2066–2073
19. Bordeerath B, Jirutitijaroen P (2012) Hybrid enumeration and conditional probability approach for reliability analysis of power systems with renewable energy sources. In: 12th PMAPS—international conference on probabilistic methods applied to power systems, Istanbul, Turkey, 10–14 June 2012
20. Leite da Silva AM, Manso LAF, Sales WS, Flávio SA, Anders GJ, Resende LC (2012) Chronological power flow for planning transmission systems considering intermittent sources. IEEE Trans Power Syst 27(4):2314–2322
21. Carvalho LM, Rosa MA, Leite da Silva AM, Miranda V (2012) Probabilistic analysis for maximizing the grid integration of wind power generation. IEEE Trans Power Syst, 27(4):2323–2331
22. Subcommittee on the Application of Probability Methods IEEE (1979) IEEE reliability test system. IEEE Trans PAS, vol PAS-99, pp 2047–2054 Nov/Dec 1979
23. Subcommittee on the Application of Probability Methods IEEE (1999) The IEEE reliability test system—1996. IEEE Trans Power Syst 14:1010–1020 Aug 1999
24. Pereira MVF, Balu NJ (1992) Composite generation/transmission reliability evaluation. Proc IEEE 80(4):470–491 Apr 1992
25. Billinton R, Allan RN (1992) Reliability evaluation of engineering systems—concepts and techniques. Plenum Press, New York
26. Li W (2005) Risk assessment of power systems—models, methods, and applications. IEEE Press/Wiley, New York
27. Billinton R, Li W (1994) Reliability assessment of electric power systems using monte carlo methods. Plenum Press, New York
28. Salvaderi L (1990) Monte Carlo simulation techniques in reliability assessment of composite generation and transmission systems, IEEE tutorial course 90EH0311-1-PWR:36–43
29. Leite da Silva AM, Manso LAF, Mello JCO, Billinton R (2000) Pseudo-chronological simulation for composite reliability analysis with time varying loads. IEEE Trans Power Syst 15(1):73–80

30. Leite da Silva AM, Resende LC, Manso LAF, Billinton R (2004) Well-being analysis for composite generation and transmission systems. IEEE Trans Power Syst 19(4):1763–1770
31. Leite da Silva AM, González-Fernández RA, Sales WS, Manso LAF (2010) Reliability assessment of time-dependent systems via quasi-sequential Monte Carlo simulation. In: 11th PMAPS—probabilistic methods applied to power systems, Singapore, pp 14–17 June 2010
32. González-Fernández RA, Leite da Silva AM (2012) Comparison between different cross-entropy based methods applied to generating capacity reliability. In: 12th PMAPS—international conference on probabilistic methods applied to power systems, Istanbul, Turkey, pp 10–14 June 2012
33. Koninklijk Netherlands Meteorological Institute (KNMI) (2010) KNMI—climate and services. Accessible on: http://www.knmi.nl/klimatologie/onderzoeksgegevens/potentiele_wind/index.cg?language=eng
34. Leite da Silva AM, Gonzalez-Fernandez RA, Singh C (2010) Generating capacity reliability evaluation based on Monte Carlo simulation and cross-entropy methods. IEEE Trans Power Syst 25(1):129–137
35. Gonzalez-Fernandez RA, Leite da Silva AM (2011) Reliability assessment of time-dependent systems via sequential cross-entropy Monte Carlo simulation. IEEE Trans Power Syst 26(4):2381–2389